DOKUZ EYLÜL UNIVERSITY
GRADUATE SCHOOL OF NATURAL AND APPLIED SCIENCES

NUMERICAL MODELING AND BACK ANALYSIS OF A RETAINING SYSTEM FOR A DEEP EXCAVATION

by

Batuhan FENLİ

October, 2016

İZMİR

NUMERICAL MODELING AND BACK ANALYSIS OF A RETAINING SYSTEM FOR A DEEP EXCAVATION

A Thesis Submitted to the
Graduate School of Natural and Applied Sciences of Dokuz Eylül University
In Partial Fullfilment of the Requirements for the Degree of Master of Science
in Civil Engineering, Geotechnical Engineering Program

by
Batuhan FENLİ

October, 2016
İZMİR

M.Sc THESIS EXAMINATION RESULT FORM

We have read the thesis entitled **"NUMERICAL MODELING AND BACK ANALYSIS OF A RETAINING SYSTEM FOR A DEEP EXCAVATION"** completed by **BATUHAN FENLİ** under supervision of **ASSOC.PROF.DR. OKAN ÖNAL** and we certify that in our opinion it is fully adequate, in scope and in quality, as a thesis for the degree of Master of Science.

Assoc.Prof.Dr. Okan Önal

Supervisor

Prof.Dr. Gürkan Özden

(Jury Member)

Y. Doç. Dr. Deniz ÜLGEN

(Jury Member)

Prof.Dr. Emine İlknur CÖCEN
Director
Graduate School of Natural and Applied Sciences

ACKNOWLEDGEMENTS

I would like to express my gratitude to my supervisor Assoc.Prof.Dr. Okan Önal for his great supervision, contribution to my academic progress and inspiring opinions throughout the research.

I am grateful to Prof.Dr. Gürkan Özden. His knowledge, experience and support has an important place in my life. I would like to thank him for believing in me.

I also want to thank Prof.Dr. Arif Ş. Kayalar and Assoc. Prof.Dr. Ali Hakan Ören and Asst.Prof.Dr. Cihan Taylan AKDAĞ for their contributions and helps for my understanding soil mechanics.

Thanks to all colleagues in KAR İNŞAAT for their support and patience.

Last but not least, I would like to thank my family for their unconditional love and support.

Batuhan FENLİ

NUMERICAL MODELING AND BACK ANALYSIS OF A RETAINING SYSTEM FOR A DEEP EXCAVATION

ABSTRACT

Today, as a result of the rapid increase in the population, intended use of the buildings began to change especially in residential and commercial buildings in urban areas. With new developments, deep excavations have become very important to improve the usage area in buildings.

The excavation support system is necessary to prevent the damage that could occur at buildings, roads and other existing structures around the excavation. Geological condition of the area and the existing structures around the excavation affects the planned retaining system.

In urban areas, generally clearance space is limited for using anchored retaining walls for deep excavations. In these situations, where anchored retaining walls cannot be employed, strutted retaining walls are preffered to provide support during the excavation.

Excessive lateral retaining wall displacements and the associated ground settlements are often the primary cause of the damage of the adjacent buildings. Deformations can be estimated with numerical methods, but these estimates should also be checked with field measurements.

In this study, strutted diaphragm wall analyses were performed using finite element method in PLAXIS 3D software. Soil models in PLAXIS 3D were compared during the analyses.

The foundation excavation analysis of Park Inn Otel/İZMİR is performed as the implementation of the finite element analysis method for deep excavation supporting systems.

The purpose of the research on deep excavations was to develop a deeper understanding of the behavior of excavation support systems.

The major aim of this study is to compare the forces and deformations measured from the diaphragm wall, to the results from the three-dimensional finite element software i.e., PLAXIS 3D.

Results from this study showed that the finite element analysis can be used to estimate the performance of the deep excavation correcty.

Keywords: Deep excavations, finite element method, inclinometer, strain-gauge, hardening soil model with small strain stiffness, PLAXIS 3D

BİR DERİN KAZI İÇİN BİR DAYANMA YAPISININ NÜMERİK MODELLENMESİ VE GERİ ANALİZİ

ÖZ

Günümüzde nüfusun hızla artması sonucu özellikle kent merkezlerindeki konut ve işyeri gibi yapılarda gereksinimler değişmeye başlamıştır. Gelişen teknolojiyle birlikte yapılarda kullanım alanını arttırmak için derin kazılar büyük önem kazanmıştır.

Kazı çevresinde bulunan bina, yol ve mevcut diğer yapılarda oluşabilecek hasarları önlemek için kazı destekleme sistemlerinin yapılması gereklidir. Zeminin jeolojik durumu ve çevrede yeralan mevcut komşu yapılar dizayn edilecek iksa sistemini etkiler.

Şehir içinde yoğun yerleşmenin olduğu bölgelerde yapılan derin kazılarda çoğu zaman ankrajlı iksa sistemlerinin kullanılması için yeterli alan bulunmaz. Ankrajlı iksa sistemlerinin kullanılamadığı durumlarda iç destekli iksa yapıları derin kazılara destek sağlamak için kullanılabilirler.

İksa sisteminde oluşan aşırı yatay deplasmanlar ve buna bağlı olarak gelişen oturmalar çevreki yapıların zarar görmesine neden olur. Deformasyonlar numerik yöntemlerle tahmin edilebilir fakat bu tahminlerin sahada yapılan deneylerle desteklenmesi gerekmektedir.

Bu tez kapsamında sonlu elemanlar yöntemi kullanılarak iç destekli diyafram duvar analizleri yapılmıştır. Bu analizler için PLAXIS 3D paket program kullanılmıştır. Analizler sırasında kullanılabilecek zemin modelleri kıyaslanmıştır.

İzmir'de yapılan Park Inn Otel projesinin iksa sistemi derin kazı örneği olarak incelenmiştir.

Derin kazı konusundaki araştırmalarındaki temel amaç destekli kazı sistemlerinin davranışını daha detaylı olarak anlayabilmektir.

Bu çalışmadaki temel amaç diyafram duvar üzerinde ölçülen deplasmanlar ve kuvvetlerin üç boyutlu sonlu elemanlar yazılımında, PLAXIS 3D, bulunan sonuçlarla karşılaştırılmasıdır.

Sonuçlar göstermiştir ki sonlu elemanlar analizi, derin kazıların performansını doğru olarak yansıtabilir.

Anahtar kelimeler: Derin kazılar, sonlu elemanlar yöntemi, inklinometre, strain-gauge, pekleşen zemin modeli, PLAXIS 3D

CONTENTS

Page

LIST OF FIGURES

Page

LIST OF TABLES

Page

CHAPTER ONE
INTRODUCTION

Excavation is inevitable at the construction of the foundations or basements, underground oil tanks, subways or mass rapid transit systems in urban areas. The need for underground space is gradually increased in populated places, where old city centres became more valuable in terms of real estate property. On the other hand, the urban renewal projects generally improve the allowable heights of the buildings in city centres, which yields extra stresses on the underlying soil layers, resulting consolidation settlements. These settlements are very problematic for old adjacent buildings, which were generally get poor engineering service and constructed by local contractors by obeying outdated regulations. The second major problem in deep excavation is the need for preventing damage to adjacent buildings during excavation stages. The excavation process changes the stress states in the ground and may cause significant deformations and ground movements. It should be noted that, the most important goal of an excavation process is to keep the usability of the adjacent structures nearby the the excavation. The contractor must ensure that, the deformation of adjacent buildings will be limited so that it can still serve its intended function.

The design of an appropriate excavation support system is curicial, in order to reduce the excavation-induced deformations. The excavation support system may be affected by large number of factors. This factors may be grouped into three major categories (Kung, 2009);

I. Inherent factors

- Stratigraphy: Such as soil strength, soil stiffness, stress history of soil and groundwater conditions. In general, larger wall deflection for an excavation could be induced in soils with lower strength and stiffness.

- Site environment: Such as adjacent buildings and traffic conditions. High-rise buildings and heavy traffic adjacent to the excavation site may cause extra wall deflection.

II. Design related factors

- Properties of retaining system: Including wall stiffness, strut stiffness and wall length. Larger wall deflection may be expected for thinner walls, having relatively lower stiffness.
- Excavation geometry: Including width and depth of excavation. Generally, the wall deflection is approximately proportioned to the excavation depth.
- Strut pre-stress: The strut pre-stress is aimed at making good connection between the strut and the wall. However, the pre-stress might reduce the wall deflection.
- Ground improvement: Such as jet grouting method, deep mixing method, compaction grouting method, electro-osmosis method and buttresses. The soil strength and stiffness could be strengthened by ground improvement, which may reduce wall deflection.

III. Construction related factors

- Construction methods: Such as the top-down method and bottom-up method.
- Over-excavation: Over-excavation prior to installation of strut may cause larger wall deflection.
- Prior construction: Such as the effect of trench excavation prior to the construction of the diaphragm wall.
- Construction of concrete floor slab: The thermal shrinkage of the concrete floor slab may result in an increase in the wall deflection.

- Duration of the construction sequence: The duration for the strut installation or the floor construction. For an excavation in clay, longer duration for installing the strut or construction the floor slab may cause larger wall deflection due to the occurrence of consolidation or creep of clay.
- Workmanship: Poorer workmanship may cause higher wall deflection.

Deep excavation analysis includes both stability and deformation analysis. Emprical methods can be used to interpolate the performance of deep excavations. By using these empirical methods, the analysis of previous published field data in different areas of the world and local experiences may be taken in to account. But the design of excavations is fundamentally a soil-structure interaction problem. Soil is a nonlinear, inelastic and anisotropic material and water content affects the behaviour of the soil. Analysis of deep excavation systems includes simulations of elasto-plastic behaviour of soil, interface behaviour between soil and retaining walls and the excavation process. Empirical based prediction methods often remain limited and does not provide accurate results. For this reason, a common approach is to employ numerical methods. The finite element method is a numerical technique for finding approximate solutions to boundary value problems for partial differential equations. The finite element method cuts a whole soil or structure into several elements. Then reconnects elements at nodes. By connecting elements together, the field quantity becomes interpolated over the entire soil or structure. This process results in simultaneous algebraic equations.

On the other hand, field monitoring is a major concern for deep excavations. The theories used for the finite element method are complicated and some of the theories are not fully developed for some specific types of soils and for their specific behaviour. Considering the complexity of the finite element method and the uncertainty of the soil property data, it is a general method to apply field measurements, in order to monitor the deformations and also to verify and back calibrate the finite element analysis. Figure 1.1 shows the general course of deep excavation design (Ou, C.Y., 2006).

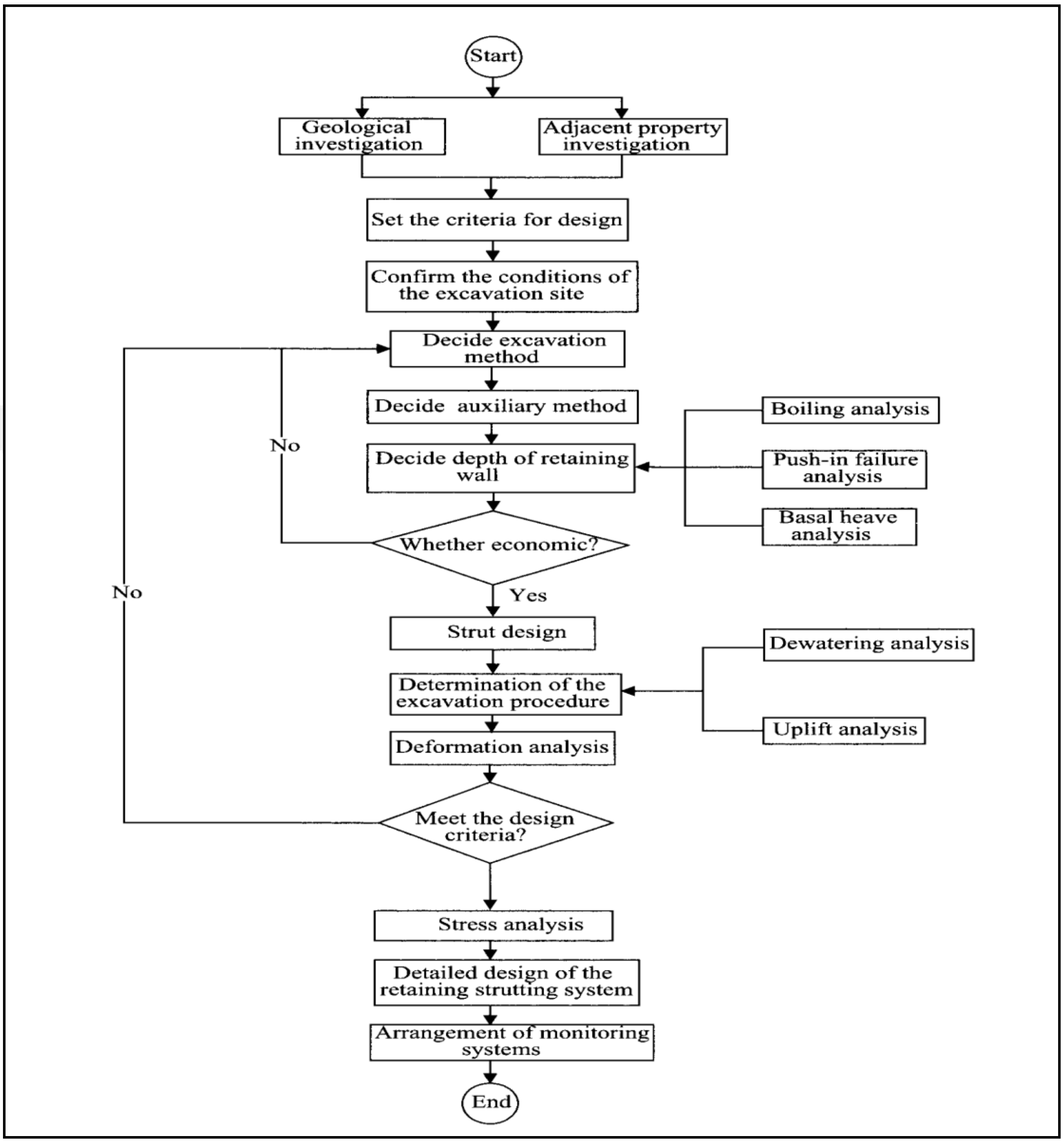

Figure 1.1 Flow chart for analysis and design of an excavation (Ou, 2006)

The purpose of the research on deep excavations was to develop a deeper understanding of the behavior of excavation support systems. There are many published case histories of deep excavations. Many researchers have used finite element analysis to study the factors that control their performance.

In scope of this dissertation, the importance of deep excavations was described as a priority. Then the effect of deep excavation to the adjacent structures was considered by finite element method which is commonly used in practice. The details of the finite element method were described in following chapter. Nevertheless, the stres-strain relationship of soils in the profile were noted. Finally, the accuracy of numerical excavation analysis was validated by comparing to the field measured data.

In Chapter 2, a review of literature on support systems for deep excavations in soil and lessons learned from the publications reviewed about factors that influence the performance of deep excavations were presented. Deep excavations often causes a complicated soil-structure interaction problem. It is, therefore, essential to take advantage of previous experience and case histories in similar conditions, e.g., the empirical methods proposed by Terzaghi (1943), Peck (1969), Bowles (1997), Clough and O'Rourke (1990), Duncan and Bentler (1998), Hsieh and Ou (1998). However, it is not reliable to extrapolate these results to deep excavations with different retaining systems, soil conditions and construction methods. For those stuations, the numerical methods should be used instead of empirical methods. There are several researches regarding the numerical analysis of deep excavations such as Ou (2006), Zaremba and Lehane (2007), Blackburn and Finno (2007), Tung and Kung (2009), Khoiri and Ou (2013), Likitlersuang et al. (2013), Hsiung and Dao (2014).

In Chapter 3, design and construction of the deep excavation support system for the Park Inn Otel Project was described. The soil and site conditions for the project were also given in this chapter.

The Park Inn Otel Project was insturemented during the excavation stage and the results of field measurements were presented in Chapter 4. In an effort to better understand the behaviour of deep excavations, field measurements were conducted during the construction process, and a number of well documented case histories have been reported, Dunnicliff (1988), Ou et al. (2000), Mikkelsen (2003), Finno et al. (2005), Blackburn and Finno (2007), Hwang et al. (2007), Zaremba and Lehane (2007), Surarak et al. (2012), Liu et al. (2011), Ng et al. (2012). The field measurement during excavation stage may provide the data for the validation of the analysis results.

Chapter 5 contains a summary of this dissertation and conclusions drawn from this study. Recommendations for future studies were also given in this chapter.

CHAPTER TWO
LITERATURE REVIEW

2.1 Introduction

Deep excavation analysis includes both stability and deformation analysis. Stability can be estimated by using simple limit equilibrium calculations. Limit equilibrium calculations involve the assessment of the classical active and passive earth pressure distributions on the back and front of the wall.

The lateral earth pressure on a retaining structure depends on several common factors. These include; the physical properties of the soil, the time dependent nature of the soil, the imposed loading, the interaction between the soil and retaining structure at the interface and the general characteristics of the deformation in the soil structure composite.

Traditionally, the Rankine's method is typically used to compute the earth pressure distribution in normally consolidated cohesive soils.

Table 2.1 Formulas for lateral earth pressure calculations

Type of Analysis	**State**	**Equation**
Effective	Rest	$K_0.\gamma'.Z_a$
Effective	Active	$K_a.\gamma'.(Z_{a-}Z_c)$
Effective	Passive	$K_p.\gamma'.Z_p + 2.c'\sqrt{k_p}$
Total	Active/Passive	$\sigma'_z(z) \mp 2C_u$
Total	Active/Passive	$\sigma'_z(z) \mp 2\lambda_u\sigma'_{vc}$

K_0 = The coefficient of earth pressure at rest

K_a = The coefficient of active earth pressure

K_p = The coefficient of passive earth pressure

$\emptyset'$ = Effective friction angle

c' = Effective cohesion

γ' = Effective unit weight

C_u = Undrained shear strength of the soil

$\sigma_z'(z)$ = The vertical effective stress at a depth Z_a

Z_a = The depth to the point of interest from surface

The most widely used load diagram for struts and anchors in soft to medium clay is that reccomended by Terzaghi/Peck (1967) as illustrated in Figure 2.1. The pressure diagram by Terzaghi and Peck was developed for flexible structures and does not include the effect of the position of struts or anchors and number of the struts.

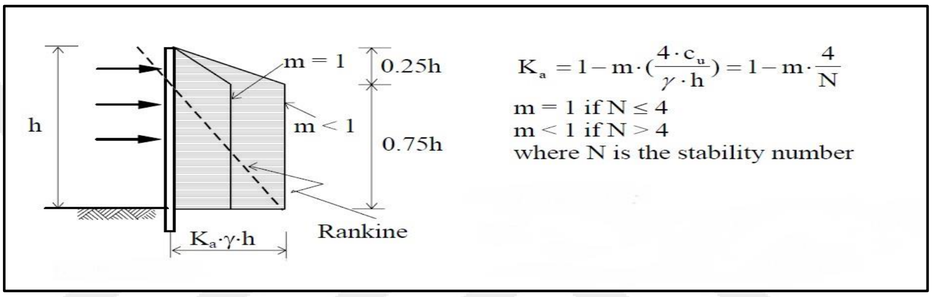

Figure 2.1 Pressure diagram for calculating loads in soft to medium clays (Gebreselassie,2003)

Heave failure is caused by the relief of the vertical stress during excavation. The two methods most commonly found in geotechnical texts for assessing basal failure, the Terzaghi (1943) and Bjerrum and Eide (1956) methods, are based on bearing capacity theory. Terzaghi (1943) was the first to develop a method for bottom heave analysis for shallow or wide excavation ($h/b < 1$).

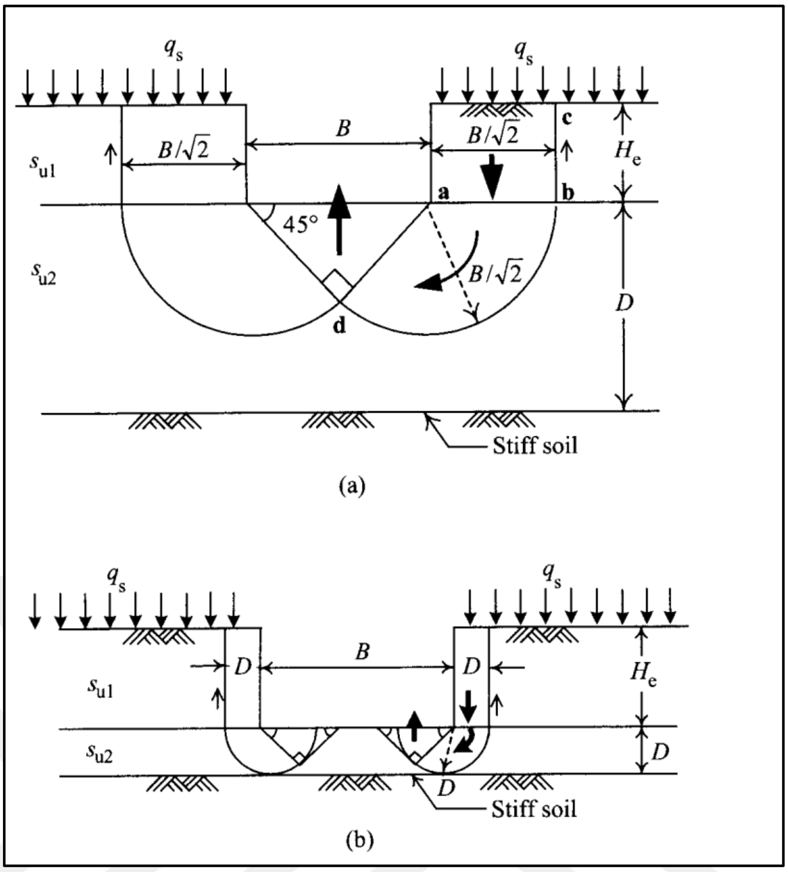

Figure 2.2 Analysis of basal heave using Terzaghi method (Ou, 2006)

$D > B/\sqrt{2}$:

$$FS_T = \frac{1}{H_e}\frac{5.7S_{u2}}{\gamma+(q_s/H_e)-(S_{u1}/0.7B)} \tag{2.1}$$

$D < B/\sqrt{2}$:

$$FS_T = \frac{1}{H_e}\frac{5.7S_{u2}}{\gamma+(q_s/H_e)-(S_{u1}/D)} \tag{2.2}$$

S_u = Undrained shear strength of the soil

γ = Unit weight of the soil

H_e = Depth of the excavation

B = Width of the excavation

q_s = The surcharge load

Bjerrum and Eide (1956) developed a method for bottom heave analysis for deep strutted excavations in soft clays ($\mathrm{h}/b > 1$)

$$FS_B = \frac{N_c\, C_u}{H\gamma + q} \tag{2.3}$$

N_c = The bearing capacity coefficient

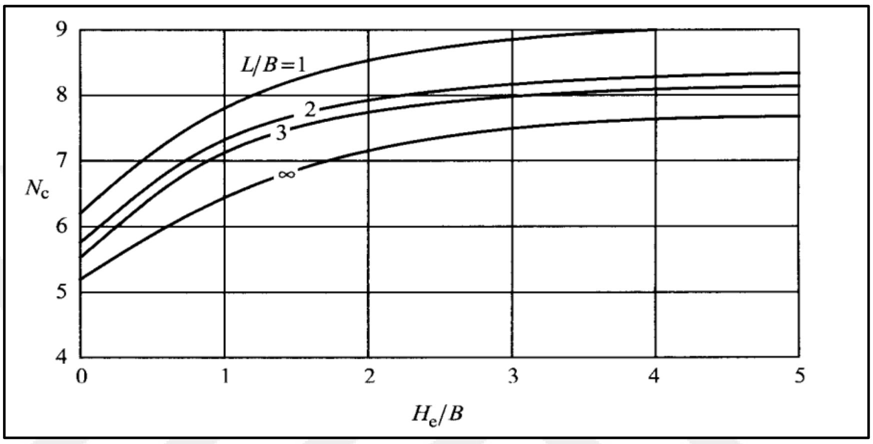

Figure 2.3 Skempton's bearing capacity factor (Skempton, 1951)

Bjerrum and Eide collected information on total or partial failure cases to analyse the base heave failure of deep excavation in soft clays. The calculated factor of safety is shown to be below 1.0 for the cases where failure occurred and just above 1.0 for the cases where partial failure occurred or no failure was observed.

Generally, the prediction of the deformation is more difficult than the prediction of the stability. In order to make the analysis of the deformation, there are several emprical methods. Emprical methods can be used to interpolate the performance of the deep excavations from the analysis of previous published field data in different areas of the world and local experiences.

When the excavation starts, soils are removed from the pit, thus the total lateral stress of the soil that subjected to the diaphragm wall is unbalanced and thereby produces lateral movement of the wall. Following this, ground settlement is expected to occur.

Ou et al. (1993) examined a number of excavation case in Taipei and showed that the range of lateral wall displacement is between 0,2% H_e and 0,5% H_e ($H_e =$ Excavation depth). The deformation of the wall in soft clay is generally greater than that in sand. Consequently, the upper bound of lateral wall displacement is recommended for soft clay while the lower bound should be used for sand.

Ou et al. (1996) proposed the plane strain ratio (PSR) of the wall displacement in terms of the excavation and the distance from the corner, as shown in Figure 2.4

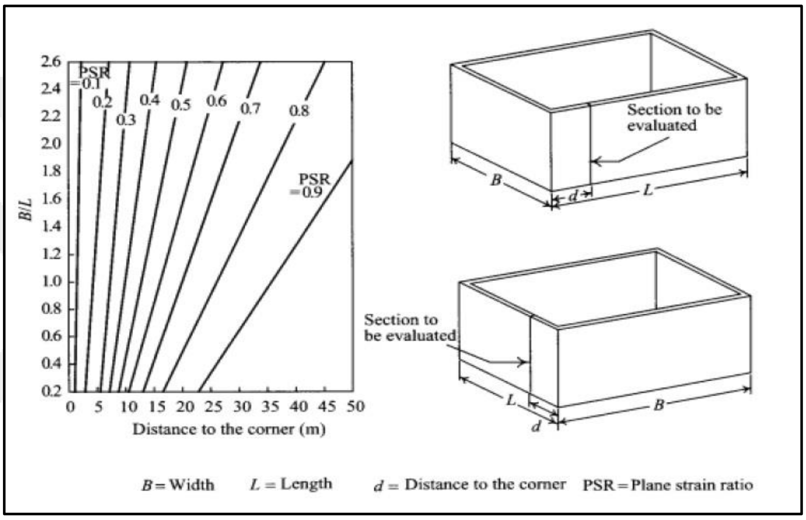

Figure 2.4 Relationship between plane strain ratio and the aspect ratio (Ou et al. 1996)

$$PSR = \frac{\delta_{hm,d}}{\delta_{hm,ps}} \tag{2.4}$$

PSR = Plane strain ratio

$\delta_{hm,d}$ = Maximum wall deflection at the distance of d from the corner

$\delta_{hm,ps}$ = Maximum wall deflection under the plane strain condition

In Figure 2.5, compiled by Clough and O'Rourke (1990), many excavation case histories are summarized. They found that, the wider excavation is, the larger the deformation of the retaining wall. The factor of safety against basal heave for soft clay decreases with the increase of the excavation width. As a result, the deformation of a retaining wall increases with the decrease of the factor of safety.

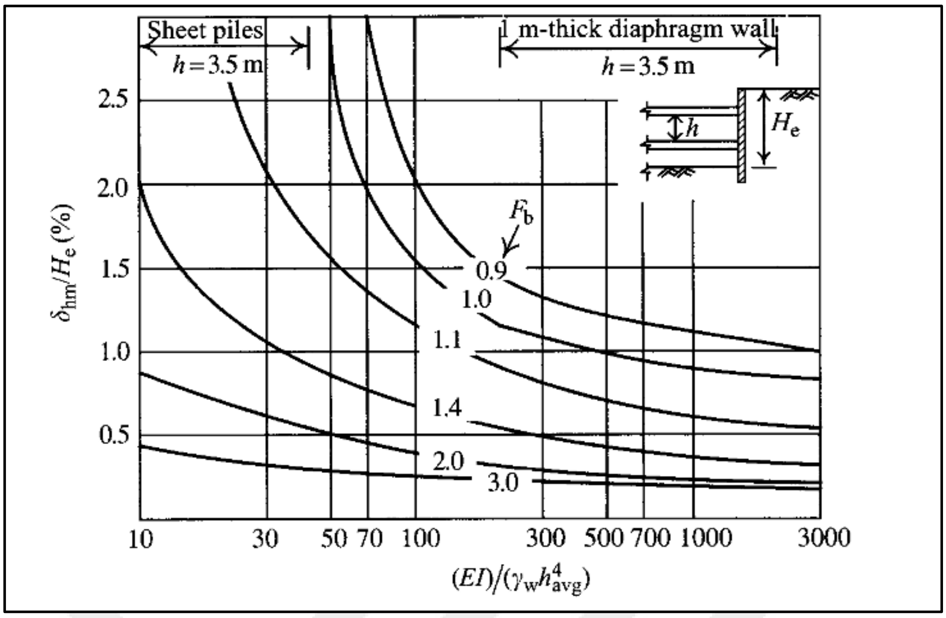

Figure 2.5 Method for estimating wall deformation (Clough and O'Rourke, 1990)

$E = Young's\ modulus$ of the wall

$I = \frac{t^3}{12}$ = The second moment of the area of the wall section

$t =$ Thickness of the wall

$\gamma_w =$ Unit weight of water

h_{awg} = The average vertical prop spacing of the multistrutted support system

The horizontal movement of wall results in the settlement of the ground behind the wall. Clough and O'Rourke (1990) had classified the shape of deformation of retaining wall as; cantilever movement and deep inward movement. The cantilever movement associated with the maximum wall deflection, occurs at the top of the wall. This type of settlements can be titled as spandrel type of settlement (Hsieh and Ou 1998). On the contrary, the deep inward movement appears when the maximum wall deformation locates near the excavation surface. This type of settlements can be titled as concave type of settlement (Hsieh and Ou 1998). The magnitude of the surface settlement depends on many factors. For example, if the wall is permitted to deflect as a cantilever, the horizontal movement can be greater than the settlements (Burland et al., 1979) and the maximum settlement usually takes place directly behind the wall. If the wall is well proped near the surface, inward movements will usually take place at a deeper depth. In such cases the horizontal surface movements will be significantly less than the settlements and the maximum settlenment may take place further from the wall.

Peck (1969) summarized the field observations of ground surface settlements around several excavations in a graphical form as shown in Figure 2.6. This method may be suitable for the spandrel-type settlement profile (Hsieh and Ou 1998).

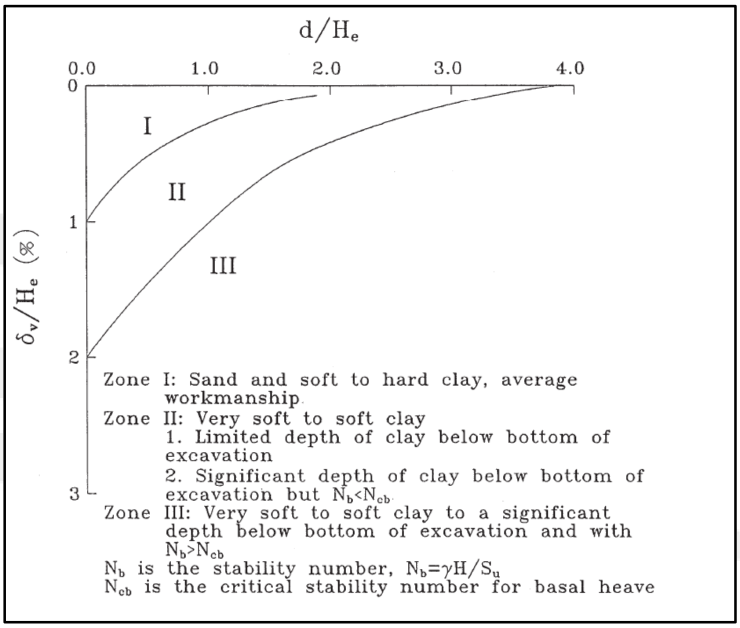

Figure 2.6 Method for estimating ground surface settlement (Peck's 1969)

Bowles (1997) proposed a method for estimating the spandrel-type settlement profile induced by excavation. The steps are given as follows:

1. Estimate the lateral wall deflection
2. Calculate the volume of lateral movement of soil mass (V_s)
3. Estimate the influence zone (D) using the method suggested by Caspe (1966) as follows:

$$D = (H_e + H_d)\tan(45 - \emptyset/2) \tag{2.5}$$

$H_e =$ Final excavation depth

$H_d =$ B for cohesive soil

$H_d = 0.5\,B\ \tan(45 + \emptyset/2)$ for cohesionless soil

$B =$ Width of the excavation

4. Estimate the maximum ground surface settlement (δ_{vm}), assuming that the maximum surface settlement occurs at the wall:

$$\delta_{vm} = 4V_s/D \qquad (2.6)$$

5. The settlement curve is assumed to be parabolic. The settlement (δ_v) at a distance from the supported wall (d) can be expressed as:

$$\delta_v = \delta_{vm}(x/D)^2 \qquad (2.7)$$

Clough and O'Rourke (1990) suggested that the settlement profile is triangular for an excavation in sandy soil or stiff clay. The maximum ground surface settlement will occur at the wall (i.e., spandrel settlement profile). The nondimensionalized profiles are shown in Figure 2.7a and Figure 2.7b, in which the corresponding settlement influence zones are $2H_e$ and $3H_e$. For an excavation in soft to medium clay, the maximum settlement usually occurs at some distance away from the wall. The trapezoidal shape of the nondimensional settlement profile was suggested, as shown in Figure 2.7c. The settlement influence zone is $2H_e$.

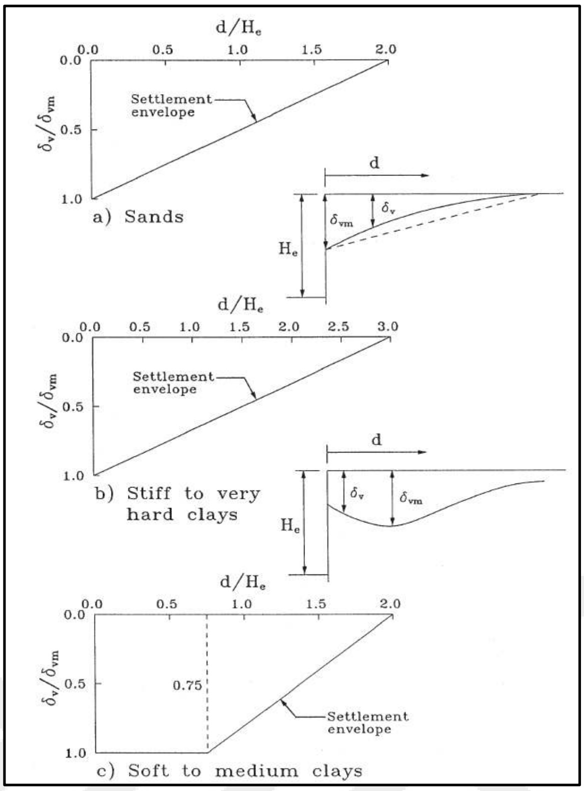

Figure 2.7 Method for estimating ground surface settlement (Clough and O'Rourke, 1990)

Ou et al. (1993) established a trilinear relationship between the normalized settlement (δ_v/δ_{vm}) and the ratio of the distance to the wall depth for the spandrel-type settlement profile.

If $d/H_e \leq 2$:

$$\delta_v = \left[-0.636\sqrt{\frac{d}{H_e}} + 1\right]\delta_{vm} \tag{2.8}$$

If $2 < d/H_e \leq 4$:

$$\delta_v = \left[-0.171\sqrt{\frac{d}{H_e}} + 0.342\right]\delta_{vm} \tag{2.9}$$

With the concave settlement profile, it is necessary to know the range of influence, surface settlement at the wall and location of maximum surface settlement to define a complete settlement profile. The distance where the maximum ground surface settlement occurs can be taken as half the final excavation depth ($H_e/2$). The settlement at the wall can be taken as $0.5\delta_{vm}$. Figure 2.8 shows the complete settlement profile used for prediction.

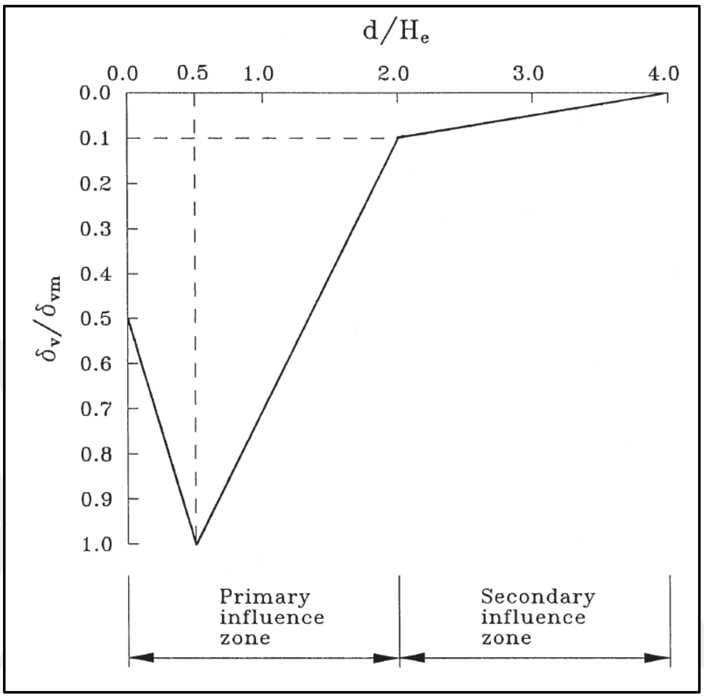

Figure 2.8 Method for estimating concave ground surface settlement (Ou, 1998)

The type of settlement profile may be related to the magnitude of the cantilever component and the deep inward component. To provide a quantative method to justify types of settlement profile induced by excavation, the area of the deep inward component (A_s) is differentiated from the wall deflection. The area of the cantilever component (A_c) is thus defined as (A_c) $= Max$ (A_{c1}, A_{c2}) where A_{c1} and A_{c2} are the area of the cantilever at the completion of the first and final stages of excavation. The concave-type settlement profile occurs if $A_s \geq 1.6A_c$. Otherwise the spandrel-type settlement profile occurs.

Clough and O'Rourke (1990) reported that the maximum horizontal wall movement is considered to be about 0.2% while the average maximum settlement is about 0.15% of the depth of excavation. This shows that the maximum settlement is about

75% of the wall maximum horizontal movement in a braced diaphragm or bored pile walls.

On the other hand, Duncan and Bentler (1998) showed that there is a wide variation in the ratio between the maximum vertical settlement and the maximum horizontal settlement. The ratio varies widely from 0.25 to 4.0.

Besides, some empirical equations developed to investigate effect of deep excavations on the adjacent buildings. Angular distortion has been used to define limiting condition for settlement under the adjacent structures. Angular distortion b is defined as the differential settlement between two points divided by the distance between them. Bjerrum (1963) presented the relations of angular distortion and building damage in Table 2.2 and it was widely adopted by many other researchers. In addition, Ou (2006) had collected the most trusted data and summarized the allowable angular distortion for reinforced concrete frames or reinforced brick structures as shown in Table 2.3

Table 2.2 Limiting values of angular distortion (Bjerrum, 1963)

Angular Distortion	**Type of damage**
1/750	Danger to machinery sensitive to settlement
1/600	Danger to frames with diagonals
1/500	Safe limit for no cracking of building
1/300	First cracking of panel walls
1/250	Visible tilting of high rigid buildings
1/150	Cracking of panel and brick walls
1/150	Danger of structural damage to most buildings

Table 2.3 Allowable angular distortion for RC frame (Ou, 2006)

Angular Distortion	**Type of damage**
1/500	Nonstructural damage
1/300	Nonstructural damage, such as cracks occur on panel walls
1/150	Structural damage

In fact, the design of excavations is fundamentally a soil-structure interaction problem. Soil is a nonlinear, inelastic and anisotropic material and water content affects the behaviour of the soil. Analysis of deep excavation systems includes simulations of elasto-plastic behaviour of soil, interface behaviour between soil and retaining walls and the excavation process. Empirical based prediction methods often remain limited and does not provide accurate results. For this reason, a common approach is to employ numerical methods. For example, finite element analysis can consider both geotechnical and structural aspects in the deep excavations such as the soil properties, details of structures and construction phases. It can be used to predict the behaviour of deep excavation in terms of stresses and deformations.

The finite element method is a numerical technique for finding approximate solutions to boundary value problems for partial differential equations. The finite element method cuts a whole soil or structure into several elements. Then reconnects elements at nodes. By connecting elements together, the field quantity becomes interpolated over the entire soil or structure. This process results in simultaneous algebraic equations.

In the finite element analysis method, any small neglect is likely to lead to wrong results. Therefore, the results of the finite element method should be examined by other methods and measured field data's.

The finite element method for soil behaviour can be split into the total stress analysis and the effective stress analysis methods and also can be divided into the undrained analysis method, drained analysis method and the partially drained analysis method. With the finite element method, the undrained behaviours of clayey soils can be analyzed by total stress analysis, effective stress analysis and coupled analysis.

2.2 Basic Principles of Finite Element Method

The finite element method is a tool to solve one dimensional, two dimensional and three dimensional structures with approximation instead of solving complicated partial differential equations. It is obvious that in one dimensional structures the element is a one dimensional member. In two dimensional structures, the element is a two dimensional plate or shell element. The three dimensional element could be a cube, prism, etc. In reality, many excavations, especially constructed for building basement, are three dimensional in geometry. However deep excavations may be represented by two dimensional model to facilitate the problem. The difference between two dimensional three dimensional models will be discussed at the end of this chapter.

If the cross section of the excavation area taken into consideration, the analysis of this section meets the the plane strain analysis condition. In this cross section, whole soil and structure is divided into many elements. According to the properties of the material of each element, the stress at any point within the element can be obtained as follows:

$$\{\sigma\} = [C]\{\varepsilon\} \tag{2.10}$$

$\{\sigma\} = stress\ matrix$

$\{\varepsilon\} = strain\ matrix$

$[C] = stress - strain\ relation\ matrix$

Under the plain strain condition, the matrices are as follows:

$$\{\sigma\} = \begin{Bmatrix} \sigma_{xx} \\ \sigma_{yy} \\ \tau_{xy} \end{Bmatrix} \tag{2.11}$$

$$\{\varepsilon\} = \begin{Bmatrix} \varepsilon_{xx} \\ \varepsilon_{yy} \\ \gamma_{xy} \end{Bmatrix} \tag{2.12}$$

$$[C] = \frac{E}{(1+\nu)(1-2\nu)} \begin{bmatrix} (1-\nu) & \nu & 0 \\ \nu & (1-\nu) & 0 \\ 0 & 0 & (1-2\nu)/2 \end{bmatrix} \tag{2.13}$$

E = Young's modulus

ν = Poisson's ratio

The displacement at any point within the element can be obtained as follows:

$$\{u\} = [f]\{\mathrm{q}\} \tag{2.14}$$

$[f]$ = displacement shape function

The strain at any point within the element can be obtained as follows:

$$\{\varepsilon\} = [d]\{u\} = [d][f]\{q\} = [B]\{q\} \tag{2.15}$$

$[d]$ = linear partial differential operator

$[B] = [d][f]$ = relation matrix between the strain and the nodal displacement

The stiffness matrix of the element as follows:

$$[K_e] = \int_V [B]^T[C][B]dV \tag{2.16}$$

Combining the relation matrices for all the elements into the global stiffness matrix:

$$[K]\{\mathrm{q}\} = \{P\} \tag{2.17}$$

$\{\mathrm{q}\}$ = nodal displacement matrix

$[K]$ = global stiffness matrix

$\{P\}$ = matrix of excavation-induced external force or equivalent nodal load at nodal points

Elasticity modulus, poisson's ratio, bulk modulus, and shear modulus can be obtained as follows:

$$E = \frac{\sigma_1}{\varepsilon_1} \tag{2.18}$$

$$\nu = -\frac{\varepsilon_2}{\varepsilon_1} = -\frac{\varepsilon_3}{\varepsilon_1} \tag{2.19}$$

$$B = \frac{\sigma_{avg}}{\varepsilon_v} = \frac{\sigma_1 + \sigma_2 + \sigma_3}{3\varepsilon_v} \tag{2.20}$$

ε_v = volumetric strain = $\Delta V/V \approx \varepsilon_1 + \varepsilon_2 + \varepsilon_3$
ΔV = change of the volume
V = volume

$$G = \frac{\tau}{\gamma} \tag{2.21}$$

γ = shear strain

If the lateral strain is 0, the constrained modulus can be obtained as follows:

$$M = \frac{\sigma_1}{\varepsilon_1} \tag{2.22}$$

According to the theory of elasticity, the relationship between the deformation parameters can be derived, as shown in Figure 2.9 (Chen and Saleeb, 1982).

	G	E	M	B	λ	ν
G, E	B	E	$\frac{G(4G-E)}{3G-E}$	$\frac{GE}{9G-3E}$	$\frac{G(E-2G)}{3G-E}$	$\frac{E-2G}{2G}$
G, M	G	$\frac{G(3M-4G)}{M-G}$	M	$M-\frac{4G}{3}$	$M-2G$	$\frac{M-2G}{2(M-G)}$
G, B	G	$\frac{9GB}{3B+G}$	$B+\frac{4G}{3}$	B	$B-\frac{2G}{3}$	$\frac{3B-2G}{2(3B+G)}$
G, λ	G	$\frac{G(3\lambda+2G)}{\lambda+G}$	$\lambda+2G$	$\lambda+\frac{2G}{3}$	λ	$\frac{\lambda}{2(\lambda+G)}$
G, ν	G	$2G(1+\nu)$	$\frac{2G(1-\nu)}{1-2\nu}$	$\frac{2G(1+\nu)}{3(1-2\nu)}$	$\frac{2G\nu}{1-2\nu}$	ν
E, B	$\frac{3BE}{9B-E}$	E	$\frac{B(9B+3E)}{9B-E}$	B	$\frac{B(9B-3E)}{9B-E}$	$\frac{3B-E}{6B}$
E, ν	$\frac{E}{2(1+\nu)}$	E	$\frac{E(1-\nu)}{(1+\nu)(1-2\nu)}$	$\frac{E}{3(1-2\nu)}$	$\frac{\nu E}{(1+\nu)(1-2\nu)}$	ν
B, λ	$\frac{3(B-\lambda)}{2}$	$\frac{9B(B-\lambda)}{3B-\lambda}$	$3B-2\lambda$	B	λ	$\frac{\lambda}{3B-\lambda}$
B, M	$\frac{3(M-B)}{4}$	$\frac{9B(M-B)}{3B+M}$	M	B	$\frac{3B-M}{2}$	$\frac{3B(2M-1)+M}{3B(2M+1)-M}$
B, ν	$\frac{3B(1-2\nu)}{2(1+\nu)}$	$3B(1-2\nu)$	$\frac{3B(1-2\nu)}{1+\nu}$	B	$\frac{3B\nu}{1+\nu}$	ν

Figure 2.9 Relations between elastic deformation parameters (Chen and Saleeb, 1982)

2.3 Stress-Strain Relationship of Soils

The model of the soil should reflect the soil characteristics by considering the strain levels. Linear elastic, perfectly plastic (e.g. Mohr Coulomb), elasto-plastic cap models (e.g. Cap, Modified Cam Clay), nonlinear-elasto-plastic cap model (e.g. Hardenin Soil with small strain stiffness) models and user defined models can be used in the finite element analysis for soils.

In general, the choice of a soil model can be examined into two groups as shown in Figure 2.10 (Obrzud, 2010).

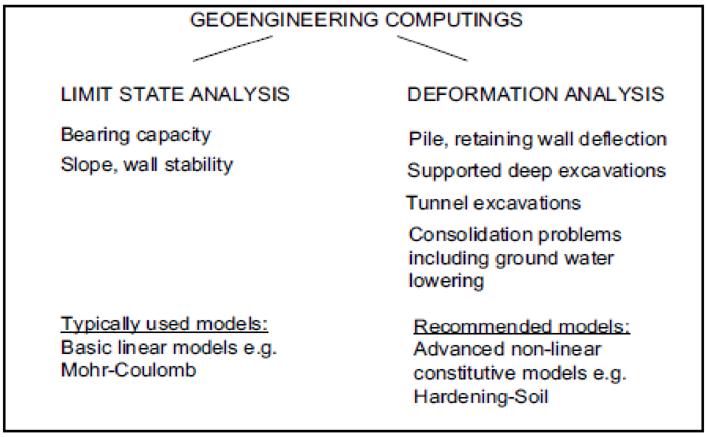

Figure 2.10 General types of geoengineering computations (Obrzud, 2010)

Soils may exhibit non-linear stress-strain behaviour even at very small strains. Stiffness of the soil vary at very small shear strains. This behaviour cannot be represented with linear elastic perfectly plastic models such as Mohr Coulomb model.

Hardening soil model is also suitable for modelling granular soils and cohesive soils. Figure 2.11 shows the recommendations for the model choice for soil type and types of analysis (Obrzud, 2010).

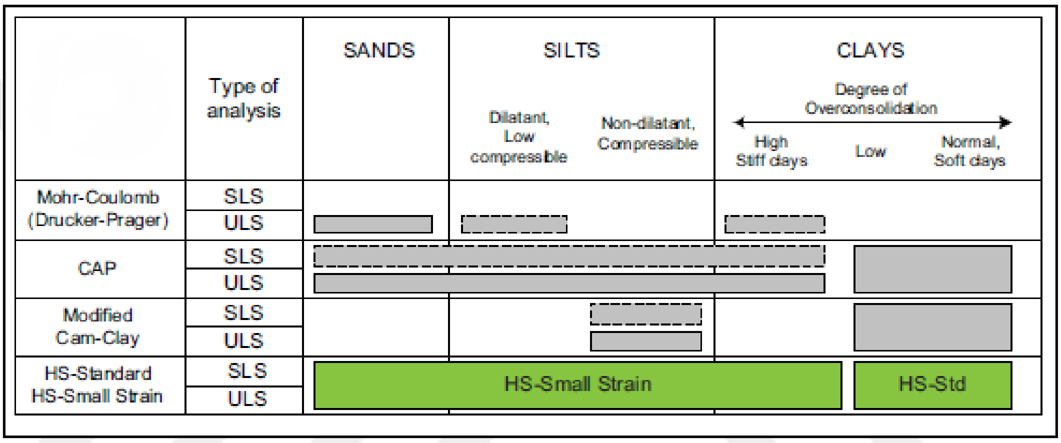

Figure 2.11 Recommendations for the model choice (Obrzud, 2010)

Dashed line: may be used but not recommended in terms of quality of results

Solid line: can be applied; Green fill: recommended

Features of hardening soil model as follows;

- Due to plastic deformations volume of voids decreases
- Due to increasing confining stress stiffness modulus increases
- Considers pre-consolidation effects
- Considers plastic yielding
- Due to shearing negative volumetric strains occurs

Hardening soil model uses three different input stiffness parameters which are the triaxial stiffness (E_{50}), the triaxial unloading-reloading stiffness (E_{ur}), and the oedometer loading modulus (E_{oed}). These features provide more realistic model for the soil.

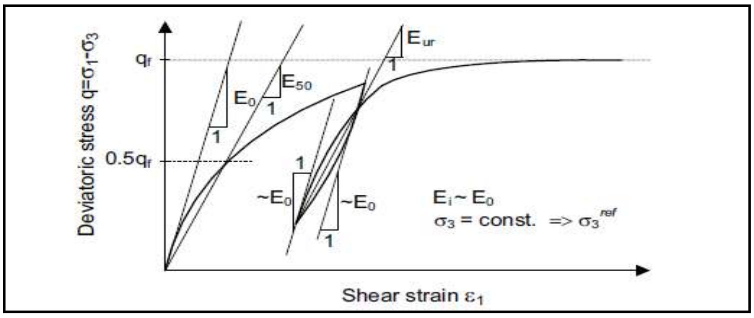

Figure 2.12 Definitions of different moduli on a typical strain-stress curve for soil (Plaxis Material Manual, 2016)

The Hardening soil model correctly reproduces the strong reduction of soil stiffness with increasing shear strain amplitudes. For unloading conditions (e.g excavation) loading and unloading stiffness modulus should be used separately, so Mohr-Coulomb model may result unrealistic lifting of the retaining wall due to excavation and also reaching the pre-consolidation pressure the shear mechanism generates no volumetric plastic strain. The model without volumetric mechanism (Mohr-Coulomb model) could significantly overestimate soil stiffness in virgin compression conditions.

During the excavation, settlements may occur behind the retaining structure. This settlement causes the plastic shear strains for granular materials such as sands and heavily consolidated cohesive soils. When using Mohr-Coulomb model or the Cap model, soil response behind the retaining structure may be underestimated.

The Hardening Soil Small Strain model is improved model of Hardening Soil model. According to Hardening Soil model, Hardening Soil model with Small Strain stiffness has strong stiffness variation and non-linear elastic stress-strain relationship even at small strains. These features provide more realistic approximation of displacement for the dynamic applications and unloading condition problems, e.g. excavations with retaining walls or tunnel excavations.

Despite being used in most cases, Hardening Soil Model and Hardening Small Strain model are incapable in some cases. Hardening Soil Model does not account for softening due to soil dilatancy and de-bonding effects and also unavailable for cyclic loading. Moreover, the model does not distinguish between large stiffness at small strains. Stiffness parameters have to be selected in accordance with the dominant strain levels. Hardening Small Strain model can be used for cycling loading but it is not suitable when softening plays a role. Besides, the hardening soil model does not incorporate the accumulation of irreversible volumetric straining nor liquefaction behaviour with cyclic loading.

2.4 Structural Materials

Retaining walls, struts, wales etc. can be used as structural material during excavation.

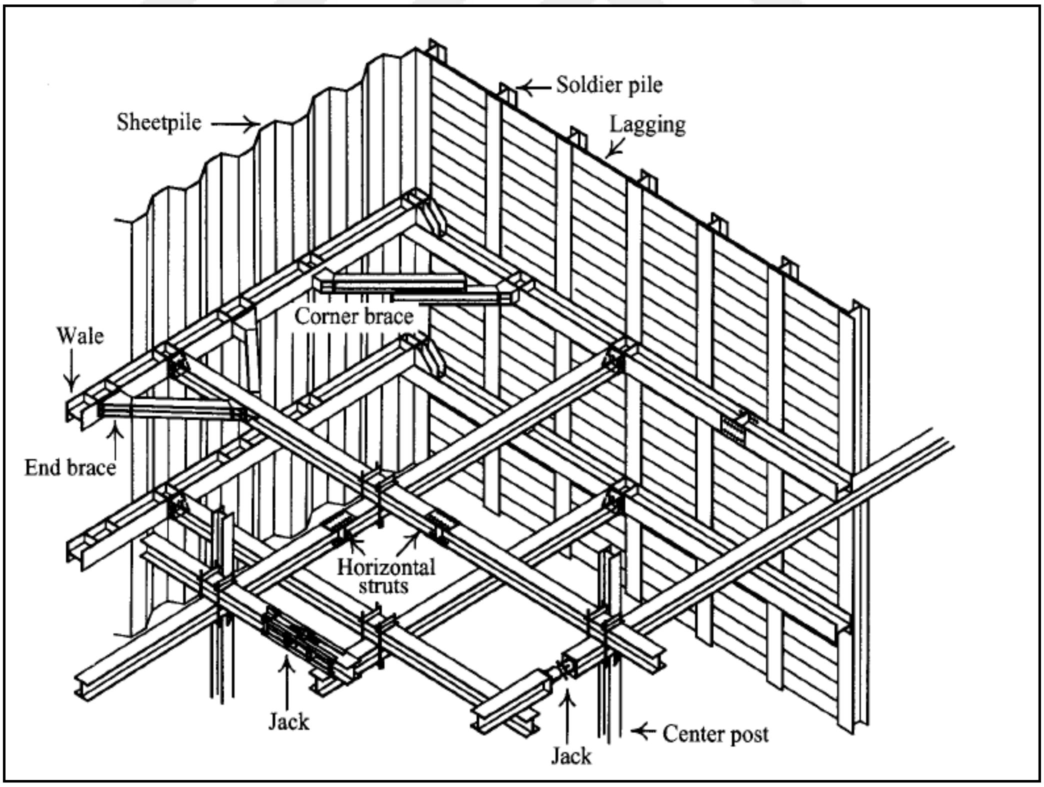

Figure 2.13 Components of a strutting retaining system (Ou, 2006)

2.4.1 Retaining Walls

Plane strain elements or beam elements can be used for analysis. If beam elements are used, the bending moment can be found at each node of the elements. If plane strain elements are used, the bending moment of the retaining wall can be computed through the stresses at the integration points within the element. For example, plane strain element has 9 integration points as Figure 2.14. The finite element method can directly obtain the stresses at the integration points.

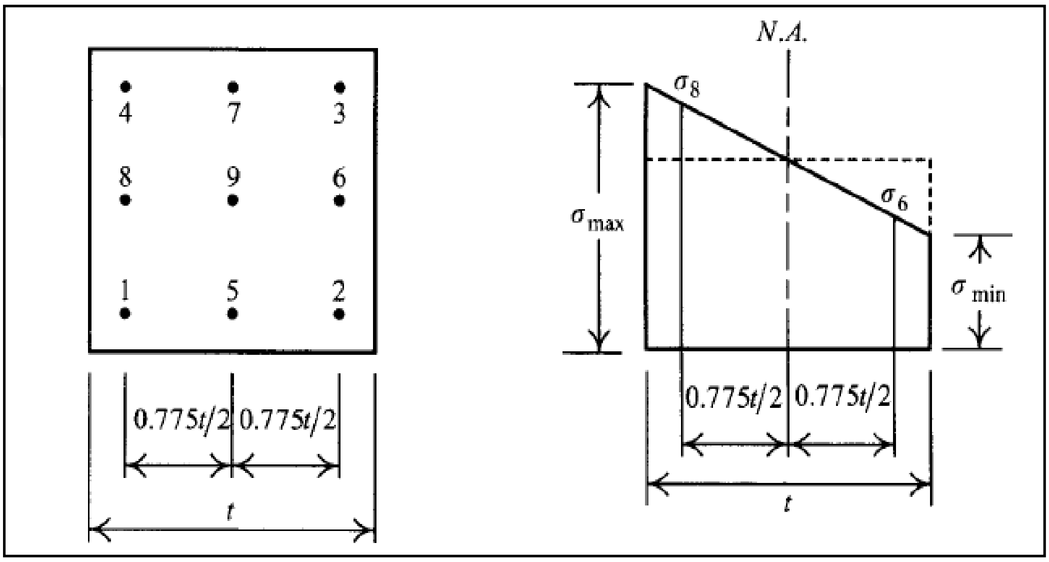

Figure 2.14 Computation of the bending moment of the retaining wall: (a) locations of the integration points and (b) stress distribution on the section (Ou, 2006)

$$\sigma_{max} = \frac{\sigma_8 - \sigma_6}{2 \times 0.775} \tag{2.23}$$

$$M_{wall} = \frac{\sigma_{max} \times t^2}{6} \tag{2.24}$$

t = thickness of the wall

Design of the wall sections should adopt the envelope of the maximum bending stresses. The bending stresses occurring at each construction stage does not take place at the same depth.

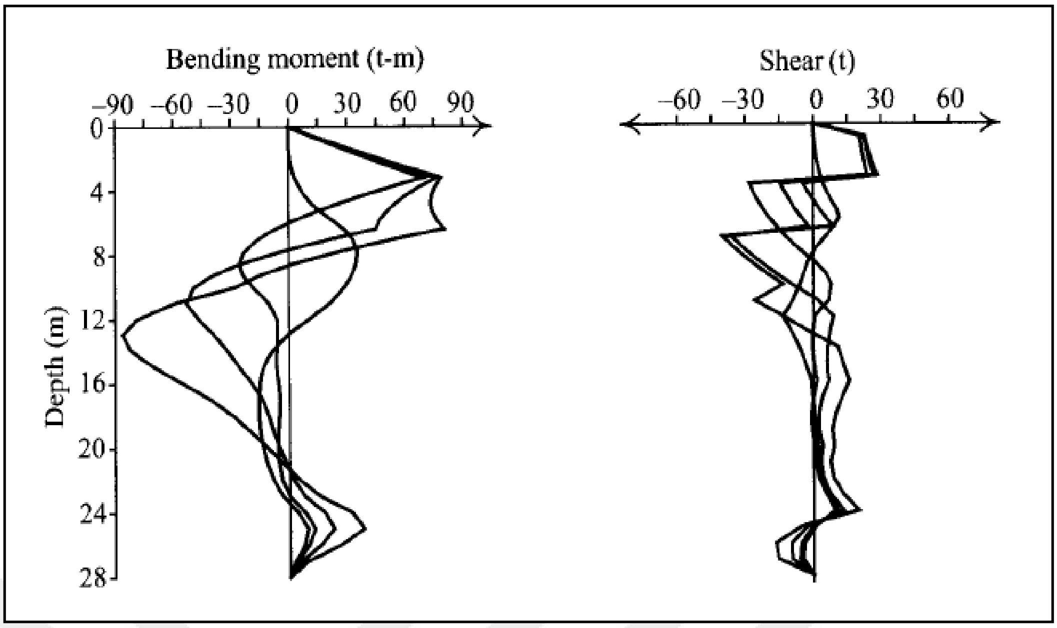

Figure 2.15 Typical bending moment and shear diagrams of a retaining wall (Ou, 2006)

2.4.2 Struts

Struts are subjected to the axial compressive load and flexural load. Axial compressive load can be computed as follows;

$$f_a = \frac{N}{A} \tag{2.25}$$

A = sectional area of the strut

N = axial load = $N_1 + N_2$

N_1 = Strut load induced by excavation

N_2 = Strut load induced by the temperature change = $\alpha.\Delta t.E.A$

α = coefficient of thermal expansion of struts; for the steel strut, $\alpha = 1.32 \times 10^{-5}$ / □

Δt = temperature change of struts ($°C$)

E = Young's modulus

Instead of N_2 term in correlations the empirical formula can be used because N_2 comes out too large. The JSA(1988) suggests N_2 = 10-15 ton or N_2 = (1.0-4.0 ton) $\times \Delta t$ where Δt is the temperature change ($°C$) in the air.

The flexural stress can be computed as follows:

$$f_b = \frac{M_1 + M_2}{S} \tag{2.26}$$

M_1 = bending moment produced by the strut weight and the live load; taking the center post as the simply supported hinge, then

$$M_1 = wL^2/8 \tag{2.27}$$

w =strut weight + live load ≅ 0.5 ton/m
L = distance between two adjacent center posts
M_2 =bending moment caused by the uplift of the center post
S =section modulus

Struts carry both the axial compressive force and the moment during excavation. The allowable axial compressive stress can be computed as follows;

$$\frac{KL}{r_y} < C_c \quad F_a = \frac{\left[1 - \frac{1}{2}((KL/r_y)/C_c)\right]F_y}{\frac{5}{3} + \frac{3}{8}[(KL/r_y)/C_c] - \frac{1}{8}[(KL/r_y)/C_c)]^3}\lambda \tag{2.28}$$

$$\frac{KL}{r_y} < C_c \quad F_a = \frac{12}{23}\frac{\pi^2 E}{(KL/r_y)^2}\lambda \tag{2.29}$$

(KL/r_y) = effective slenderness ratio of the strut on the flexural plane where K can be taken as 1.0
L = unsupported lenght of the strut
r_y = radius of gyration of the cross section of the strut in the direction of the weak axis
C_c = critical slenderness ratio = $\sqrt{2\pi^2 E/F_y}$
E = Young's modulus of struts
F_y = yielding stres of struts
λ = short-term magnified factor of the allowable stres

According to the AISC Specifications, the stress on each section of a strut should satisfy the following equation:

$$\frac{f_a}{F_a} \leq 15\% \qquad \frac{f_a}{F_a} + \frac{f_b}{F_b} \leq 1.0 \tag{2.30}$$

$$\frac{f_a}{F_a} > 15\% \qquad \frac{f_a}{F_a} + \frac{C_m f_b}{(1 - f_a^{'}/F_e^{'})F_b} \leq 1.0 \tag{2.31}$$

C_m = coefficient of modification = 0.85

$1/(1 - f_a^{'}/F_e^{'})$ = amplification factor

$F_e^{'}$ = allowable Euler stres = $\lambda.\, 12\pi^2\, E/[23(KL/r_x)^2]$

KL/r_x = effective slenderness ratio on the flexural plane

r_x = radius of gyration of the strut in the direction of the strong axis

E = Young's modulus of struts

λ = short-term magnified factor of the allowable stres

2.4.3 Wales

The wales are subjected to the moment and the axial force. For computing bending moment and shear force of wales, the wales can be observed as simply supported beams with struts as supporting hinges or fixed end beams as shown in Figure 2.16

For simply supported beam assumption following equation can be used:

$$M_{max} = \frac{1}{8}pL^2 \tag{2.32}$$

$$Q_{max} = \frac{1}{2}pL \tag{2.33}$$

For fixed end beam assumption following equation can be used:

$$M_{max} = \frac{1}{12} pL^2 \tag{2.34}$$

$$Q_{max} = \frac{1}{2} pL \tag{2.35}$$

M_{max} = maximum bending moment of the wale

Q_{max} = maximum shear of the wale

L = distance between struts

P = earth pressure

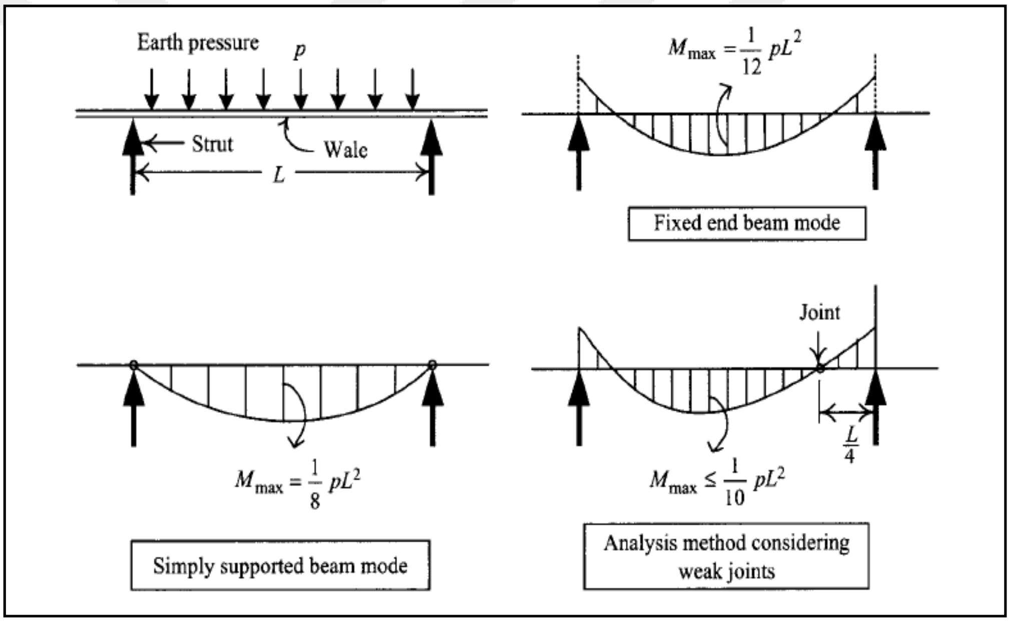

Figure 2.16 Computation of the bending moment of a wale (Ou, 2006)

2.5 Excavation Analysis Methods

2.5.1 Direct Analysis and Back Analysis

In the direct analysis, soil parameters obtained from soil tests can be used directly. If the soil model and soil parameters can thoroughly simulate the soil behaviors, the direct analysis can obtain reasonable and accurate results. Besides, the measured field data can also be used to calibrate and verify finite element analysis. In the back analysis, measurement data may be taken as a reference as to modify the parameters of the soil model so to make the analysis results match the measurements. Modified soil parameters can be used for the prediction of excavation behaviors. If all parameters are assumed unknown, back analysis will be very time consuming, expensive and sometimes results are impossible to match the site deformations. Therefore, parameters which cannot be obtained from laboratory and field tests should be estimated with back analysis.

2.5.2 Total Stress Analysis and Effective Stress Analysis

The total stress parameters such as S_u and $\emptyset = 0$ (for saturated clay) or C_T and $\emptyset_T$ (for unsaturated clay) are used for total stres analysis. The effective stress parameters such as c' and $\emptyset'$ are used for effective stres analysis.

Effective stress parameters should be used for drained analysis. Besides either the total stress parameters and effective stress parameters can be used for undrained analysis.

2.5.3 Drained Analysis, Undrained Analysis and Partially Drained Analysis

When drained analysis performed the excess pore water pressure is assumed to be completely dissipated and soil goes through a volume change accordingly. Drained analyses are mainly applied to granular soils and for the long-term behavior of clayey soils so effective stress parameters should be used.

When undrained analysis performed, the excess pore water pressure is assumed to be not dissipated at all. If the soil is in the saturated state, the volume change would not arise.

In some cases, the behaviors of clay are in between drained and undrained state, called the partially drained. The analysis of the partially drained behavior of clay can be carried out through undrained analysis, which takes advantage of the known excess pore water pressure at each stage. The pore water pressure can be obtained by using piezometer.

When using hyperbolic soil model, the undrained analysis for short-term behavior of saturated clay has to adopt the total stress analysis (S_u and $\emptyset = 0$). The undrained analysis of unsaturated clay directly adopts the result of the triaxial UU test (c_T and $\emptyset_T$). For granular soils the effective stress analyses has to be performed ($c^{'}$ and $\emptyset^{'}$).

When using elasto-plastic soil model, the undrained analysis for short-term behavior of saturated clay can adopt either the effective stress analysis or the total stress analysis. If adopting the effective stress analysis, strength of the soil increases with the increase of the average effective stress ($p^{'}$). If adopting the total stress analysis, strength of the soil does not increase with the increase of the average total stress (p).

2.6 Density of Meshes

Density of meshes should be finer in the crucial areas. The mesh in the transition zone between the wall and the surrounding soils and also on the bottom of the excavation in the excavation zone should be as fine as possible. Away from the wall, lower density of mesh can be used.

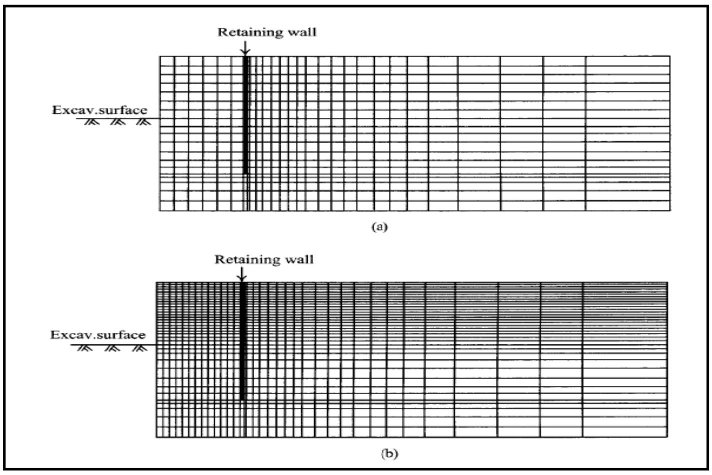

Figure 2.17 The finite element meshes used in the analysis of excavation: (a) bad mesh and (b) good mesh (Ou, 2006)

2.7 Boundary Conditions

When boundary conditions move farther from the retaining wall, more accurate results can be obtained. Minimum recommended distance of boundary condition is illustrated in Figure 2.18

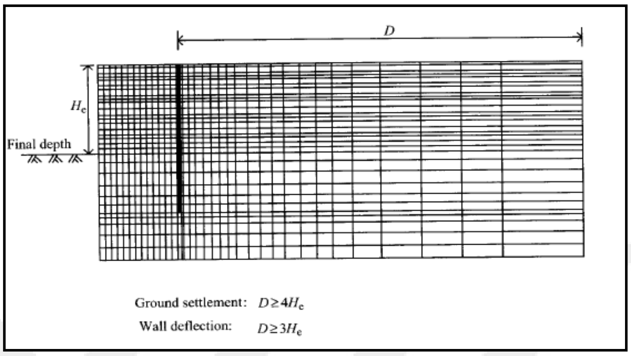

Figure 2.18 Distance of the boundary required for the analysis (Ou, 2006)

The symmetric boundary of an excavation should be equipped with rollers to restrain the lateral displacement and allow vertical displacement. According to Ou and Shiau (1998) for analyzing movement in an excavation, rollers will be more efficient than hinges placed on the boundary of soil which is illustrated in Figure 2.19.

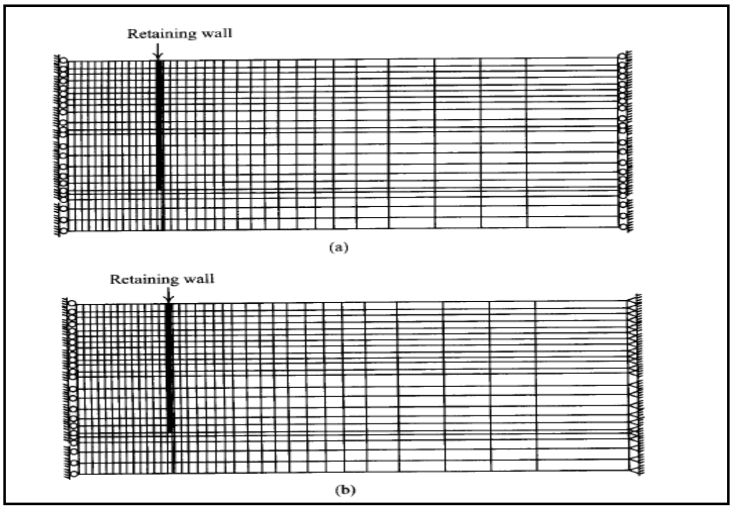

Figure 2.19 Boundary conditions of the finite element mesh: (a) boundary outside the excavation zone is allocated with rollers and (b) boundary outside excavation zone is allocated with hinges (Ou, 2006)

2.8 Two Dimensional Analysis and Three Dimensional Analysis

As mentioned earlier, many excavations, especially constructed for building basement, are three dimensional in geometry. However, two dimensional models may be used for pre calculations or for facilitating the problem.

But three-dimensional effects caused by the higher stiffness at the corners of an excavation lead to smaller ground movements near the corners and larger ground movements toward the middle of the excavation wall.

Three dimensional analysis can be used to obtain more realistic prediction of excavation behaviour. Two dimensional plane strain analysis will overestimate the results. On the other hand St. John (1975) studied an unsupported square excavation in stiff London Clay using three dimensional as well as two dimensional axisymmetric and plane strain linear elastic analyses. The results showed that good agreement was obtained between the 3D and 2D axisymmetric analyses, but that two dimensional plane strain analysis significantly over predicted horizontal movements. Burland et al. (1979) also suggested that an assumption of axial symmetry is more appropriate to computations for square excavations than is plane strain.

However, this assumption is valid for unsupported excavations. It is difficult to model excavations that are irregularly shaped or supported by strutting systems with 2D analysis, Lin and Woo (2007).

Ou and Shiau (1998) indicated that 2D plane strain finite element analysis of deep excavation can be affected by the restraint of wall corners.

Liu (1995) carried out several numerical analyses on a bottom-up excavation. Back analysis of field data using 2D and 3D finite element analyses showed that wall movement below excavation level is much better predicted by 3D analyses whereas 2D analyses consistently over predicted wall movement.

2.9 Soil Model Parameters

As discussed in Chapter 2.2 some soil models are used in finite element method. (e.g. The Mohr Coulomb model, Hardening soil model, Hardening soil model with small strain stiffness). The soil parameters used in in these models as follows;

2.9.1 The Mohr-Coulomb Model

The Mohr-Coulomb (MC) model is a basic soil model for analyzing deep excavation problem. This model can be used for a first analysis of the problem considered (Plaxis References Manual, 2016). Required input parameters for the Mohr-Coulomb model as follows;

E : Young's modulus (kN/m^2)
ν_r: Poisson's ratio (-)
φ : Friction angle (°)
c : Cohesion (kN/m^2)
Ψ : Dilatancy angle (°)

2.9.2 Hardening Soil Model

The hardening soil model was developed as an extension of the Mohr-Coulomb Model (Nordal, 1999). Soil stiffness is described more accurately in this model. Required input parameters for the hardening soil model is as follows;

φ : (Effective) Friction angle (°)
c : (Effective) Cohesion (kN/m^2)
R_f : Failure Ratio (-)
Ψ : Dilatancy angle (°)
E_{50}^{ref} : Secant stiffness in standard drained triaxial test (kN/m^2)
E_{oed}^{ref} :Tangent stiffness for primary oedometer loading (kN/m^2)
E_{ur}^{ref} : Unloading / reloading stiffness (kN/m^2)

m: Power for stress-level dependency of stiffness (-)

ν_{ur}: Poisson's ratio for unloading / reloading (-)

K_0^{nc} : K_0 value for normal consolidation (-)

2.9.3 Hardening Soil Model with Small-Strain Stiffness

Hardening Soil Model with small-strain stiffness is an advanced version of hardening soil model. Soils exhibit a higher stiffness at low strain levels than engineering strain levels and this stiffness varies non-linearly with strain. This behavior of soil can be examined with hardening soil model with small-strain stiffness. Required input parameters as follows;

φ : (Effective) Friction angle (°)

c : (Effective) Cohesion (kN/m^2)

R_f : Failure Ratio (-)

Ψ : Dilatancy angle (°)

E_{50}^{ref} : Secant stiffness in standard drained triaxial test (kN/m^2)

E_{oed}^{ref} :Tangent stiffness for primary oedometer loading (kN/m^2)

E_{ur}^{ref} : Unloading / reloading stiffness (kN/m^2)

m : Power for stress-level dependency of stiffness (-)

ν_{ur}: Poisson's ratio for unloading / reloading (-)

K_0^{nc} : K_0 value for normal consolidation (-)

G_0^{ref} : Reference shear modulus at very small strains ($\varepsilon < 10^{-6}$) (kN/m^2)

$\gamma_{0.7}$: Shear strain at which $G_s = 0.722G_0$ (-)

OCR : Over-consolidation ratio

CHAPTER THREE
AN EXAMPLE FOR A DEEP BRACED EXCAVATION

Following chapters includes a study to set light for deep excavation application of Park Inn Hotel–İzmir. Soil profile and the finite element analysis of deep excavation project were examined in this Chapter.

3.1 Project Description

The site locates in İzmir/Konak with given map sections of layout: 79, site block: 1007 and lot: 5. The location of the project may be seen in Figure 3.1

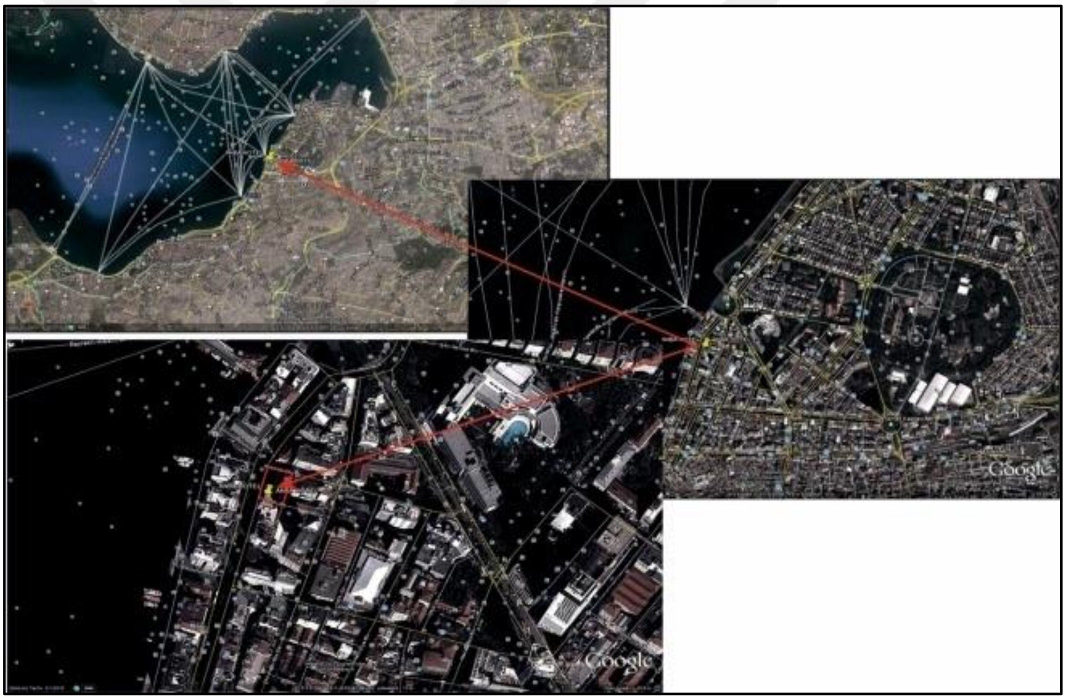

Figure. 3.1. The location of the Park Inn Otel project

The existing building in the field was planned to be demolished, which is called Anba Hotel. (Figure 3.2)

Figure 3.2 Existing building, Anba Otel and its demolition

The new project, Park Inn Hotel, has totally 12 floors with 3 basement floors, 1 ground floor, 7 normal floors and 1 roof floor (Figure 3.3). The base area of the project is approximately 663 m^2. The other necessary information was taken from the architectural and structural projects pertaining to the structure can be summarized as follows:

- The total height of the building at the tallest section was determined as H= 33.50m.
- Load carrying structural system consists of reinforced concrete frame elements. In the structural projects, the foundation system was given as a flat raft. The raft has thicknesses of t=100cm.
- The bottom elevation of the raft places at a depth of 11.50m (Figure 3.4). The given depth was evaluated with respect to the natural ground surface level (±0.00 m).
- The fair average depth of the ground water table was 1m from the natural ground surface.
- The excavation of the basement will be approximately 32m tall and 20m wide.
- Deep excavation was planned to be supported with 60cm thick diaphragm wall and steel struts.

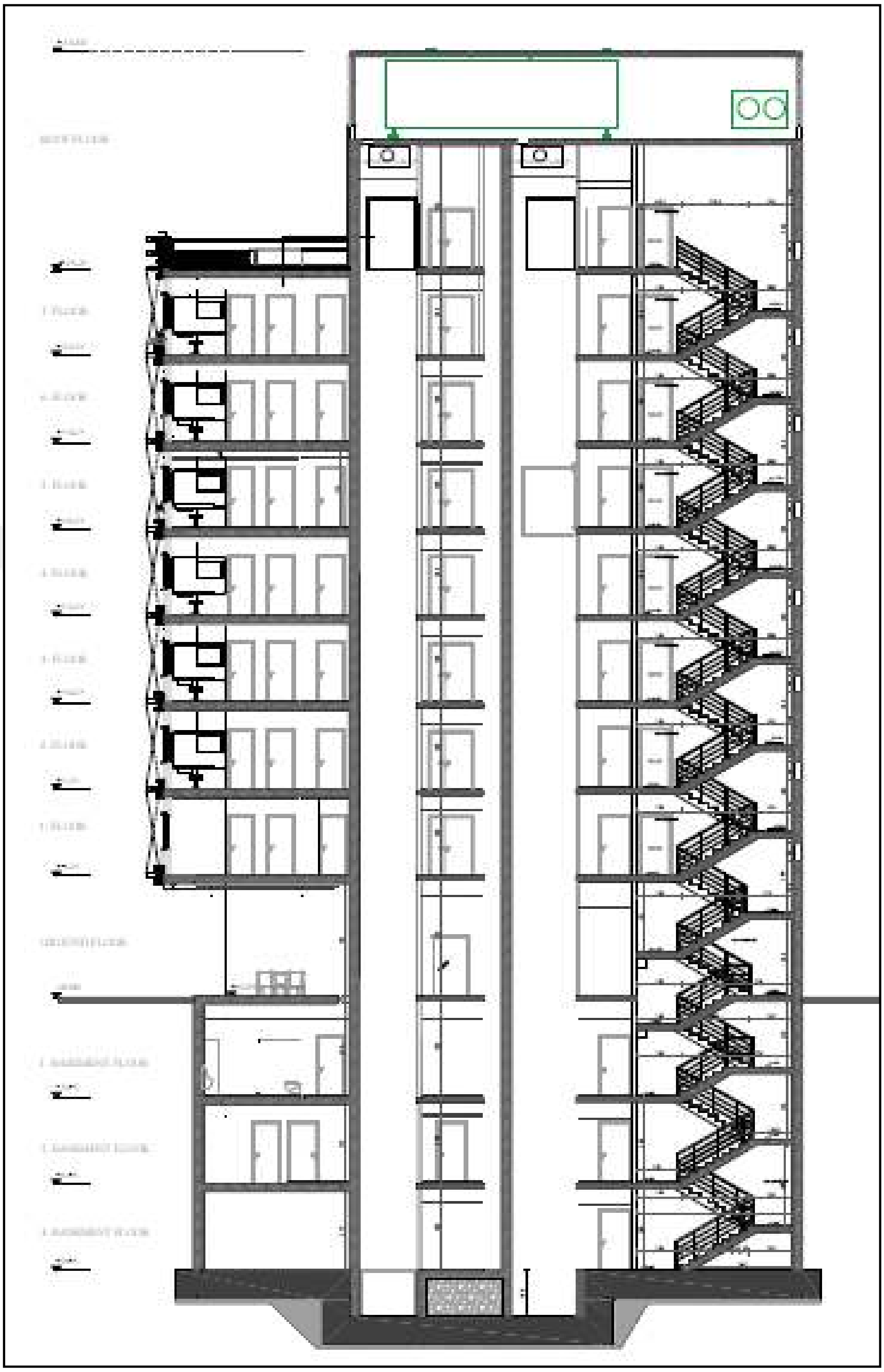

Figure 3.3 B-B Section of Park Inn Hotel

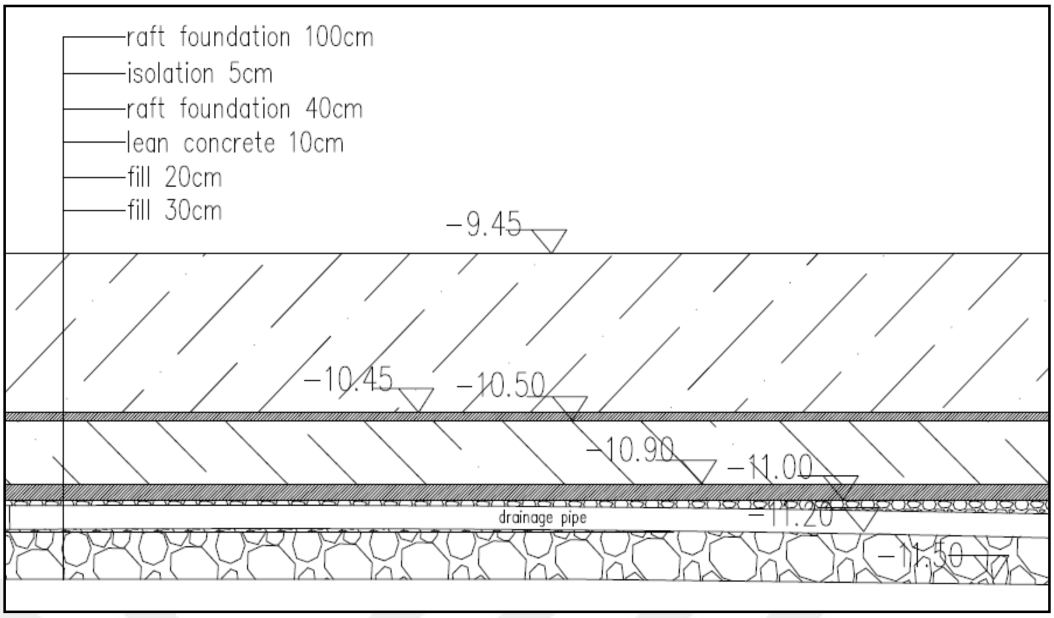

Figure 3.4 Section of raft foundation

3.2 Site Soil Description

There are two boreholes drilled in the field for specify soil parameters. The depth of the drillings performed for BH-1 and BH-2 were 30.0 m. According to the results of completed boreholes; Andesite fill layer, silty sand with gravel layer, silty clay layer, silty clay layer with sand, silty clayey gravel, clayey sand layer is located, respectively.

3.2.1 Field Tests

Standard penetration test was conducted for each 1.5m. Data obtained from the experiment results are shown in Table 3.1 and Table 3.2.

Table 3.1 SPT results of BH-1

BH-1	Depth (m)	0-15 cm	15-30 cm	30-45 cm	N30	Soil Classification
SPT - 1	1.50-1.95	15	13	12	25	Fill
SPT - 2	3.00-3.45	8	9	8	17	Fill
SPT - 3	4.50-4.95	R	-	-	R	Fill
SPT - 4	6.00-6.45	9	7	6	13	Fill
SPT - 5	7.50-7.95	2	2	2	4	SM
SPT - 6	9.00-9.45	1	2	2	4	CH
SPT - 7	10.50-10.95	3	3	3	6	CH
SPT - 8	12.00-12.45	3	3	3	6	CH
SPT - 9	13.50-13.95	3	3	5	8	CH
SPT - 10	15.00-15.45	6	7	11	18	CH
SPT - 11	17.00-17.45	5	5	6	11	CL
SPT - 12	18.00-18.45	8	13	5	18	GW-GC
SPT - 13	19.50-19.95	6	7	5	12	CL
SPT - 14	21.00-21.45	31	40	R	R	GW-GC
SPT - 15	22.50-22.95	31	10	9	19	GP-GC
SPT - 16	24.00-24.45	21	19	11	30	CL
SPT - 17	25.50-25.95	20	13	8	21	CL
SPT - 18	27.00-27.45	8	8	9	17	CL
SPT - 19	28.50-28.95	10	9	7	16	CL
SPT - 20	30.00-30.45	12	11	6	17	GC

Table 3.2 SPT results of BH-2

BH-2	Depth (m)	0-15 cm	15-30 cm	30-45 cm	N30	Soil Classification
SPT - 1	1.50-1.95	16	11	12	23	Fill
SPT - 2	3.00-3.45	7	10	8	18	Fill
SPT - 3	4.50-4.95	6	8	5	13	Fill
SPT - 4	6.00-6.45	8	8	5	13	Fill
SPT - 5	7.50-7.95	2	2	2	4	SM
SPT - 6	9.00-9.45	1	1	1	2	CH
SPT - 7	10.50-10.95	2	2	2	4	CH
SPT - 8	12.00-12.45	4	3	5	8	CH
SPT - 9	15.00-15.45	4	5	5	10	CH
SPT - 10	18.00-18.45	9	12	6	18	GP-GC
SPT - 11	19.50-19.95	5	5	5	10	CL
SPT - 12	21.00-21.45	8	25	30	R	GW-GC
SPT - 13	22.50-22.95	33	13	6	19	GP-GC
SPT - 14	24.00-24.45	20	17	12	29	CL
SPT - 15	25.50-25.95	18	11	6	17	CL
SPT - 16	27.00-27.45	9	9	6	15	CL
SPT - 17	28.50-28.95	9	8	10	18	CL
SPT - 18	30.00-30.45	10	12	7	19	GC

3.2.2 Laboratory Tests

In order to determine the soil index and mechanical properties; Sieve analysis, consistency limits, water content, shear box test, uniaxial compression test, triaxial test, consolidation test and unit weight determination test were performed. Tests results as follows:

Table 3.3 Classification of soil layers (BH-1)

BH-1	Atterberg Limits			Water Content (%)	Sieve Analysis		Soil Classification
	LL	PL	PI		+#10	-#200	
6.00 – 6.45m	-	-	-	39.1	42	16	SM
7.50 – 7.95m	-	-	-	35.2	28	31	SM
9.0 – 9.45m	55	25	30	34.8	0	86	CH
10.50-10.95m	62	28	34	40.4	0	95	CH
11.50-12.00 (UD)	66	31	35	36.5	0	97	CH
13.50-13.95m	70	30	40	45.9	7	77	CH
17.00-17.45m	44	22	22	26	6	83	CL
21.00-21.45m	-	-	-	9.3	65	8	GW-GC
23.00-24.00m (B.hole sample)	45	22	23	26.4	2	86	CL
27.00-27.45m	44	22	22	27.5	4	70	CL
29.00-30.00m (B.hole sample)	30	20	10	12.3	48	22	GC

Table 3.4 Basic characteristics properties of soil layers (BH-1)

BH-1	Plasticity Index	Liquidity Index	Activity	Relative Consistency	Swelling Potential	Compression Index	Void Ratio
	PI	LI	A	I_c	S	C_c	e_0
9.0 – 9.45m	30	0.327	0.35	0.673	12.44	0.4941	1.48525
10.50-10.95m	34	0.365	0.36	0.635	18.66	18.66	1.62275
11.50-12.00 (UD)	35	0.157	0.36	0.843	20.45	0.5931	173.275
13.50-13.95m	40	0.398	0.52	0.603	22.48	0.6291	182.275
17.00-17.45m	22	0.182	0.27	0.818	5.63	0.3951	123.775
21.00-21.45m	-	-	-	-	-	-	-
23.00-24.00m (B.hole sample)	23	0.191	0.27	0.809	6.51	0.4041	126.025
27.00-27.45m	22	0.250	0.31	0.750	4.75	0.3951	123.775
29.00-30.00m (B.hole sample)	10	0.770	0.45	1.770	0.22	0.2691	0.92275

Table 3.5 Classification of soil layers (BH-2)

BH-2	Atterberg Limits			Water Content (%)	Sieve Analysis		Soil Classification
	LL	PL	PI		+#10	-#200	
9.0 – 9.45m	65	29	36	40.8	0	95	CH
10.50-10.95m	66	30	36	40	0	95	CH
13.50-14.00 (UD)	70	30	40	48.6	4	83	CH
15.00 – 15.45m	46	23	23	30.6	1	94	CL
16.50-17.00m	44	22	22	29.1	1	96	CL
18.00-19.50m (B.hole sample)	42	22	20	20.6	5	77	CL
21.00-22.50m (B.hole sample)	32	19	13	17	14	35	SC
22.50-22.95m	-	-	-	8.8	66	11	GP-GC

Table 3.6 Basic characteristics properties of soil layers (BH-2)

BH-2	Plasticity Index	Liquidity Index	Activity	Relative Consistency	Swelling Potential	Compression Index	Void Ratio
	PI	**LI**	**A**	I_c	**S**	C_c	e_0
9.0 - 9.45m	36	0.328	0.38	0.672	21.45	0.5841	171.025
10.50-10.95m	36	0.278	0.38	0.722	21.45	0.5931	173.275
13.50-14.00 (UD)	40	0.465	0.48	0.535	24.23	0.6291	182.275
15.00 – 15.45m	23	0.330	0.24	0.670	7.11	0.4131	128.275
16.50-17.00m	22	0.323	0.23	0.677	6.52	0.3951	123.775
18.00-19.50m (B.hole sample)	20	0.070	0.26	1.070	4.14	0.3771	119.275
21.00-22.50m (B.hole sample)	13	0.154	0.37	1.154	0.66	0.2871	0.96775

Figure 3.5 SPT step for Park Inn Otel project

3.3 Soil Profile

3.3.1 Fill Layer

Andesite blocks was observed between 0m and 6.5m depth. This fill layer was created to fill the sea to gain more space for buildings.

3.3.2 Silty Sand Layer

Silty sand layer exists for 2m below the depth of 6.5m fill. This layer was observed gray in color. This layer has the silt and sand character.

Table 3.7 Soil characteristics of silty sand layer

Water Content	W_n	%35 - %39
Sieve Analysis	Gravel - Sand	%69 - %84
	Clay - Silt	%16 - %31
Atterberg Limits	Liquid Limit (LL)	NP
	Plastic Limit (PL)	NP
	Plasticity Index (PI)	NP
Standard penetration test	N_{30}	4
Soil Classification	**SM**	

3.3.3 Silty Clay Layer

Gray colored silty clay layer lies between 8.5m and 14.5m depth. Brown colored silty clay layer exist for 3,5m below the gray colored silty clay and also this layer observed between 19.5m-20.5m and 23.5m-28.5m.

Table 3.8 Soil characteristics of silty clay layers

Water Content	W_n	%20 - %48
Sieve Analysis	Gravel - Sand	%3 - %30
	Clay - Silt	%77 - %97
Atterberg Limits	Liquid Limit (LL)	42 - 70
	Plastic Limit (PL)	22 - 31
	Plasticity Index (PI)	22 - 40
Standart penetration test	N_{30}	2 - 30
Soil Classification	**CH-CL**	

3.3.4 Clayey Gravel Layer

Brown colored clayey gravel layer was observed after 18m depth.

Table 3.9 Soil characteristics of clayey gravel layer

Water Content	W_n	%8 - %12
Sieve Analysis	Gravel - Sand	%78 - %92
	Clay - Silt	%8 - %22
Atterberg Limits	Liquid Limit (LL)	30
	Plastic Limit (PL)	20
	Plasticity Index (PI)	10
Standart penetration test	N_{30}	17-R
Soil Classification	**GP – GW - GC**	

3.3.5 Clayey Sand Layer

Brown colored clayey sand layer lies between 20,5m and 21,5m depth. This layer has the clay and sand character predominantly.

Table 3.10 Soil characteristics of clayey sand layer

Water Content	W_n	17%
Sieve Analysis	Gravel - Sand	65%
	Clay - Silt	35%
Atterberg Limits	Liquid Limit (LL)	32
	Plastic Limit (PL)	19
	Plasticity Index (PI)	13
Standart penetration test	N_{30}	-
Soil Classification	**SC**	

3.3.6 Idealized Soil Profile

The visual assessments and boring surveys (BH-1, BH-2) carried out at the construction site and the soil mechanics laboratory test results indicated that the soil strata compose of clays and gravels with different shear characteristics and rare silty sand layers. According to the liquefaction analysis, there is no layer with liquefaction potential. Considering all those engineering researches, the estimated idealized soil profile of this site was given in Figure 3.6

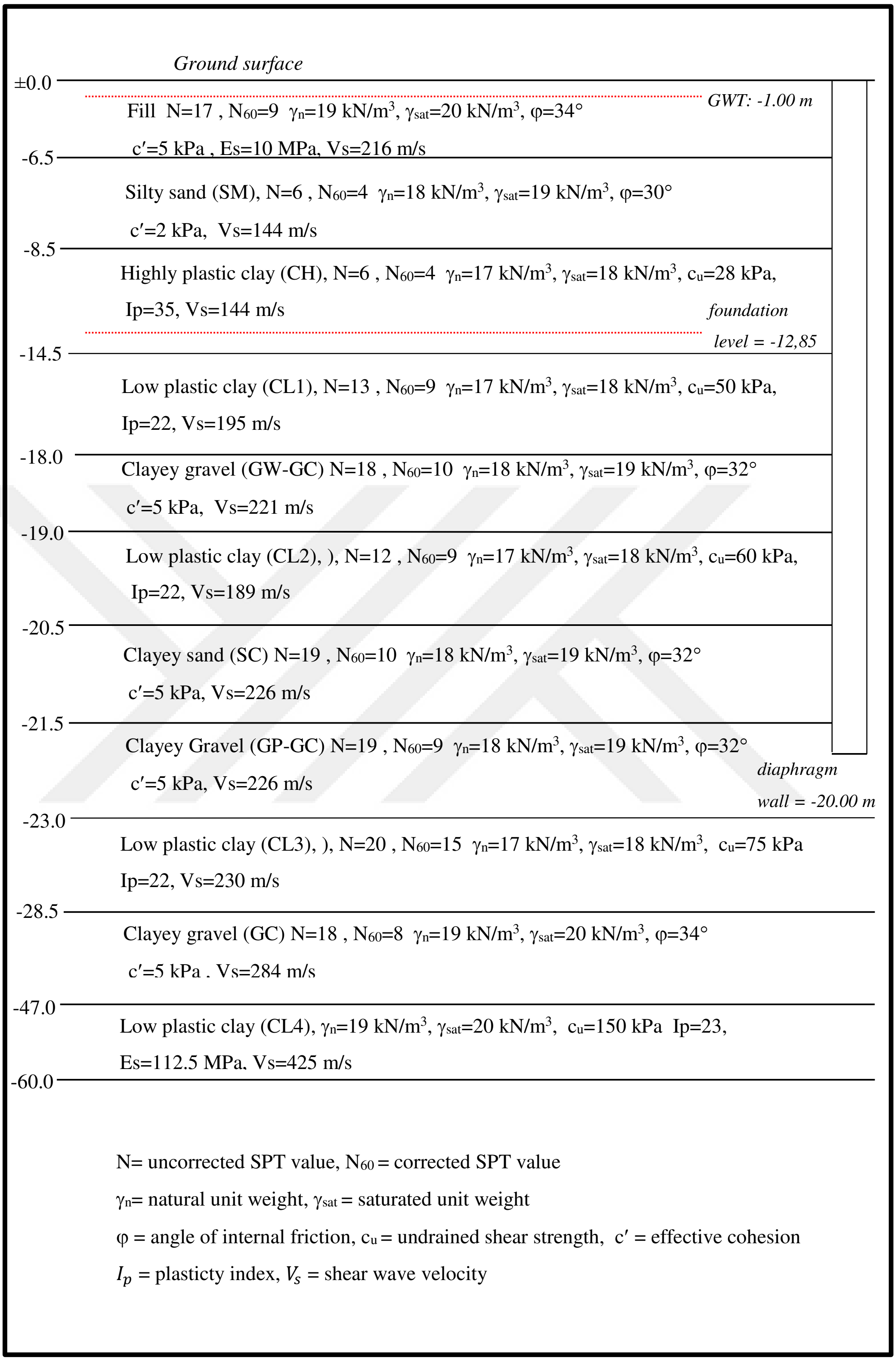

Figure 3.6 Idealized soil profile

3.4 3D Analysis of Excavation

In this study numerical analyses were performed with PLAXIS 3D software. PLAXIS 3D is a three dimensional finite element program. Some of the general features of PLAXIS 3D is as follows;

- Staged construction mode
- Multiple borehole wizard
- Inverse analysis for soil test parameter
- DXF, DWG, 3DS import of geometries
- Advanced Material Models and User defined soil models
- Plastic calculation, consolidation analysis and safety analysis
- Parallels Meshing
- Connections (Hinges, dilation joints)

Following the excavation analysis, depth of excavation and adjacent buildings are considered in excavation simulation. Model dimensions are 200x200x60 m. Meshing operations were performed by PLAXIS 3D. Model compose of 117921 elements with 160552 nodes. General view of model is shown in Figure 3.7

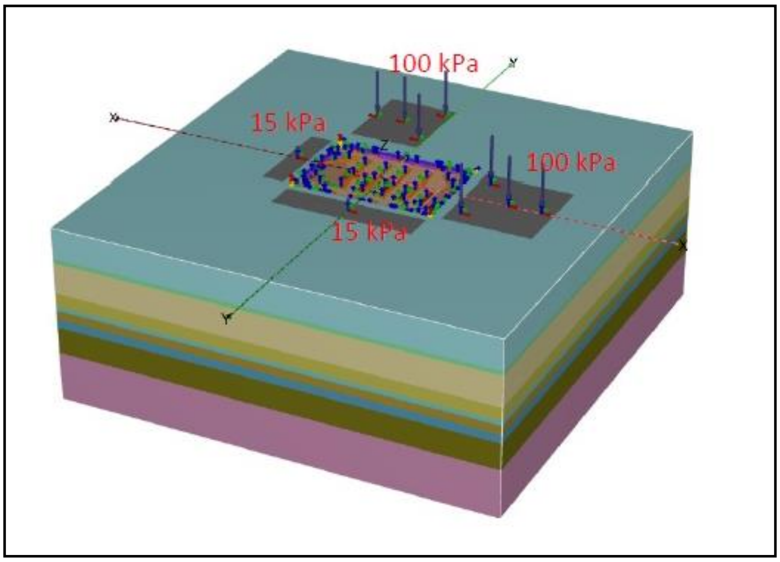

Figure 3.7 Three dimensional model

The shape of the excavation was average about 34m in length 24m in width. The excavation was completed in four stages with the maximum excavation depth of 11.5m. A diaphragm wall, which was 0,6m thick and 20m deep was used as the retaining structure. The diaphragm wall system was braced with steel struts at three levels and the horizontal spacing of the struts was average about 5m. Each level of internal bracing properties is shown in Figures 3.8, 3.9, 3.10, 3.11

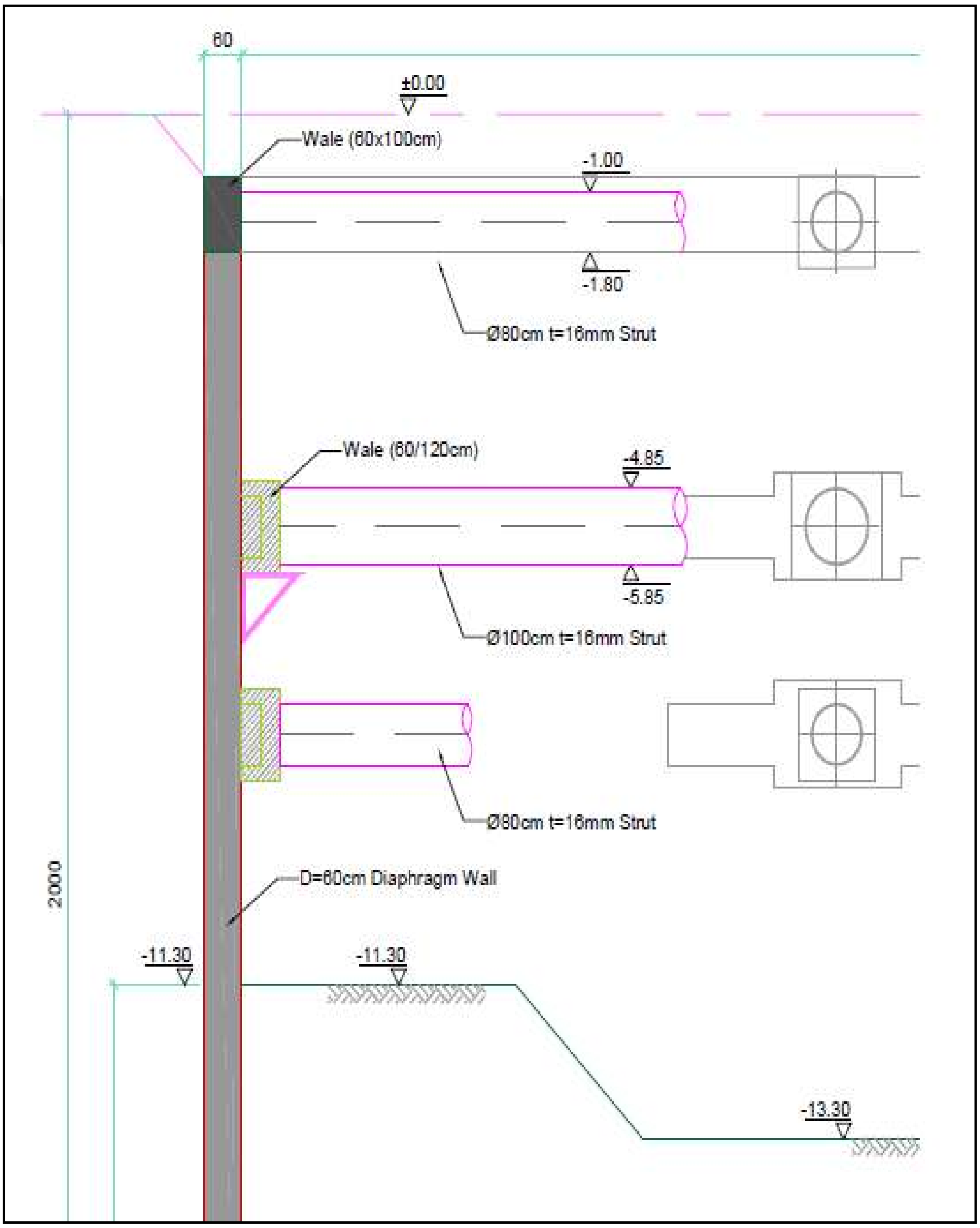

Figure 3.8 Section of the excavation and retaining structure

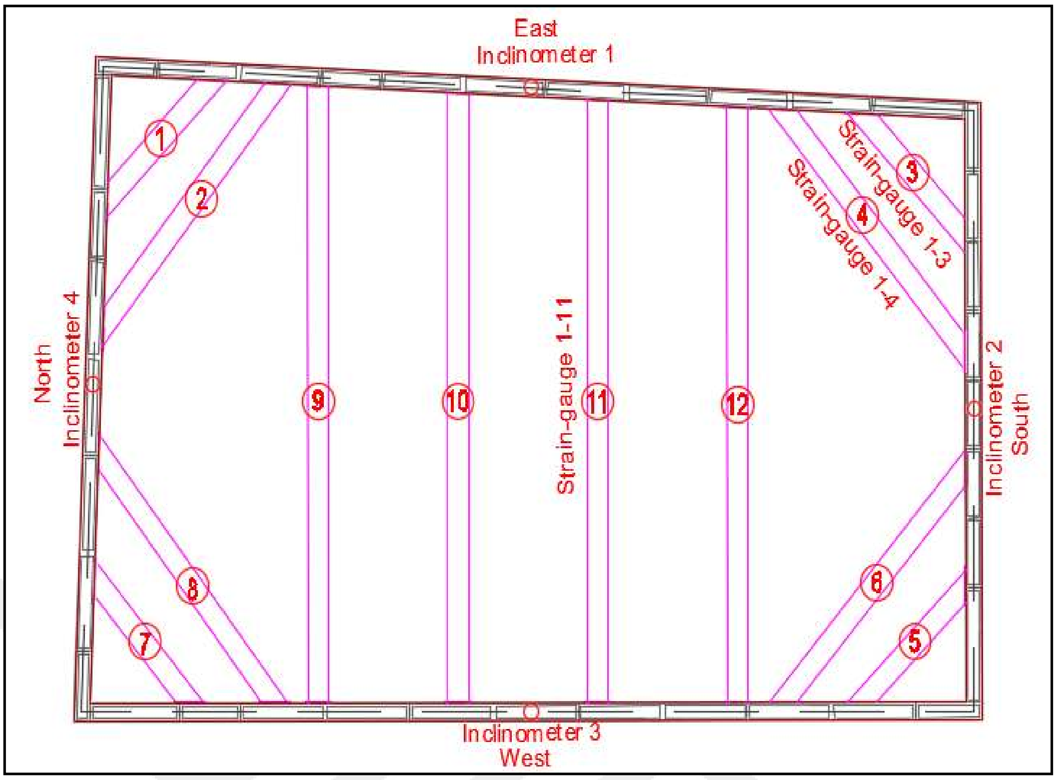

Figure 3.9 The first level strut plan (-1.40m)

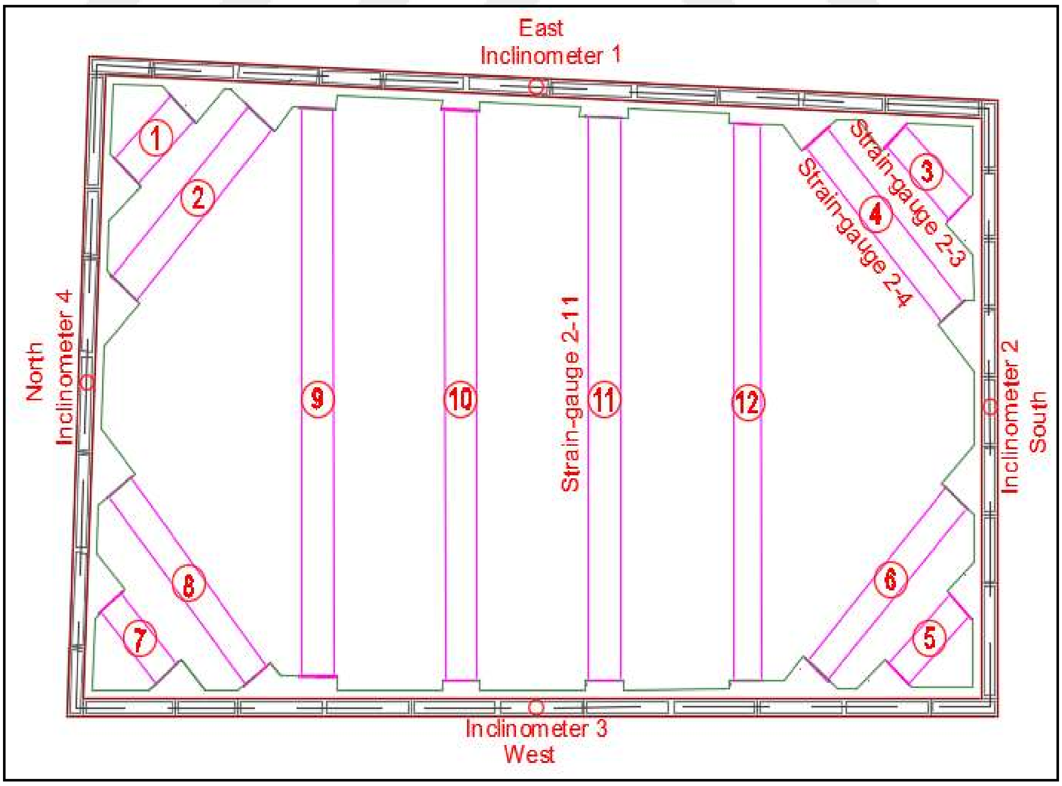

Figure 3.10 The second level strut plan (-5.35m)

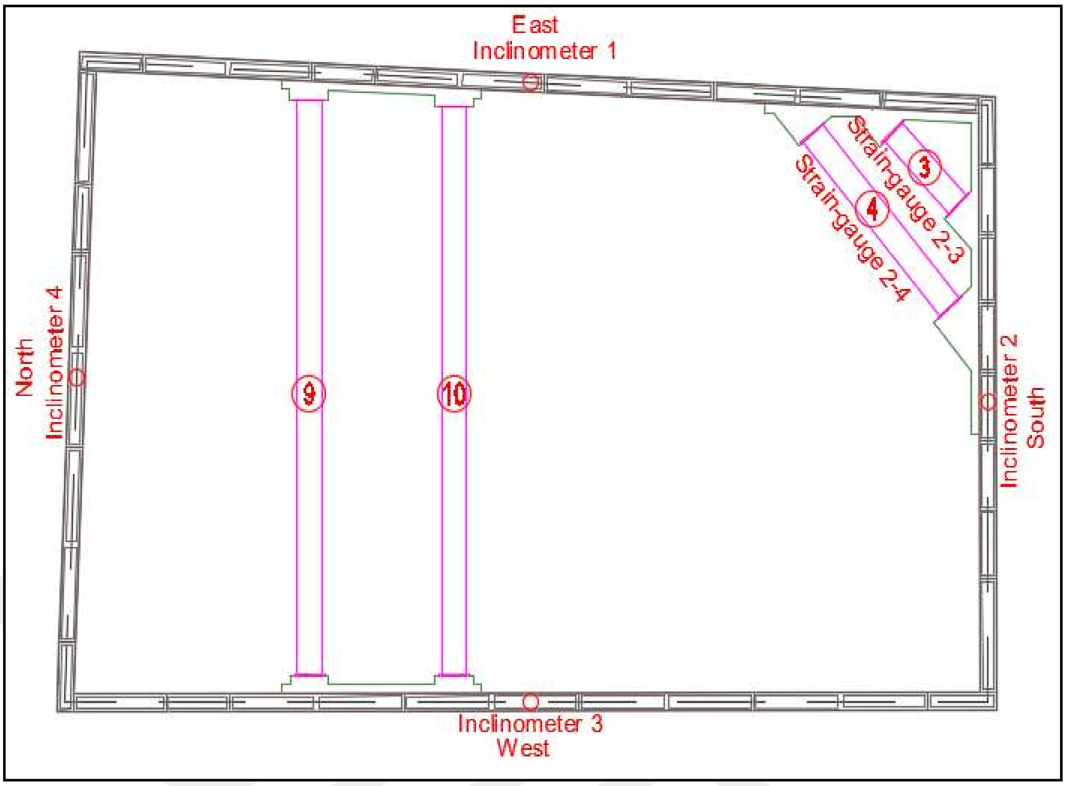

Figure 3.11 The third level strut plan (-8.05m)

The ground water level inside the pit was lowered to depth of 1.0m below each excavation level before each stage of excavation to make a convinient space for construction process of excavation. The wall is to behave as a cantilever at the first stage of excavation because the steel struts at the first level have not installed and preloaded. The wall then displays the deep inward movements at subsequent stages of excavation.

In order to represent soil properties of the problem, Hardening Soil Small Strain model (HSsmall) was used. Different soil layers were defined with borehole in PLAXIS 3D.

The undrained analysis is performed by effective stres approach for the fine grained soil layers. The drained analysis is performed for the coarse grained soil layers. It is generally true that drained condition governs the safety of deep excavation but it is very important to check the undrained behaviour in very soft clay. (Magus et al. 2005) (Undrained A or undrained B) Undrained B option was selected in this study.

Table 3.11 Features of Undrained A and Undrained B analysis

Undrained A	**Undrained B**
Effective stres analysis	Effective stres analysis
Effective strength parameters: ϕ', c', ψ'	Total strength parameters: $\phi_u = 0,\ c = C_u, \psi = 0$
Effective stiffness parameters: E'_{50}, ν'	Effective stiffness parameters: E'_{50}, ν'

3.4.1 Input Parameters for Soil

As mentioned Section 2.9 the soil parameters used in models shown in Table 3.12

Table 3.12 Input soil parameters for different soil models

Input parameters				
Mohr-Coulomb Model	Hardening Soil Model	Hardening soil model with small strain stiffness		
x	x	x	ϕ'	Internal friction angle
x	x	x	c'	Cohesion
x			E'	Young’s modulus for elasticity
x			ν'	Poisson’ ratio for elasticity
x	x	x	ψ	Dilatancy angle
x	x	x	K_0	Coefficient of earth pressure at rest
	x	x	R_f	Failure ratio
	x	x	E_{50}^{ref}	Ref. secant stiffness
	x	x	E_{oed}^{ref}	Ref. tangent stiffness
	x	x	E_{ur}^{ref}	Ref. unloading/reloading stiffness
	x	x	m	Power for stres-level dependency of stiffness
	x	x	ν_{ur}	Unloading/reloading Poisson's ratio
		x	G_0^{ref}	Reference small strain shear modulus
		x	$\gamma_{0.7}$	Shear strain magnitude at at 0.722Gmax

Strength parameters are the same in these three model but stiffness parameters are different. In Mohr-Coulomb model stiffness parameters are constant, where as in Hardening Soil model stiffness parameters are stres dependent.

Strength parameters can be obtained easily from laboratory tests and correlations but stiffness parameters depend on physical properties. It is difficult to get undisturbed samples for sandy soils and some test apparatus are elaborate and costly. (i.e. triaxial test apparatus)

As a result, stiffness parameters are often obtained from the empirical equations or back analyses. The Mohr-Coulomb model represents Young's modulus of soil in the situ stress state. The Hardening Soil Small Strain model represents its three moduli at the reference pressure (Plaxis Material Models Manual, 2016).

$$\boldsymbol{E_{50} = E_{50}^{ref}\left(\frac{c\cos\phi - \sigma_3' \sin\phi}{c\cos\phi + p^{ref}\sin\phi}\right)^{m}} \tag{3.1}$$

E_{50}^{ref} = a reference minor principal stress of $-\sigma_3' = p^{ref}$
$p^{ref} = 100$ stress units
$m =$ Power for stress-level dependency of stiffness

E_{ur}^{ref}, $E_{oed}^{ref} = 3E_{50}^{ref}$, E_{50}^{ref} as suggested Schanz and Vermeer (1998) and Schweiger (2009).

But it must be noted that, when using Undrained (B) in the Hardening Soil model or the Hardening Soil Small Strain model, the stiffness moduli in the model are no longer stres-dependent. The model exhibits no compression hardening, although the model retains its seperate unloading-reloading modulus and shear hardening. Consolidation analysis should not be performed after the undrained calculation.

The parameter of m was taken as 0.5 for sands and 1 for the clay layers. Dilatancy angle can be assumed as $\psi' = 0^\circ$ with $\phi' \leq 30^\circ$ and $\psi' = \phi' - 30^\circ$ with $\phi' \geq 30^\circ$.

Interface value, $R_{interface}$, was assumed 0,8 for the interaction of sand/concrete and 0,7 for the interaction of clay/concrete as suggested Brikgreeve and Shen (2011).

$\mathrm{R_f}$, ν_{ur}, $K_0 = (1 - \sin\phi)$ (Jaky, 1944) are default settings for the Plaxis.

The initial or very small-strain shear modulus G_0, can be obtained by the following equation:

$$G_0 = \rho V_s^2 = \frac{\gamma}{g} V_s^2 \text{ (kPa)} \tag{3.2}$$

$\rho =$ density of soil
γ = unit weight of soil (kN/m^3)
g = gravitational acceleration (m/s^2)
V_s = shear wave velocity soil (m/s)

The reference shear modulus at very small strain level then obtained as follows:

$$G_0 = G_0^{ref} \left(\frac{\sigma_3'}{p^{ref}}\right)^m \tag{3.3}$$

The shear strain level $\gamma_{0.7}$ at which the secant shear modulus G_s = 0.722 G_0 can be obtained from Plaxis Material Models Manual, 2016.

As a result, used parameters of Hardening Soil Small Strain model are shown in Table 3.13.

Table 3.13 HSsmall model parameters for idealized soil profile

	γ kN/m3	γ_{sat} kN/m3	$\phi^{'}$	$c^{'}$ (kN/m2)	ϕ_u	C_u (kN/m2)	ψ	R_{int}	E_{50}^{ref} (kN/m2)	E_{oed}^{ref} (kN/m2)	E_{ur}^{ref} (kN/m2)	m	G_0^{ref} (kN/m2)	$\gamma_{0.7}$
F	19	20	34	5	-	-	4	0.8	13	13	39	0.5	1.58E+05	1.00E-04
SM	18	19	30	2	-	-	0	0.8	5.5	5.5	16.5	0.5	4.38E+04	1.00E-04
CH	17	18	-	-	0	28	-	0.7	14	14	42	1	3.59E+04	4.00E-04
CL1	17	18	-	-	0	50	-	0.7	25	25	75	1	6.58E+04	2.00E-04
GW-GC	18	19	32	5	-	-	2	0.8	14	14	42	0.5	6.95E+04	1.00E-04
CL-2	17	18	-	-	0	60	-	0.7	30	30	90	1	6.18E+04	2.00E-04
SC	18	19	32	5	-	-	2	0.8	14	14	42	0.5	6.83E+04	1.00E-04
GP-GC	18	19	32	5	-	-	2	0.8	13	13	39	0.5	6.63E+04	1.00E-04
CL3	17	18	-	-	0	75	-	0.7	37.5	37.5	112.5	1	9.22E+04	2.00E-04
GC	19	20	34	5	-	-	4	0.8	28	28	84	0.5	8.38E+04	1.00E-04
CL4	19	20	-	-	0	150	-	0.7	112.5	112.5	337.5	1	3.50E+05	2.10E-04

3.4.2 Input Parameters for Structure Elements

Plate elements were used to simulate the diaphragm wall and also beam elements were used to simulate the wallings and struts. Required parameters for plate elements and beam elements as follows in Table 3.14, 3.15, 3.16, 3.17.

Table 3.14 Input parameters for diaphragm wall

Diaphragm Wall – Plate Element		
Thickness	d	0.6 m
Unit weight	γ	7 $\mathrm{kN/m^3}$
Young's Modulus	E_1	3.0E+07 $\mathrm{kN/m^2}$
Poisson's ratio	ν_{12}	0,2
In-plane Shear Modulus	G_{12}	12.5E+06 $\mathrm{kN/m^2}$

Table 3.15 Input parameters for strut (80cm diameter)

Strut 1 – 80cm diameter 16mm thickness – Beam Element		
Cross section area	A	0.03938 $\mathrm{m^2}$
Unit weight	γ	78.5 $\mathrm{kN/m^3}$
Young's Modulus	E	2.1E+08 $\mathrm{kN/m^2}$
Moment of inertia against bending around the third axis	I_3	3.03E-03 $\mathrm{m^4}$
Moment of inertia against bending around the second axis	I_2	3.03E-03 $\mathrm{m^4}$

Table 3.16 Input parameters for strut (100cm diameter)

Strut 1 – 100cm diameter 16mm thickness – Beam Element		
Cross section area	A	0.04944 $\mathrm{m^2}$
Unit weight	γ	78.5 $\mathrm{kN/m^3}$
Young's Modulus	E	2.1E+08 $\mathrm{kN/m^2}$
Moment of inertia against bending around the third axis	I_3	5.98E-03 $\mathrm{m^4}$
Moment of inertia against bending around the second axis	I_2	5.98E-03 $\mathrm{m^4}$

Table 3.17 Input parameters for wallings

Wallings – Beam Element		
Cross section area	A	0.24 m^2
Unit weight	γ	25 $\mathrm{kN/m}^3$
Young's Modulus	E	3.0E+07 $\mathrm{kN/m}^2$
Moment of inertia against bending around the third axis	I_3	12.8E-03 m^4
Moment of inertia against bending around the second axis	I_2	1.8E-03 m^4

Unit weight of plate was substracted from the value of soil unit weight because the wall was modelled as non-volume elements (Plaxis References Manual, 2016).

3.5 Calculation Steps

Calculation phases and construction stages used in PLAXIS are as follows:

Phase 1 : Initial Phase
Phase 2 : Surface Loads (adjacent building loads)
Phase 3 : Consolidation
Phase 4 : Structure (diaphragm wall construction)
Phase 5 : Excavation 1 (excavation to -1.80m)
Phase 6 : Strut 1 (strut installation to -1.40m)
Phase 7 : Excavation 2 (excavation to -5.85m)
Phase 8 : Strut 2 (strut installation to -5.35m)
Phase 9 : Excavation 3 (excavation to -8.45m)
Phase 10 : Strut 3 (strut installation to -7.95m)
Phase 11 : Excavation 4 (excavation to -11.50 m and excavation for elevator pits to -13.50 m)

In the third phase of the calculation the settlements due to adjacent buildings loads were discarded using the reset displacements to zero option.

3.6 Finite Element Analysis Results

According to used soil and structure parameters analysis results as follows;

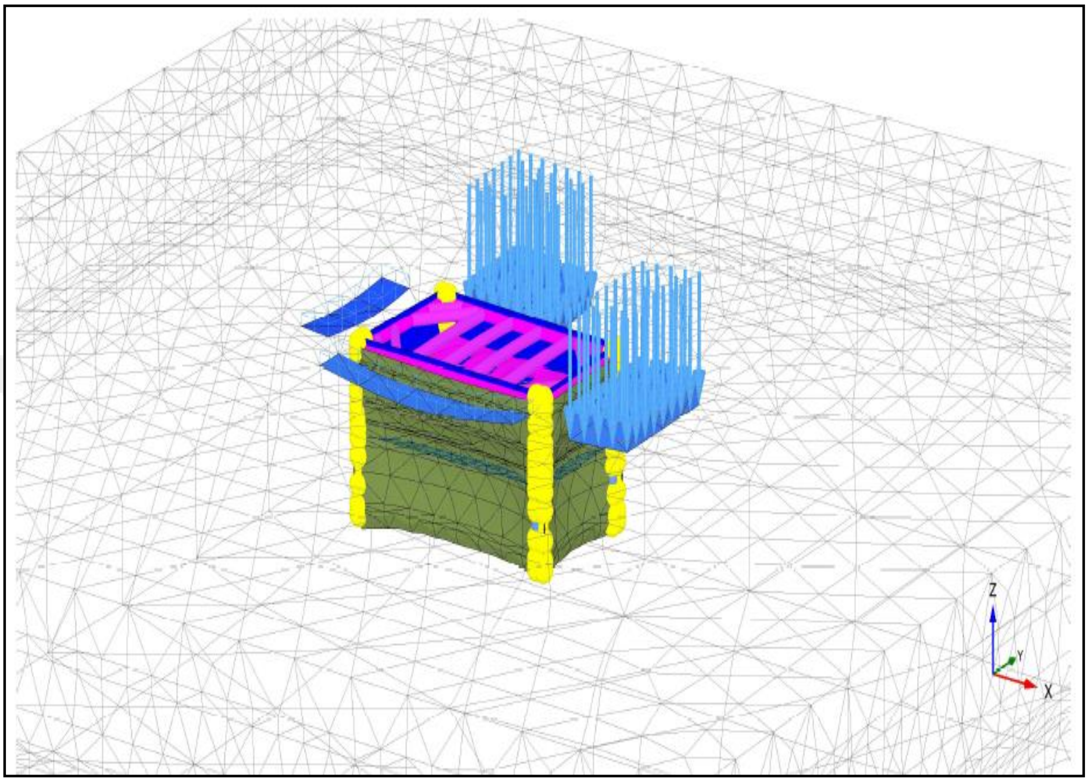

Figure 3.12 Deformed finite element model

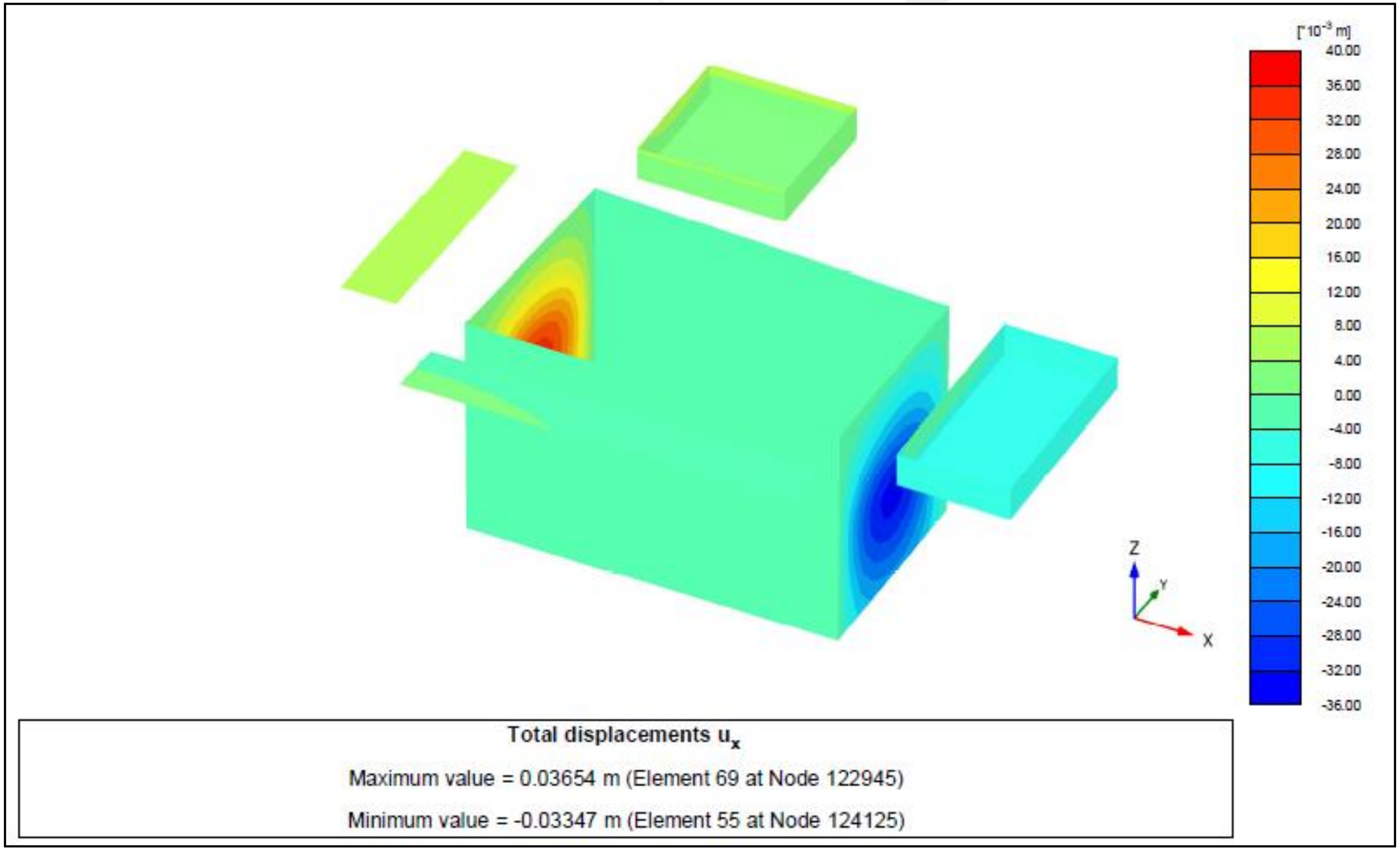

Figure 3.13 Displacement contours in x direction for diaphragm wall

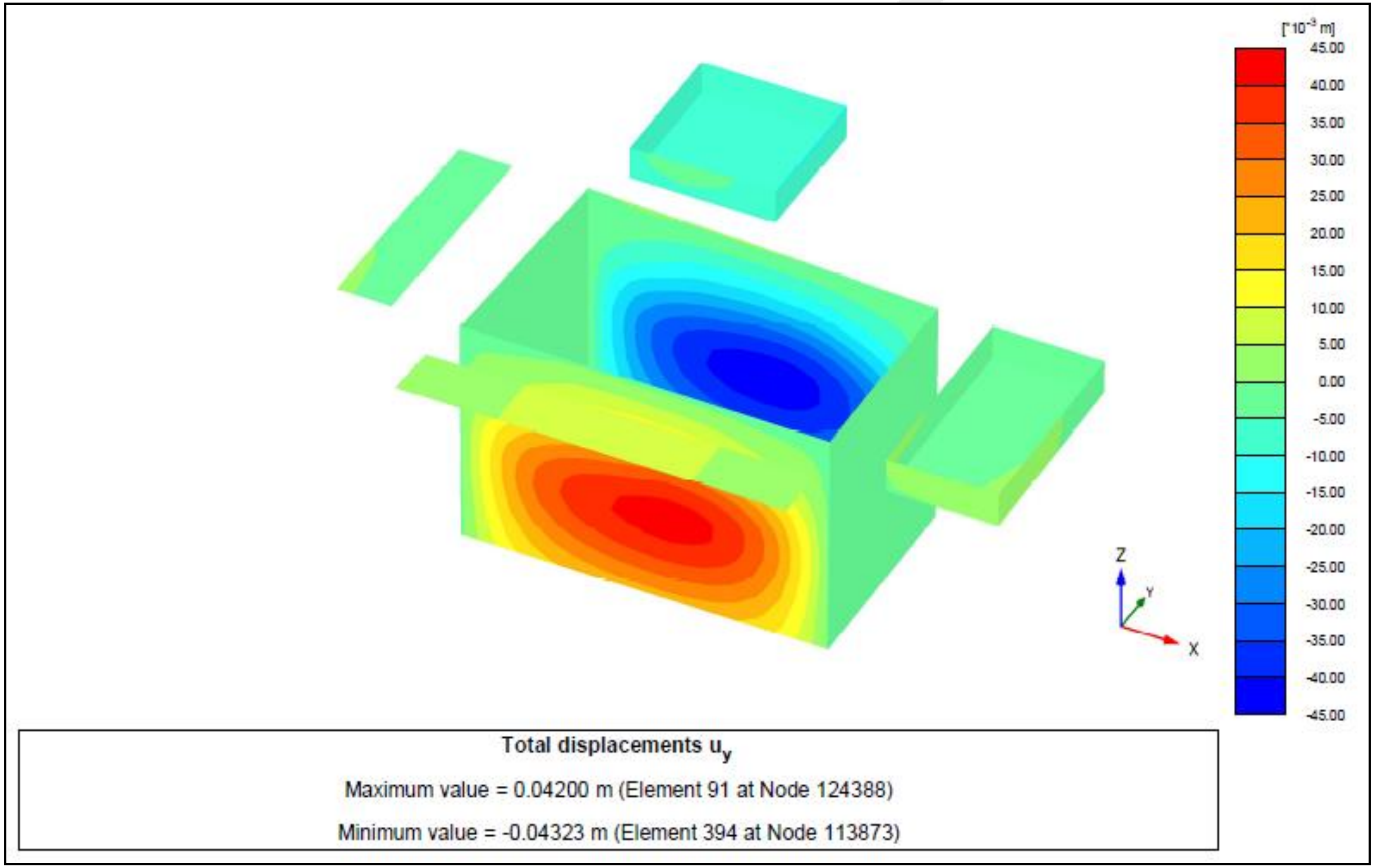

Figure 3.14 Displacement contours in y direction for diaphragm wall

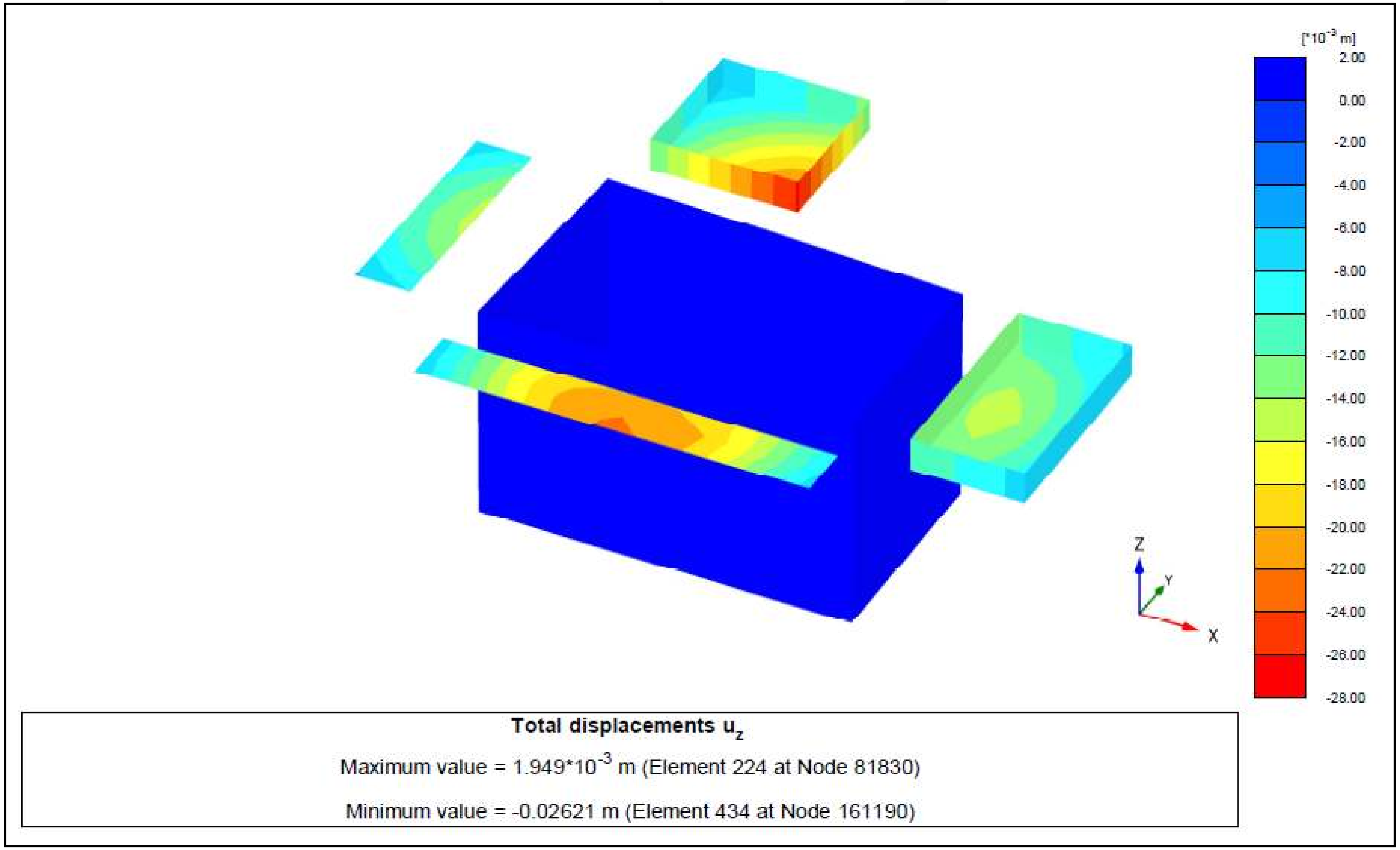

Figure 3.15 Displacement contours in z direction for constructions

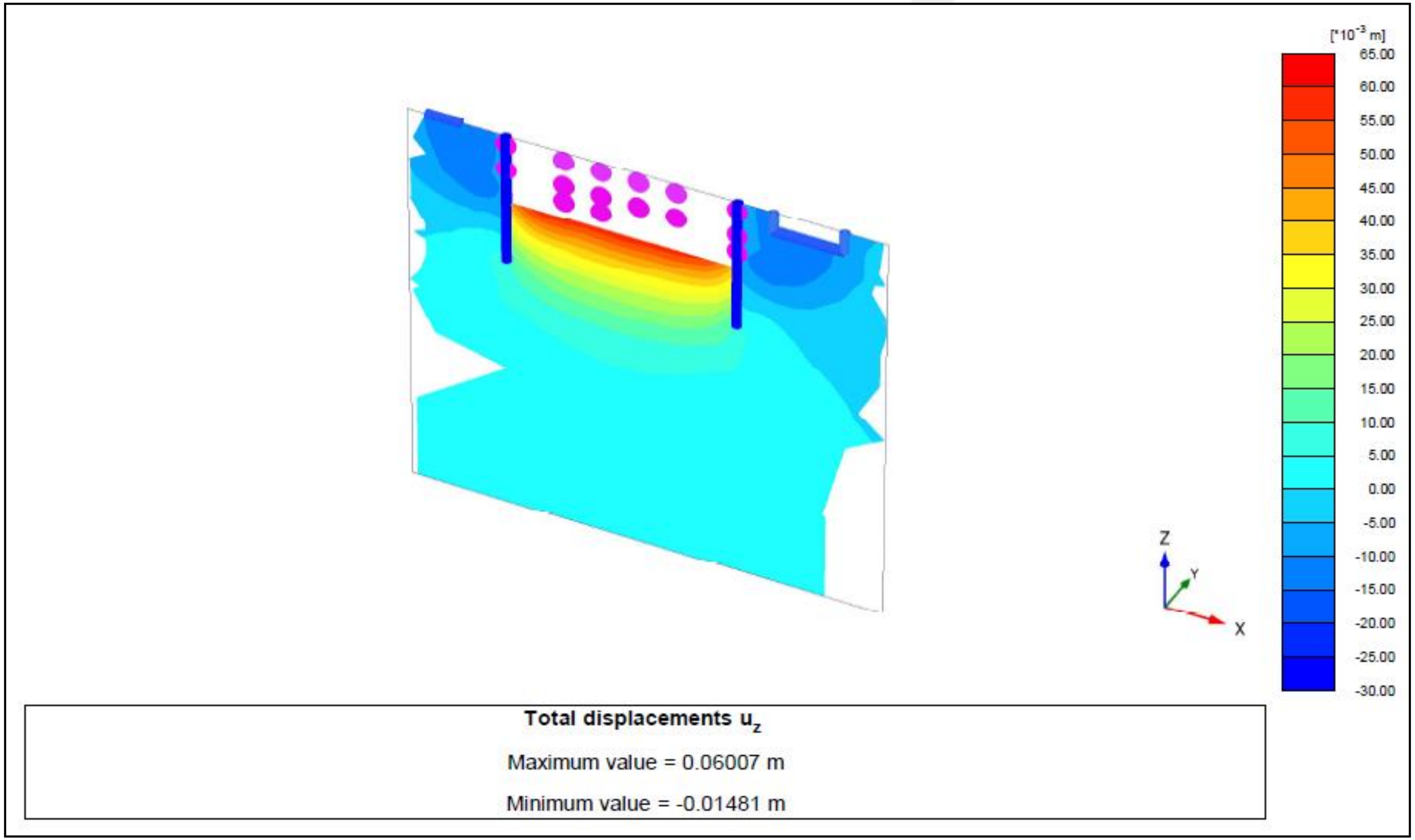

Figure 3.16 Displacement contours in z direction for x-x cross section

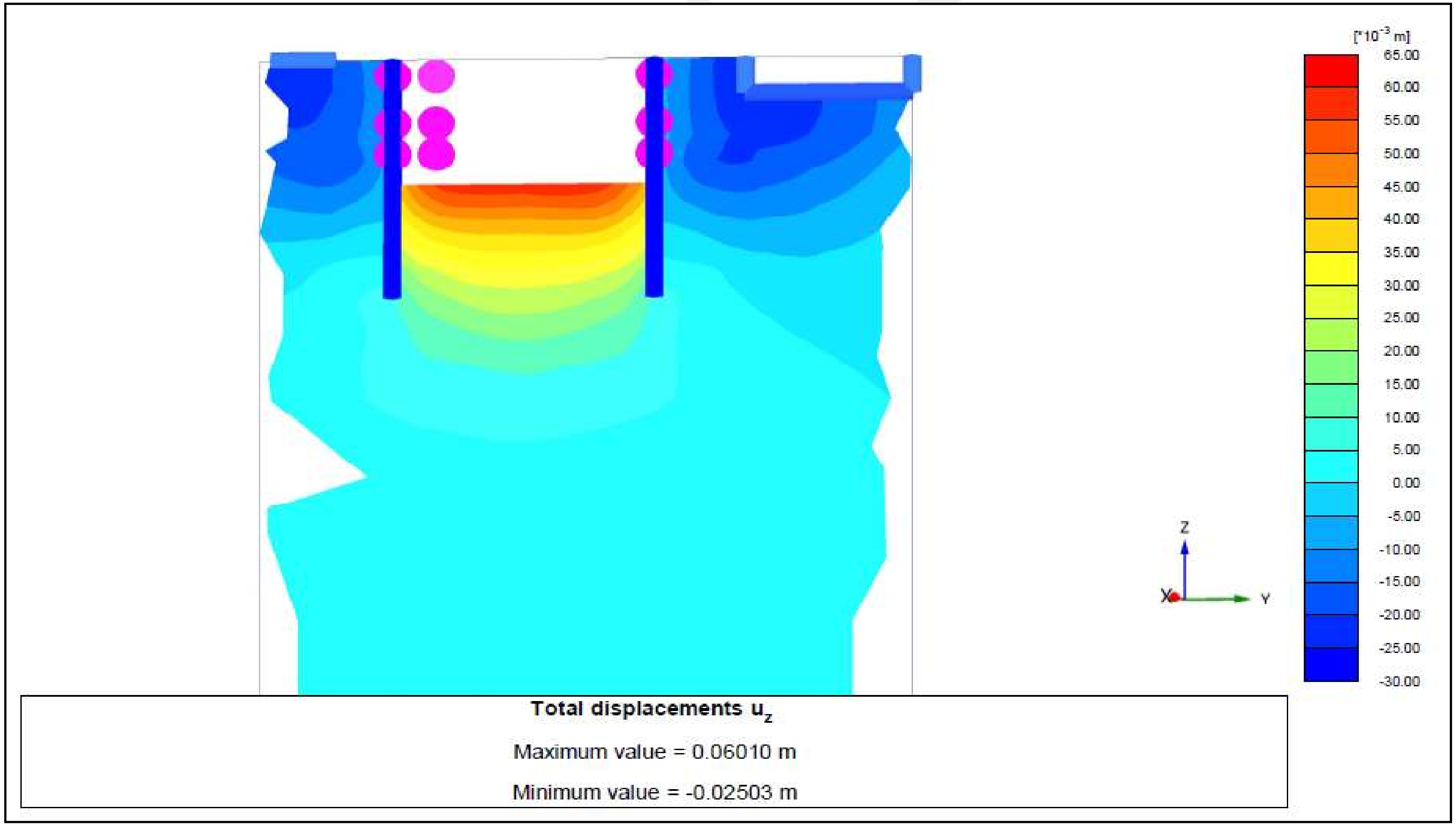

Figure 3.17 Displacement contours in z direction for y-y cross section

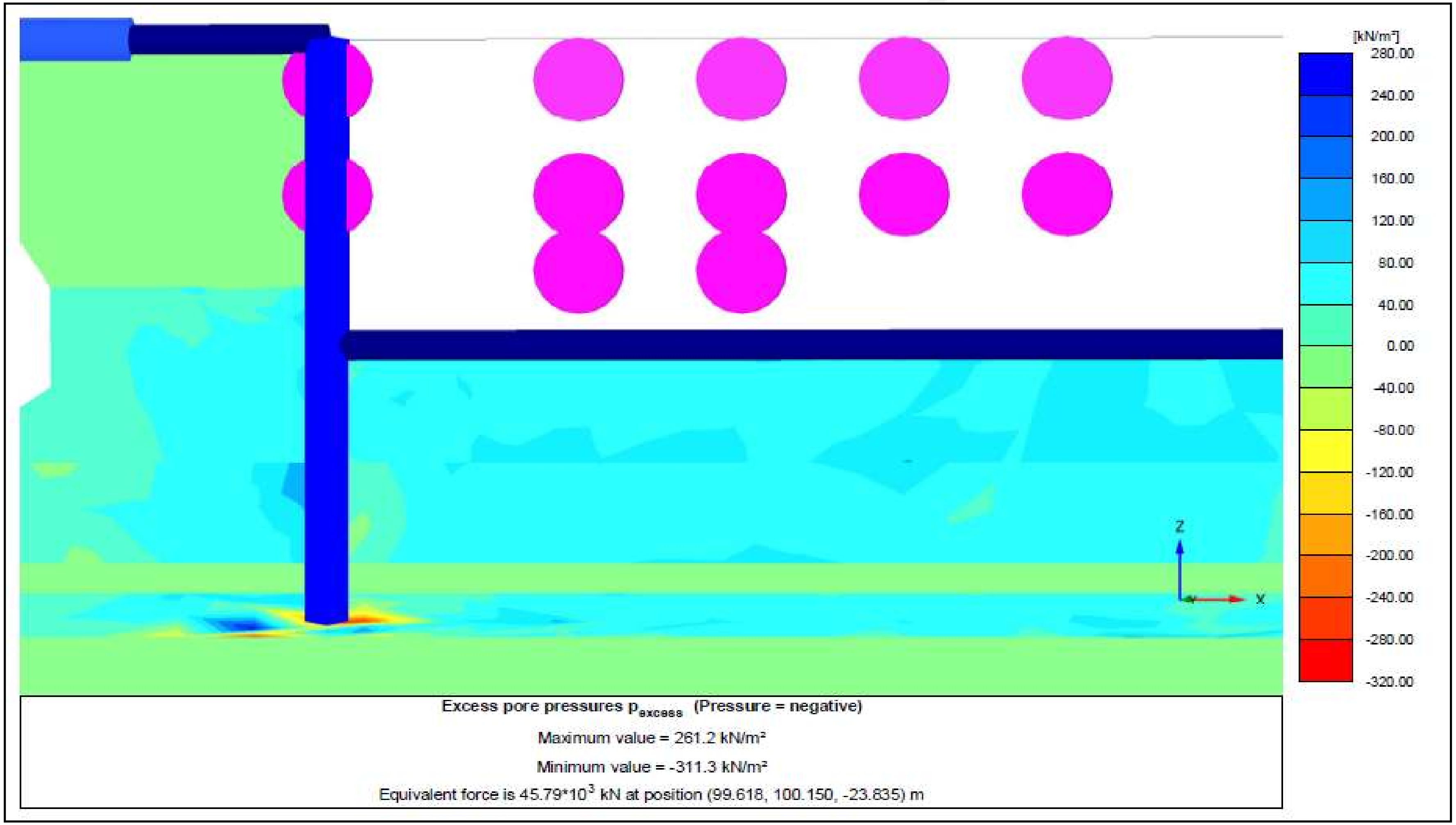

Figure 3.18 Excess pore pressure contours

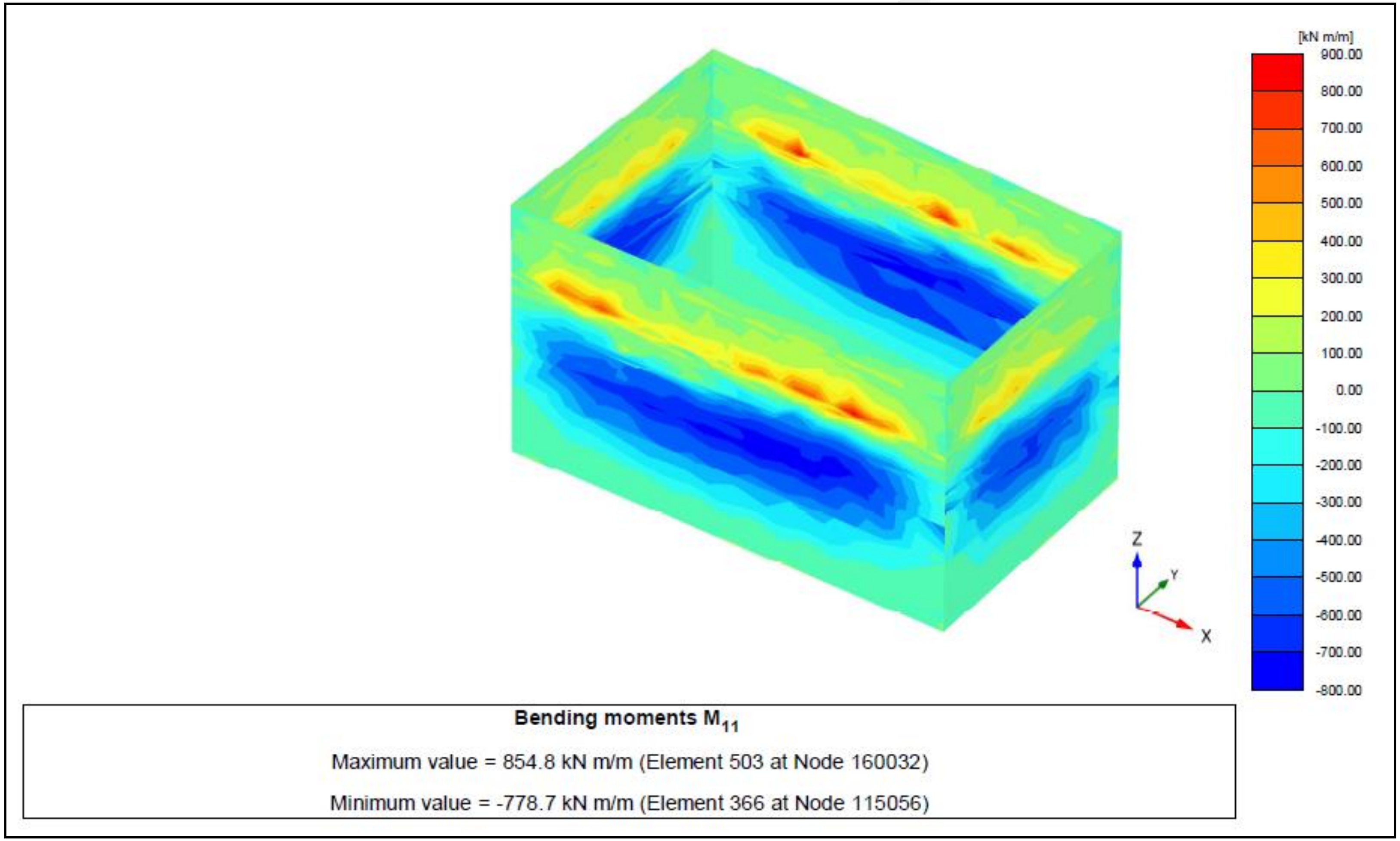

Figure 3.19 Bending moments contours for diaphragm wall (M_{11})

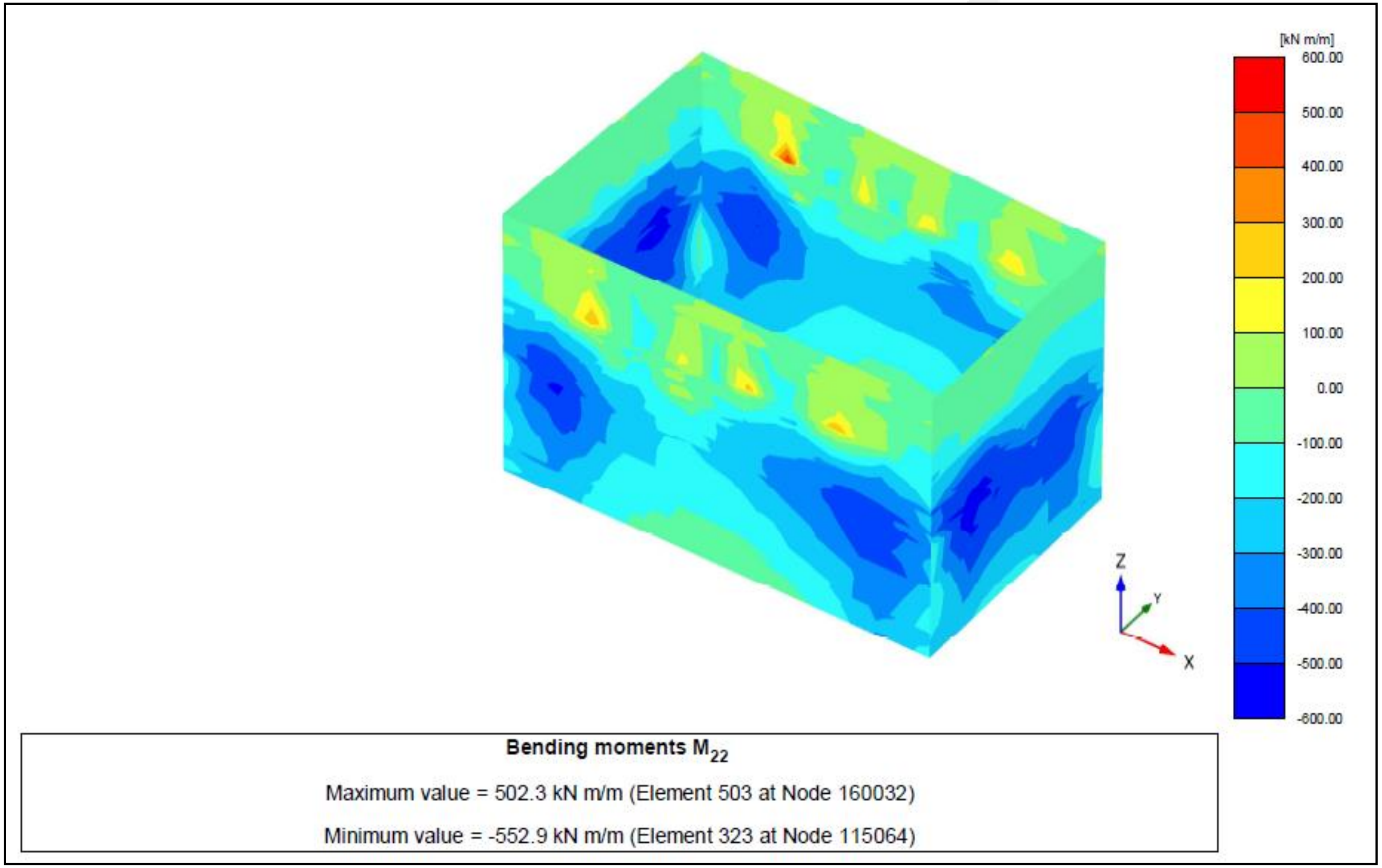

Figure 3.20 Bending moments contours for diaphragm wall (M_{22})

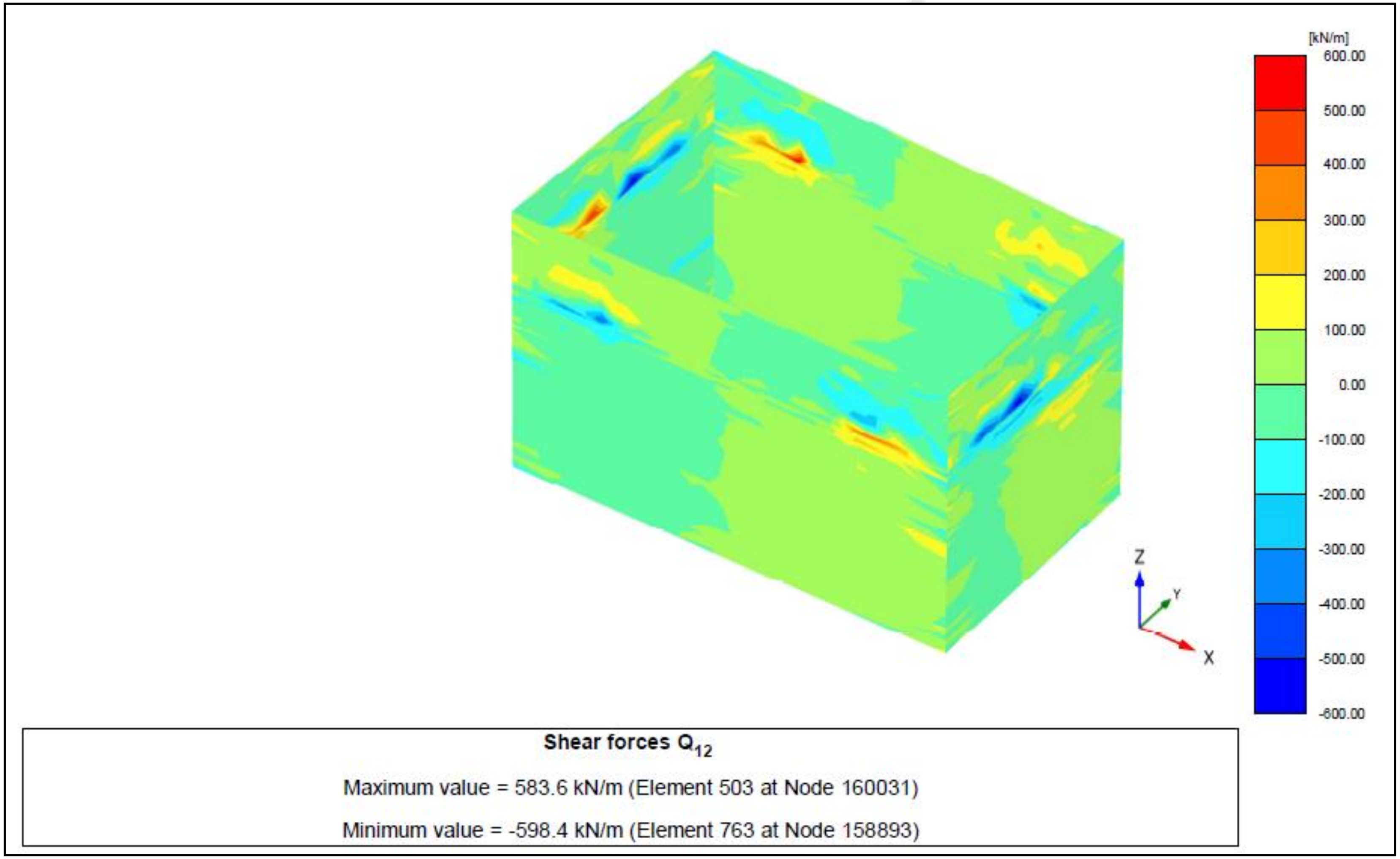

Figure 3.21 Shear forces contours for diaphragm wall (Q_{12})

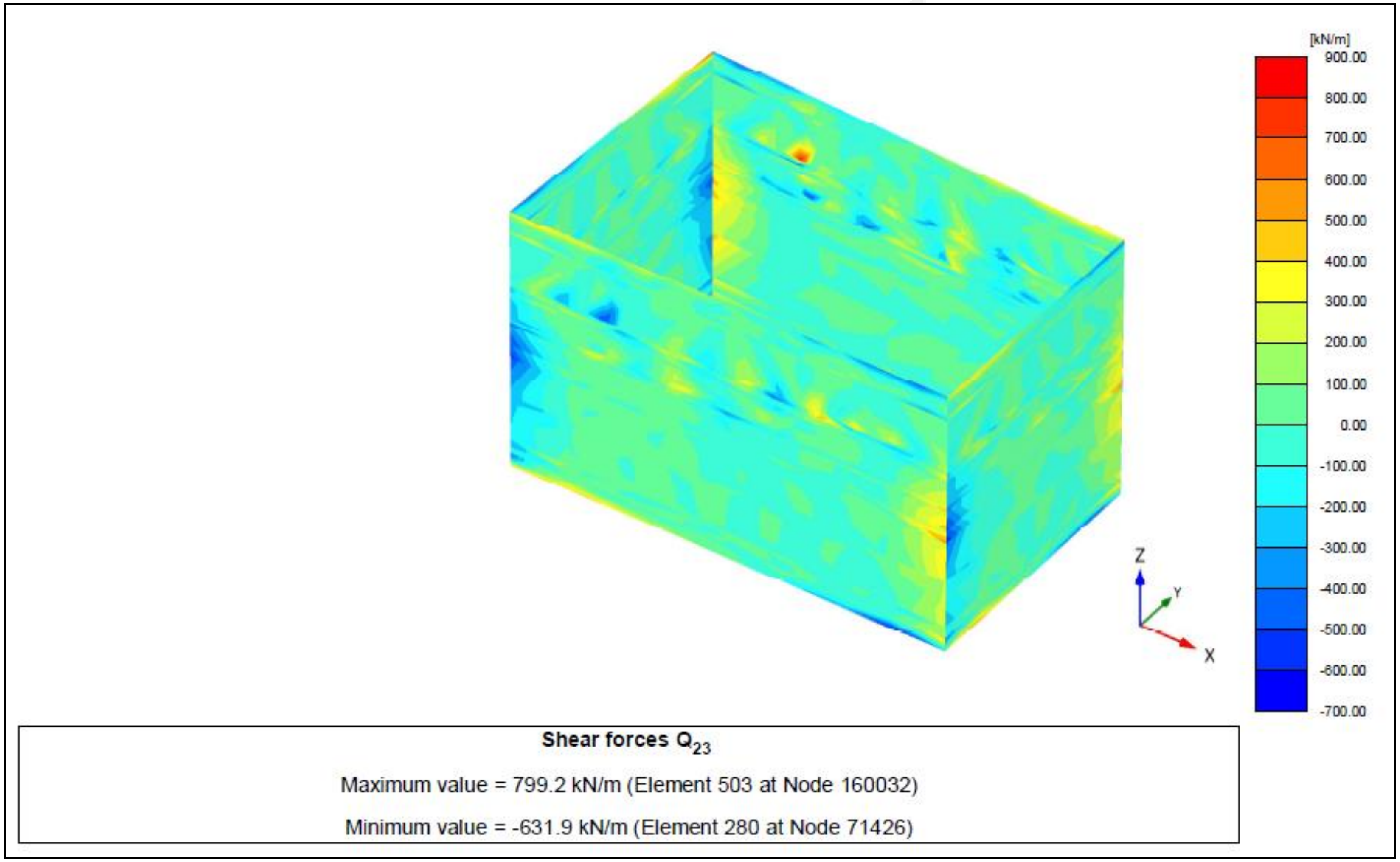

Figure 3.22 Shear forces contours for diaphragm wall (Q_{23})

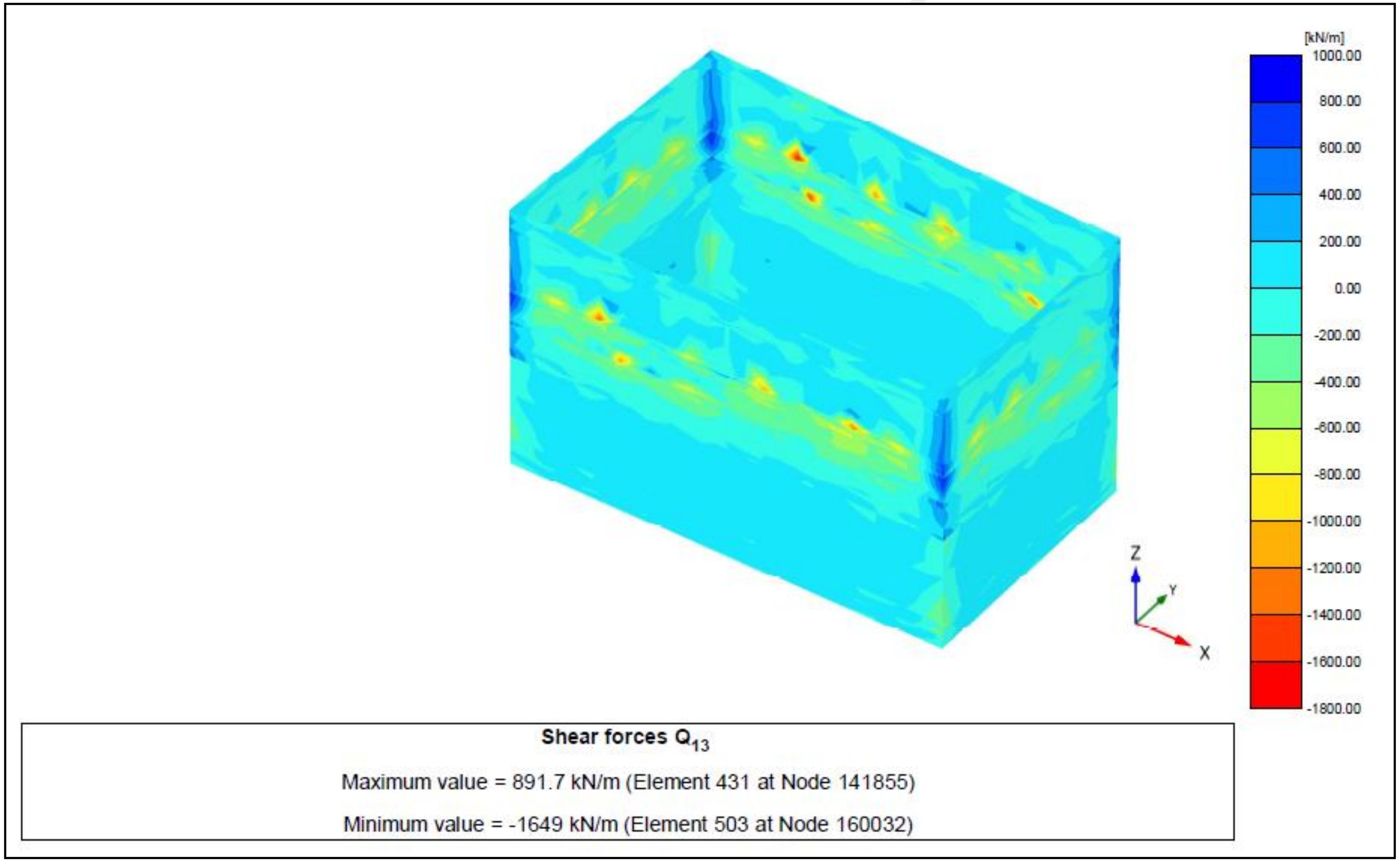

Figure 3.23 Shear forces contours for diaphragm wall (Q_{13})

Table 3.18 Axial forces in instrumented struts

	1S3	1S4	1S11	2S3	2S4	2S11	3S3	3S4
1. Excavation	-	-	-	-	-	-	-	-
2. Excavation	825.9 kN	847.5 kN	1080 kN	-	-	-	-	-
3. Excavation	569.3 kN	657.1 kN	779.1 kN	1833 kN	1891 kN	2215 kN	-	-
4. Excavation	497.9 kN	443.8 kN	573.4 kN	1596 kN	1737 kN	3267 kN	1830 kN	2356 kN

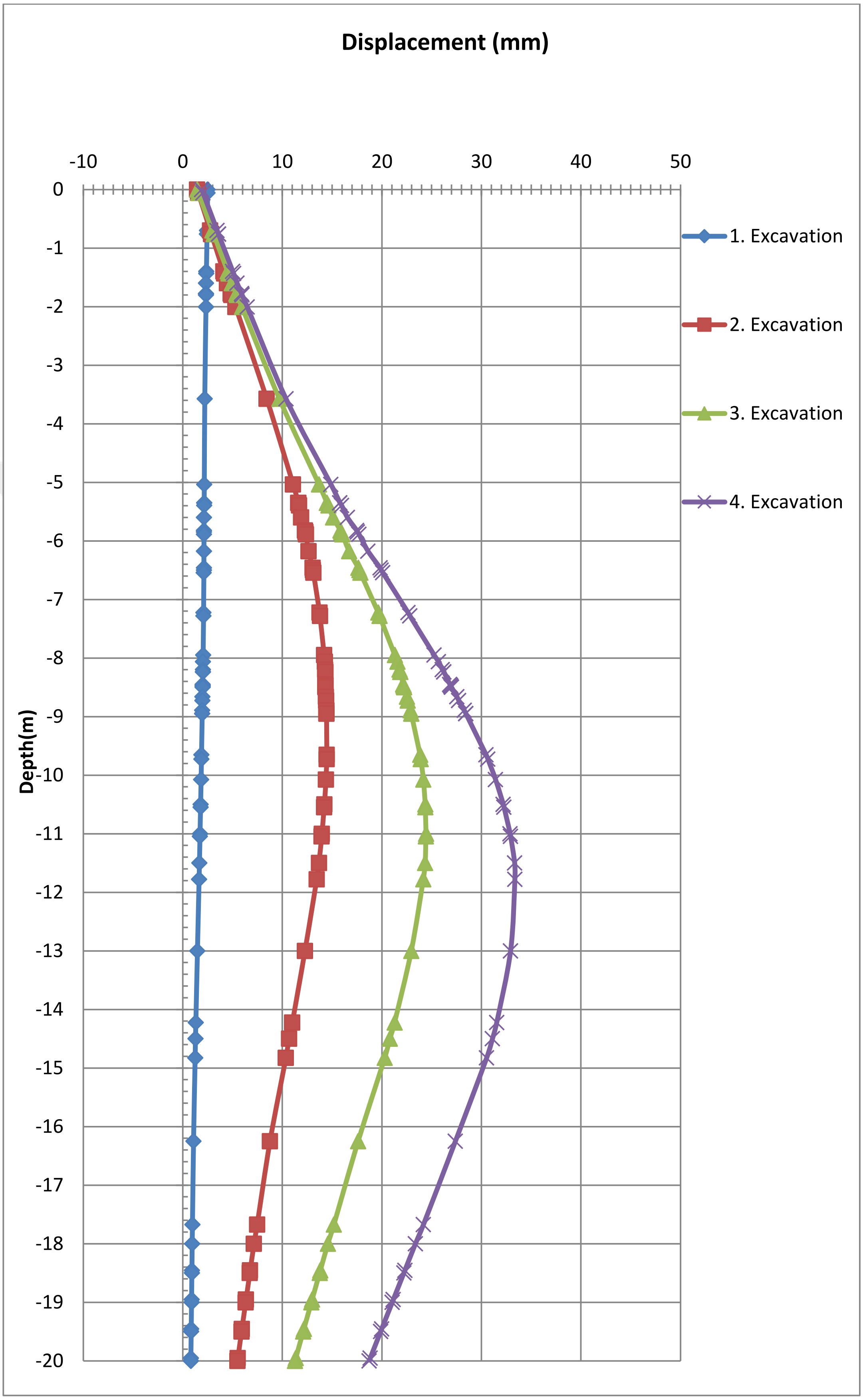

Figure 3.24 Displacements in x direction for south wall

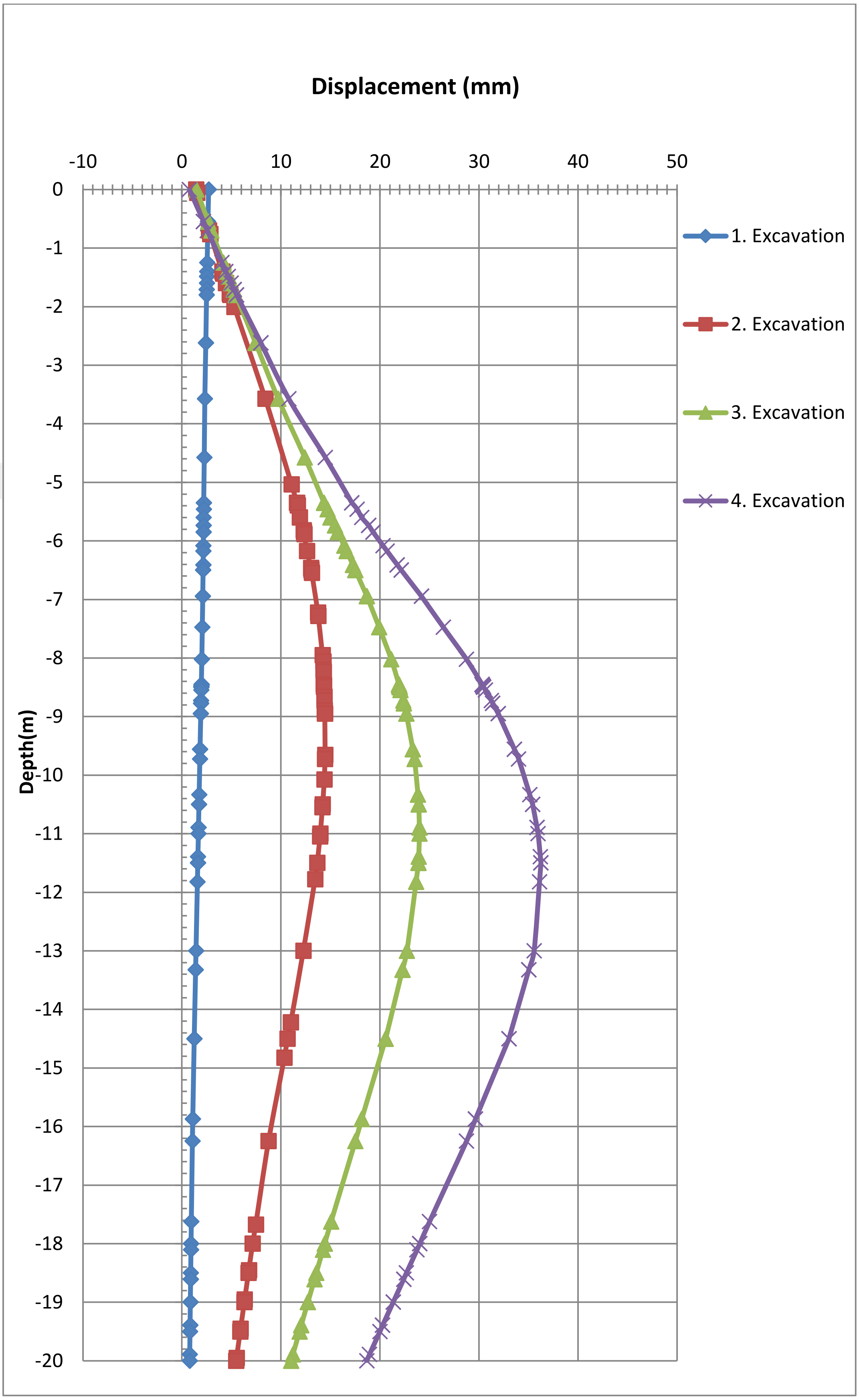

Figure 3.25 Displacements in x direction for north wall

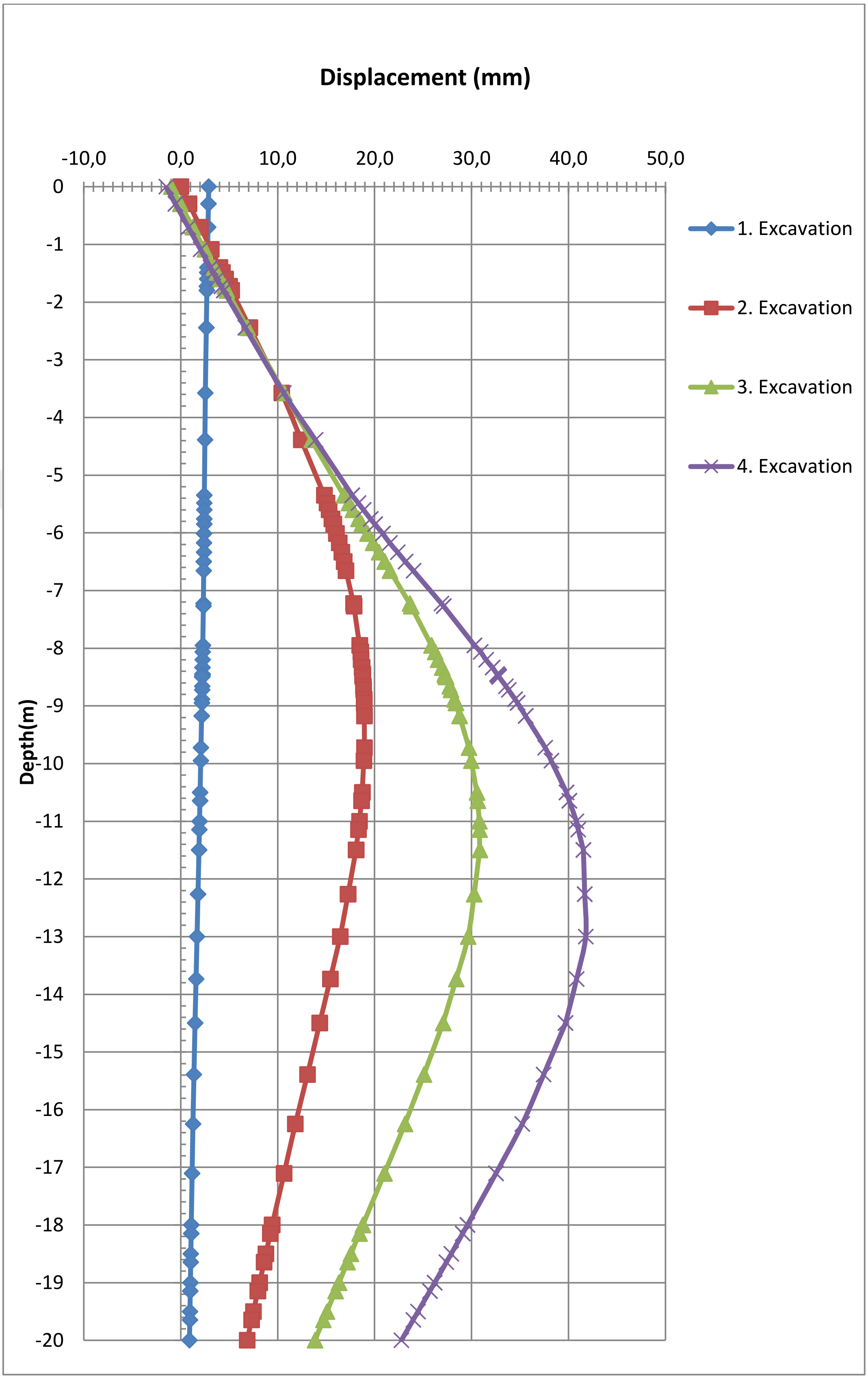

Figure 3.26 Displacements in y direction for west wall

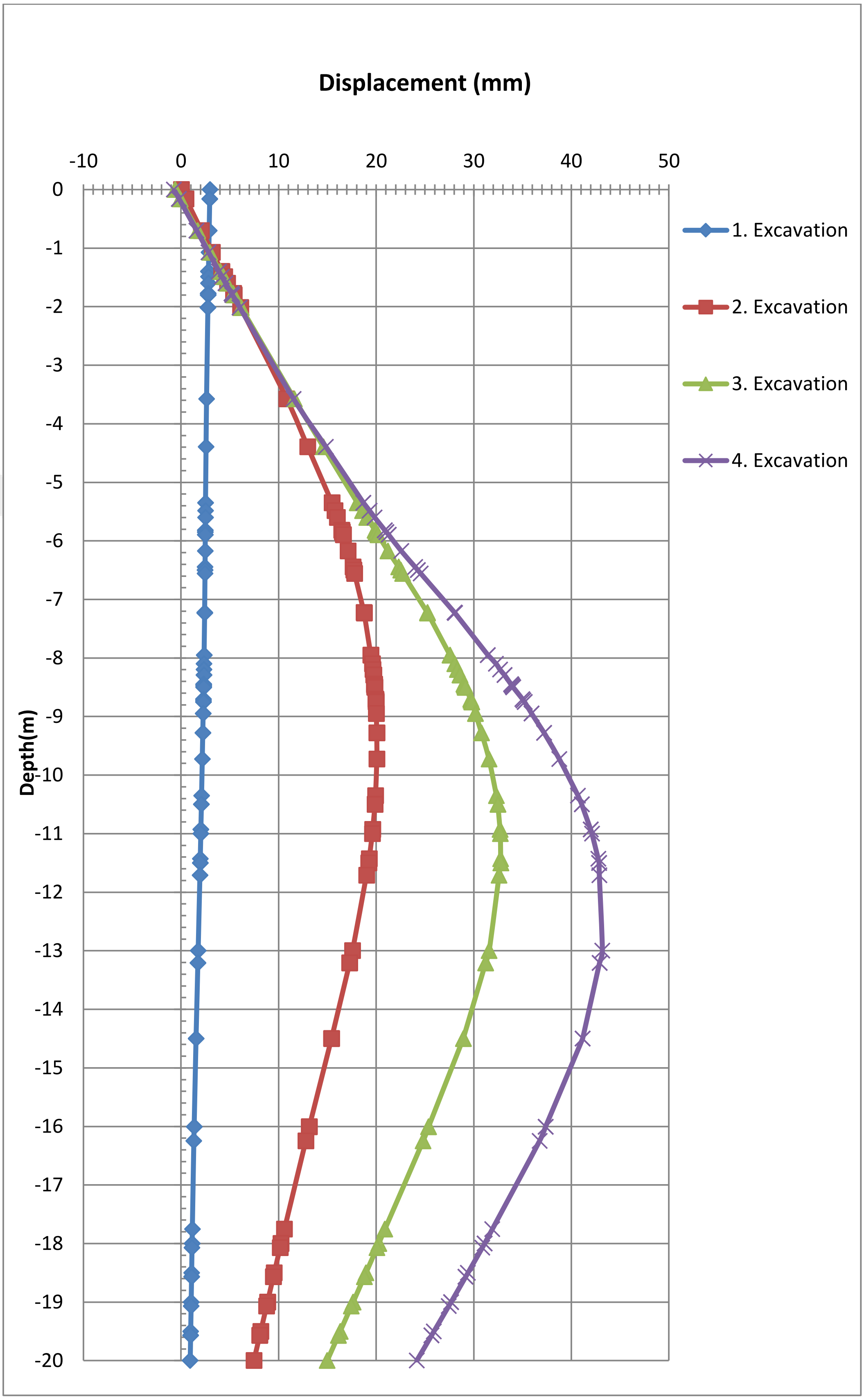

Figure 3.27 Displacements in y direction for east wall

The maximum wall deflections are showed in Figure 3.12 and Figure 3.13. As can be seen, the maximum wall deflection at the final excavation stage is equal to 4.323cm.

Figure 3.14 showed the maximum settlement below the adjacent buildings due to excavation is 2.62cm. For the building behind the location of maximum ground surface settlement, angular distortion was found as 1/830.

Finally, phi-c reduction method is used for determining the factor of safety. Phi-c reduction can be used to determine the critical slip surface and the corresponding factor of safety. The shear strength parameters ϕ and c are progressively reduced by the safety factor SF until non-convergence of the calculation is reached.

$$\frac{\boldsymbol{c}}{\boldsymbol{c_r}} = \frac{\tan\emptyset}{\tan\emptyset_r} = \sum \boldsymbol{M_{sf}} \tag{3.4}$$

$\boldsymbol{c}$ = cohesion
$\emptyset$ = friction angle
$\boldsymbol{c_r}$ = reduced cohesion
$\emptyset_r$ = reduced friction angle
$\sum \boldsymbol{M_{sf}}$ = total multiplier

The reduction of parameters is controlled by the total multiplier $\sum M_{sf}$. This parameter is increased step by step until failure occurs. The safety factor is then defined as the value of $\sum M_{sf}$ at failure. Safety factor against collapse is found as 3.597 > 1.5 (Figure 3.27)

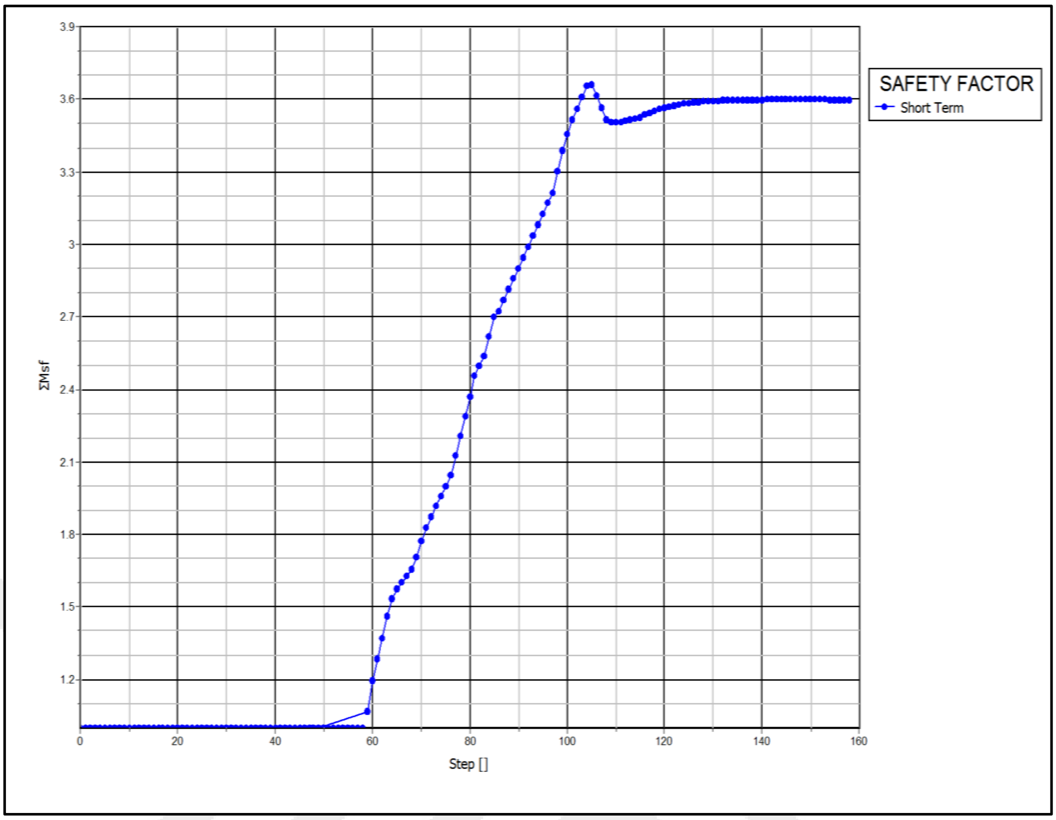

Figure 3.28 $\sum Msf$ values and factor of safety value

Do et al. (2013) suggested that intersection method can be used to determine factor of safety against basal heave. Figure 3.29 shows the displacement versus stregth reduction (SR) values. At the beginning, the displacement increases slightly but then continues to increase rapidly for large safety factor values. Such behaviours are denoted as the lower and upper parts of the curve. As extended, these two parts will intersect each other at an intersection point. The corresponding strength reduction value as the factor of safety of excavations. A pronouncing intersection point, corresponding to the SR value of 1.7, can be observed at the maximum wall displacement versus SR curve.

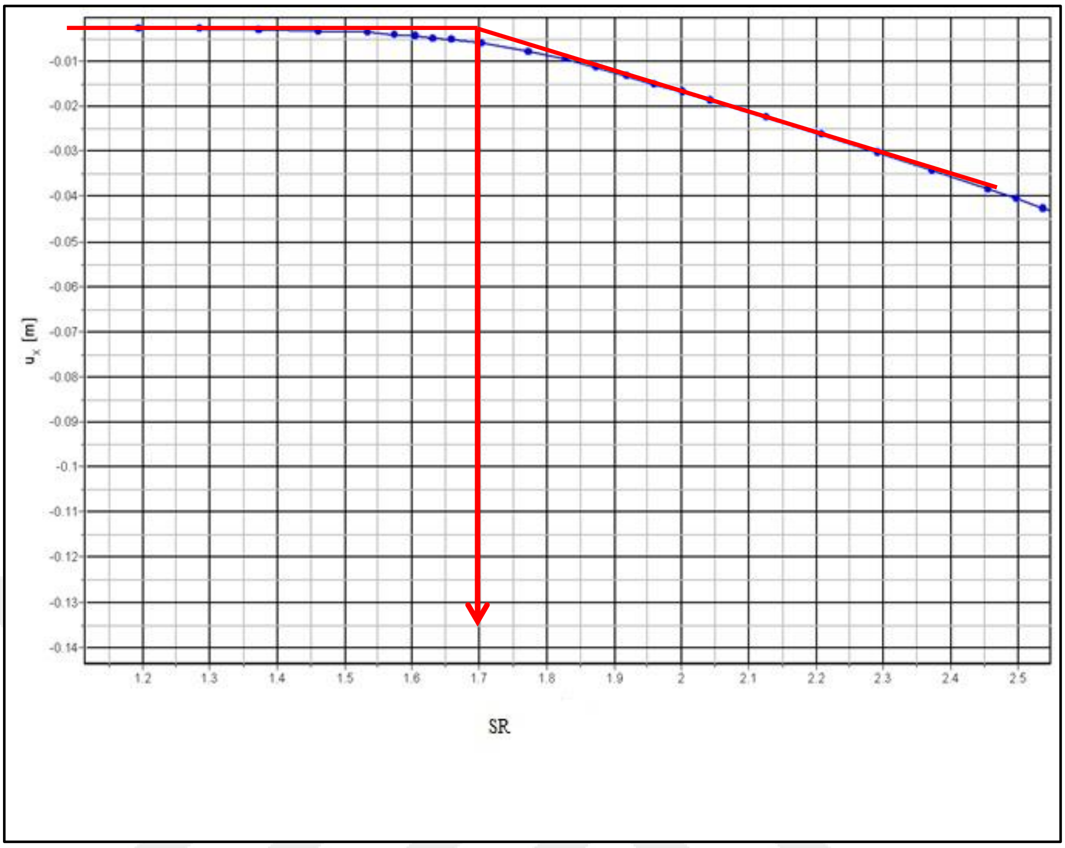

Figure 3.29 Displacement versus SR curve

3.7 Empirical Analysis Results

3.7.1 Factor of Safety Against Basal Heave

According to Terzaghi method (Terzaghi, 1943):

$$FS_T = \frac{1}{H_e} \frac{5.7 S_{u2}}{\gamma + (q_s/H_e) - (S_{u1}/0.7B)}$$

$$FS_T = \frac{1}{11.5m} \frac{5.7 \times 60 kN/m^2}{17 kN/m^3 + \left(\frac{100 kN/m^2 - 17 kN/m^3 \times 3m}{11.5m}\right) - \left(\frac{30}{0.7 \times 20m}\right)}$$

$$FS_{T1} = 1.56$$

According to Bjerrum and Eide (1956) safety factor against basal heave can be found as:

$$FS_B = \frac{N_c \times S_{u\,avg}}{\gamma \times H_e + q_s}$$

$$\frac{L}{B} = \frac{32m}{20m} = 1.6$$

$$\frac{H_e}{B} = \frac{11.5}{20} = 0.58$$

$N_c = 6.7$ (from Figure 2.3)

$$FS_B = \frac{6.7 \times 60\,kN/m^2}{17\,kN/m^3 \times 11.5m + (100\,kN/m^2 - 17kN\,/\,m^3\ \times 3m)}$$

$$FS_B = 1.64$$

3.7.2 Lateral Wall Deformations

Clough and O'Rourke (1990) established that the deformation of a retaining wall increases with the decrease of the factor of safety as illustrated in Figure 2.5.

$$\frac{EI}{\gamma_w \times h_{avg}^4} = \frac{30e6\ kN/m^2 \times 0.018m^3}{9.81\ kN/m^3 \times (3.95m)^4} \cong 225$$

$$F = 1.7\ (assumption\ from\ Chapter\ 3.6)$$

$\frac{\delta_{hm}}{H_e} = 0.45$ (from Figure 2.5)

$$\delta_{hm} = 5.175cm$$

Ou et al. (1993) examined that the range of maximum lateral wall displacement is between 0,2% H_e and 0,5% H_e.

$2.3cm < \delta_{hm} \leq 5.75cm$

3.7.3 Ground Surface Settlements

Figure 2.7c can be used to find the displacements 6 meters away from the wall. According to Clough and O'Rourke (1990) $\delta_{v\,6meter}$ should be equal to δ_{vmax}. The maximum ground surface settlement occurs in the range of $0 \leq d/H_e \leq 0.75$.

And also Clough and O'Rourke reported that the maximum settlement is about 75% of the wall maximum horizontal movement in a braced diaphragm walls.

δ_{hm} = 4.32cm (from Chapter 3.6)

$\delta_{v\,6meter}$ = 3.24cm

According to Hsieh and Ou (1998), the excavation induced ground surface settlement in back of the wall can be predicted based on the following procedure:

1. Estimate the maximum lateral displacement of the wall. (i.e. empirical methods, the finite element method or the beam on elastic foundation method) ($\delta_{hm} = 4.32cm$).

2. Concave type ground movements occurs in this problem (Chapter 2.1)

3. Estimate the value of δ_{vmax} on the basis of the relations between the maximum settlement and the maximum lateral displacement. (i.e. Clough and O'Rourke (1990), $\delta_{vmax} = 75\%\delta_{hmax}$, and δ_{vmax} = 3.24cm).

4. From Figure 1.6, $\delta_{v\,6meter} \cong \delta_{vmax}$, $\delta_{v\,6meter}$ = 3.24cm, can be found.

3.8 Parametric Study

In order to study the sensitivity of soil and structure parameters on the displacements and strut loads, a series of numerical analysis are performed using PLAXIS. Variations of the parameters have been considered. These variations are listed as follows;

1. Analysis-1 : Reference parameters in Table 3.12, 3.13, 3.14, 3.15, 3.16

2. Analysis-2 : Same with Analysis-1, but the unit weight of diaphragm wall was selected $25kN/m^3$. Variation of this parameter had an appreciable effect on the settlement results but had little effect on the horizontal displacement of the wall.

3. Analysis-3 : Same with Analysis-1, but the Young's modulus of diaphragm wall and steel strut reduced. Considering the occurence of cracks in the diaphragm wall due to bending and considering repeated uses as well as improper installation of steel struts, stiffness of the wall and steel struts were reduced by 20% and 30% as suggested by Ou (2006). As a result of this change horizontal displacement of the wall increase about 1.1 times. But some changes observed for strut load distribution. Even though the first level of strut loads increase, the loads of lower strut loads have been observed to decrease.

4. Analysis-4 : Same with Analysis-1, but $R_{interface}$ values was selected 0.67 for all soil layers. Variation of this parameter had a negligible effect on the horizontal displacement of the wall and the strut loads. This changes are approximately 1%.

5. Analysis-5 : Same with Analysis-4, but E_{50}^{ref} values was increased by a factor of 1.5. Variation of this parameter have a significant influence on the

predictions of horizontal displacement of the wall. Variation in the 50% range cause 20% change in displacement.

6. Analysis-6 : Same with Analysis-5, but G_0^{ref} values was increased by a factor of 2. Same results observed in analysis-5. Variation in the 50% range cause 20% change in displacement of the wall.

The importance of parametric study has been discussed in Chapter Five.

CHAPTER FOUR
FIELD MEASUREMENTS OF EXCAVATION

4.1 Introduction

A braced excavation may cause deformations. Lateral displacement of the wall and vertical displacement of the ground surface occur simultaneously.

Vertical displacement determines the level of damage in the adjacent structure and lateral displacement may cause the entire underground support system to fail.

Designers can estimate deformations using semiemprical methods or results of numerical modelling. Deformations can be monitored during construction. These observations would be used in inverse analysis to control the construction process and guide for the development of improved soil models suitable for representing soil response during excavation as illustrated in Figure 4.1

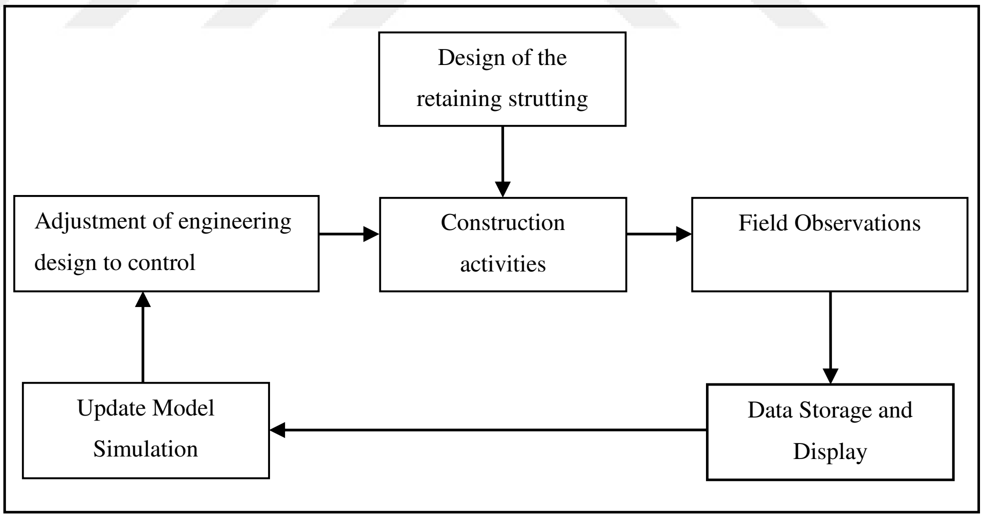

Figure 4.1 Deformation control during excavation

Some of the measurements methods of a deep excavation as follows;

- Geodetic Methods;
- Topographic Methods

    - Total Station
    - Levelling Instrument
- Photogrammetric Methods
    - Cameras
    - Laser Scanning

➢ Physical Methods;

- Inclinometer
- Tiltmeter
- Strain-gauges
- Piezometers
- Load Cells
- Extensometers

In this study, instrument readings include inclinometers placed in the support wall and strain-gauges on the bracing system. The excavation procedure is divided into stages, listed as in Table 4.1

Table 4.1 Excavation stage information

Stage	Activity	Dates	Cons. Days
1	Diaphragm wall installation	15.04.2014 – 26.05.2014	42
2	Excavation to -1.80 m	02.07.2014 – 13.08.2014	43
3	Strut installation (-1.40 m)	01.08.2014 – 15.08.2014	15
4	Excavation to -5.85 m	13.08.2014 – 21.08.2014	9
5	Strut installation (-5.35 m)	26.08.2014 – 14.09.2014	20
6	Excavation to -8.45 m	08.09.2014 – 20.09.2014	13
7	Strut installation (-7.95 m)	18.09.2014 – 02.10.2014	15
8	Excavation to -11.50 m and excavation for elevator pits to -13.50 m	08.10.2014 – 25.10.2014	18

4.2 Inclinometer Observations

The inclinometers are developed for monitoring landslide movements and slope stability monitoring and then evolved to monitore deformations of structures. The inclinometer system can measure relative deformations.

Types of inclinometers summarized as follows;

- Traversing inclinometer system
  - Manually moving the probe
  - Measurement are made both axis
  - Control cable provides to transmit electrical signals and repeatable depth control

- IPI inclinometer system
  - Real time using
  - Automated data acquisition
  - Higher cost per measuring
  - More complex

Inclinometer instrumentation composed of several components as illustrated Figure 4.2 and Figure 4.3

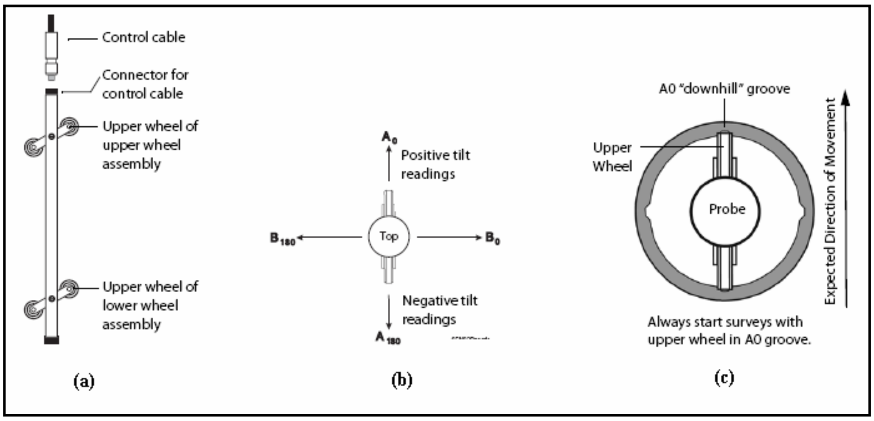

Figure 4.2 Schematic of inclinometer a. Inclinometer components b. Inclinometer casing (Machan, 2008)

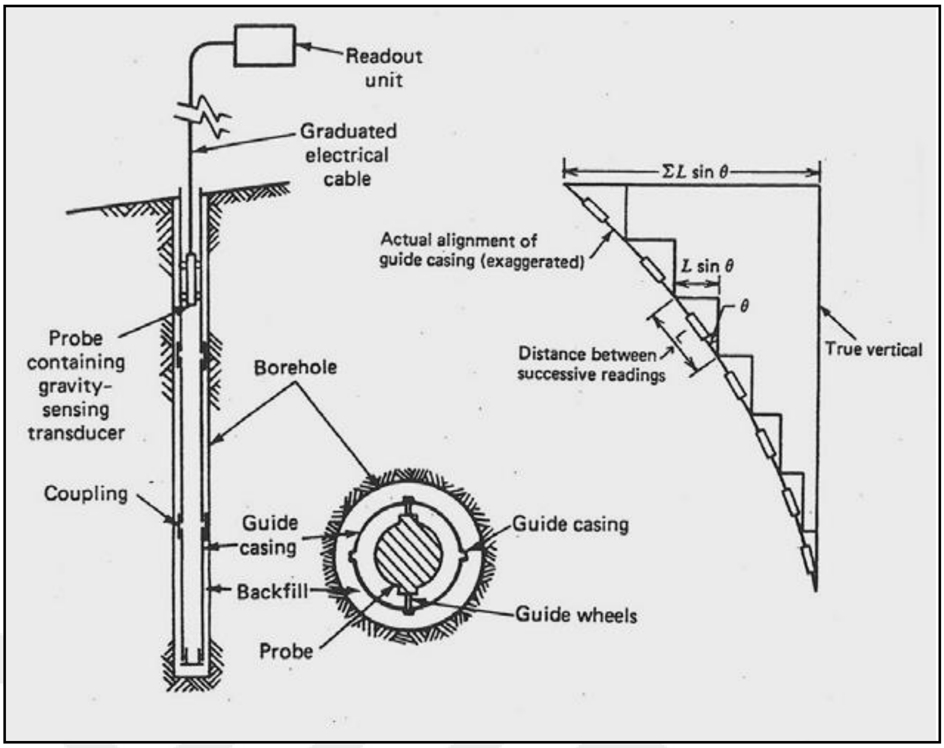

Figure 4.3 Schematic of inclinometer measurement (Machan, 2008)

Inclinometer casing is used to guide the inclinometer probe within the casing with four longitudinal wheel grooves 90° apart (Figure 4.2c).

The casing can be installed vertically in boreholes adjacent to the wall face or can be embedded within or attached to structural elements. In this project the 0.6m thick diaphragm panels were provided with reinforcing steel cages. Inclinometer casings were installed on the steel cages as illustrated Figure 4.4.

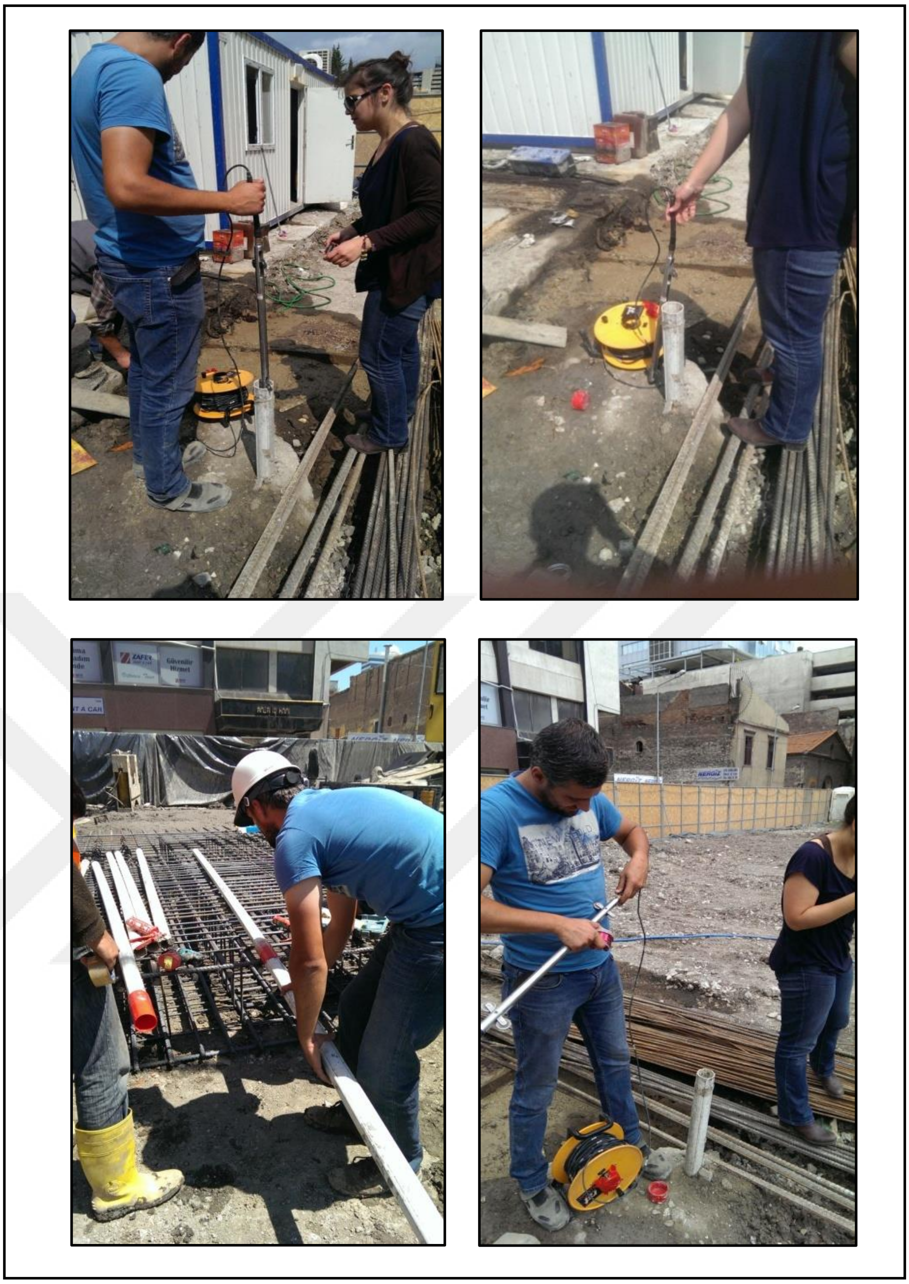

Figure 4.4 Placing inclinometer casings to steel cages

When inclinometer readings are utilized, random and systematic errors and mistakes must be taken into consideration, which are operator inconsistencies errors, bias shift errors, rotation errors, sensivity drift errors and depth positioning errors. This errors and mistakes must be evaluated carefully (Mikkelsen, 2003).

Despite above mentioned corrections, this does not mean that inclinometers always give reliable results. It is usually assumed that the toes of inclinometer casing will not move. In this project, the toe of diaphragm wall did not extend into a hard stratum, so the braced wall structure floated in the soft clay. Because of the inclinometer casing was not in stable ground, readings often indicated false outward wall movements and inclinometer readings have to be calibrated for the toe movements of wall. Readings can be calibrated if the movements at the top of the inclinometers are measured. But it may not always be possible. Toe movements can be estimated by assuming the strut level of the wall will no longer move or move inward by only small amounts (Hwang, 2007).

Figure 4.5 shows the inclinometer plan but measurements could not be made at number 1 which was damaged during construction. Figure 4.6, Figure 4.7, Figure 4.8, Figure 4.9 shows the inclinometer results.

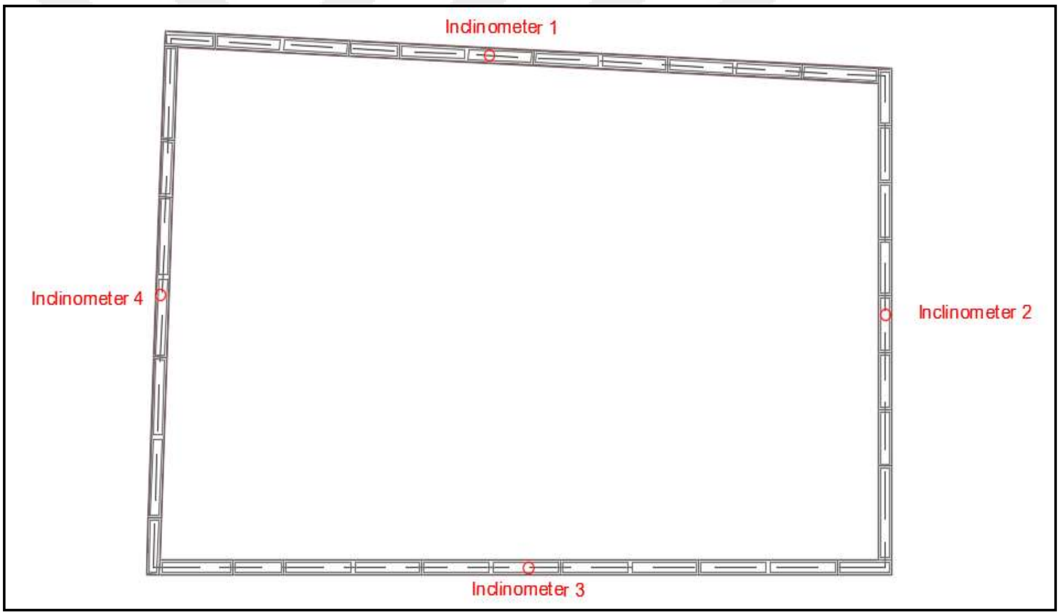

Figure 4.5 Inclinometer plan

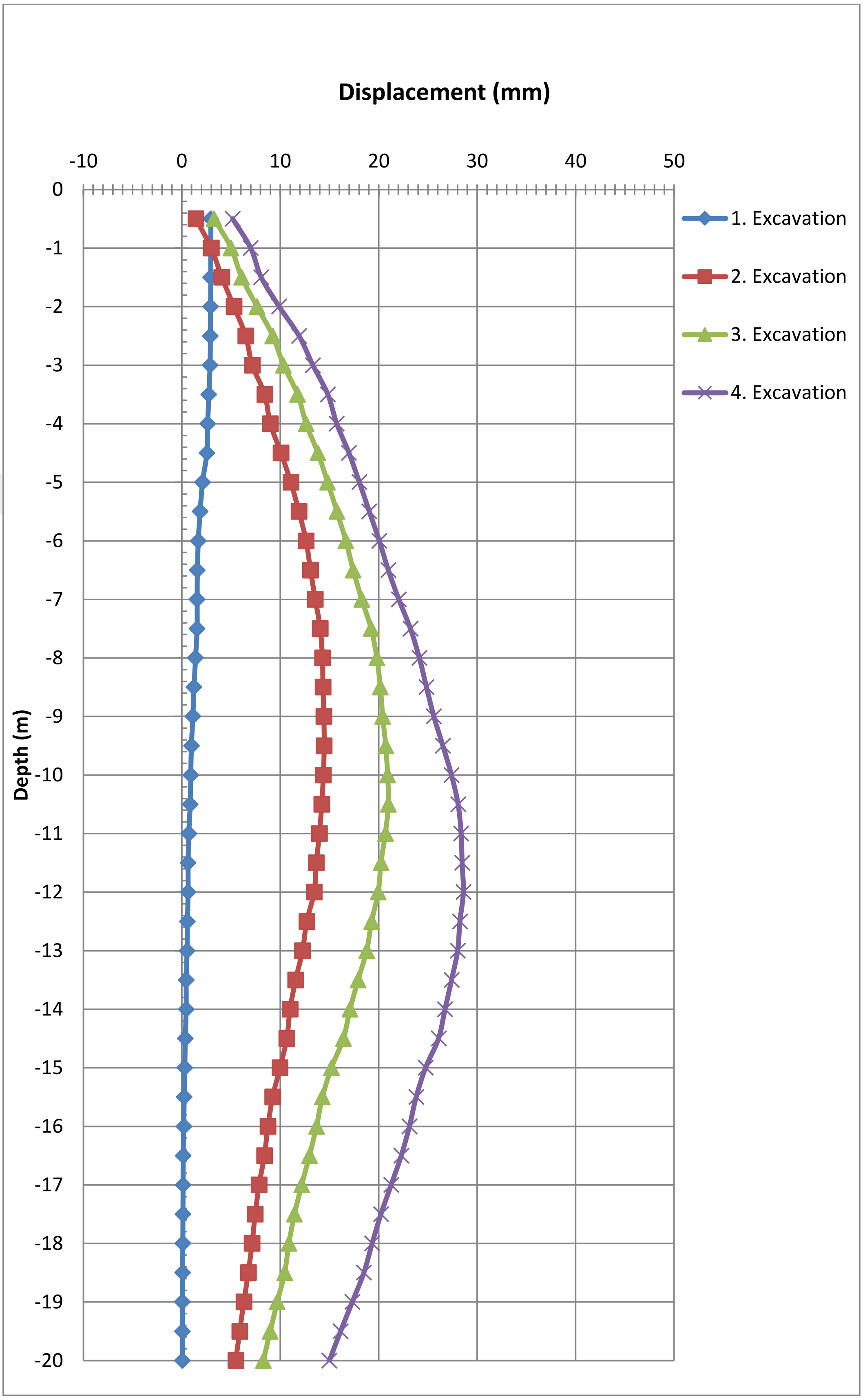

Figure 4.6 Inclinometer-2 reading results

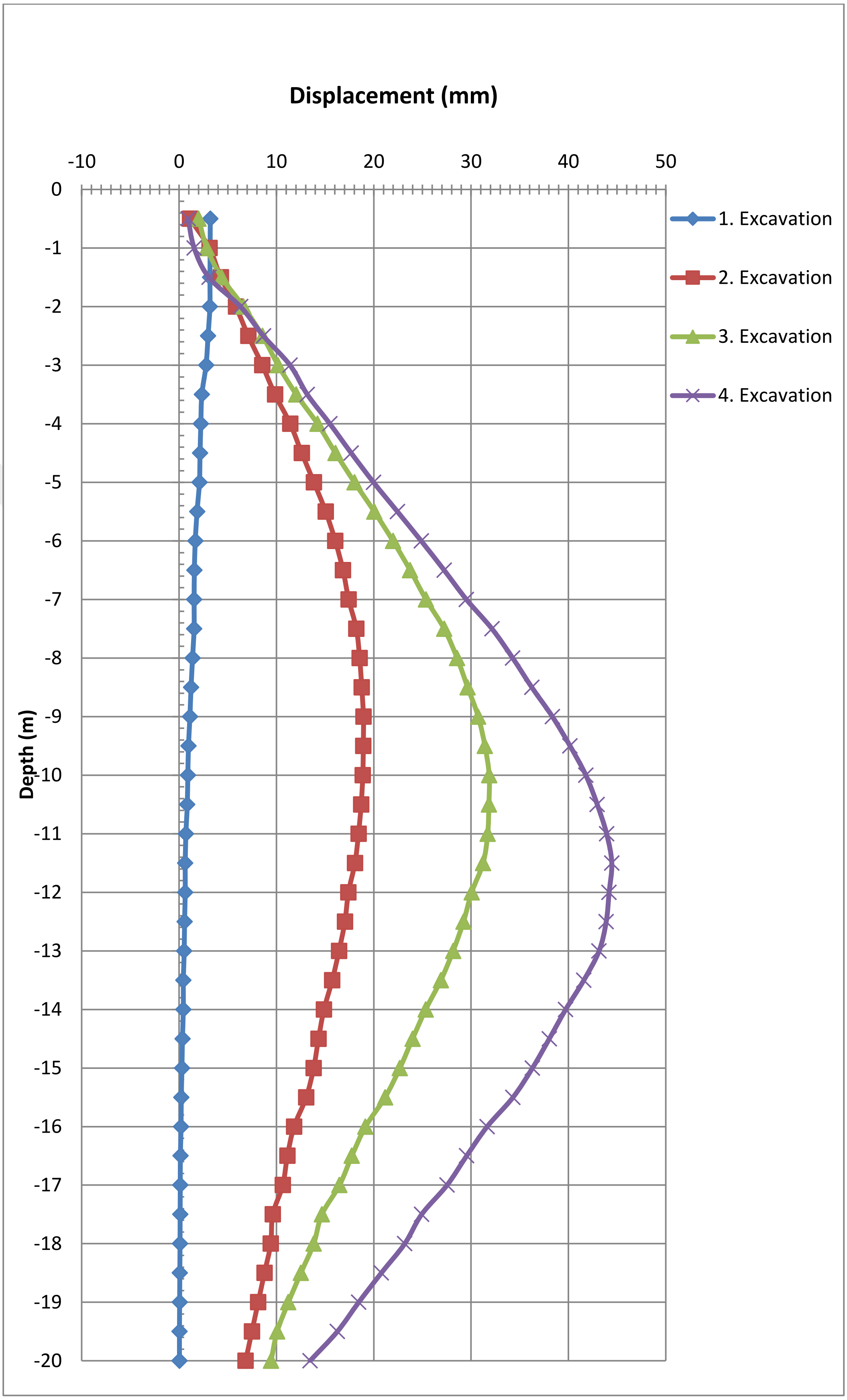

Figure 4.7 Inclinometer-3 reading results

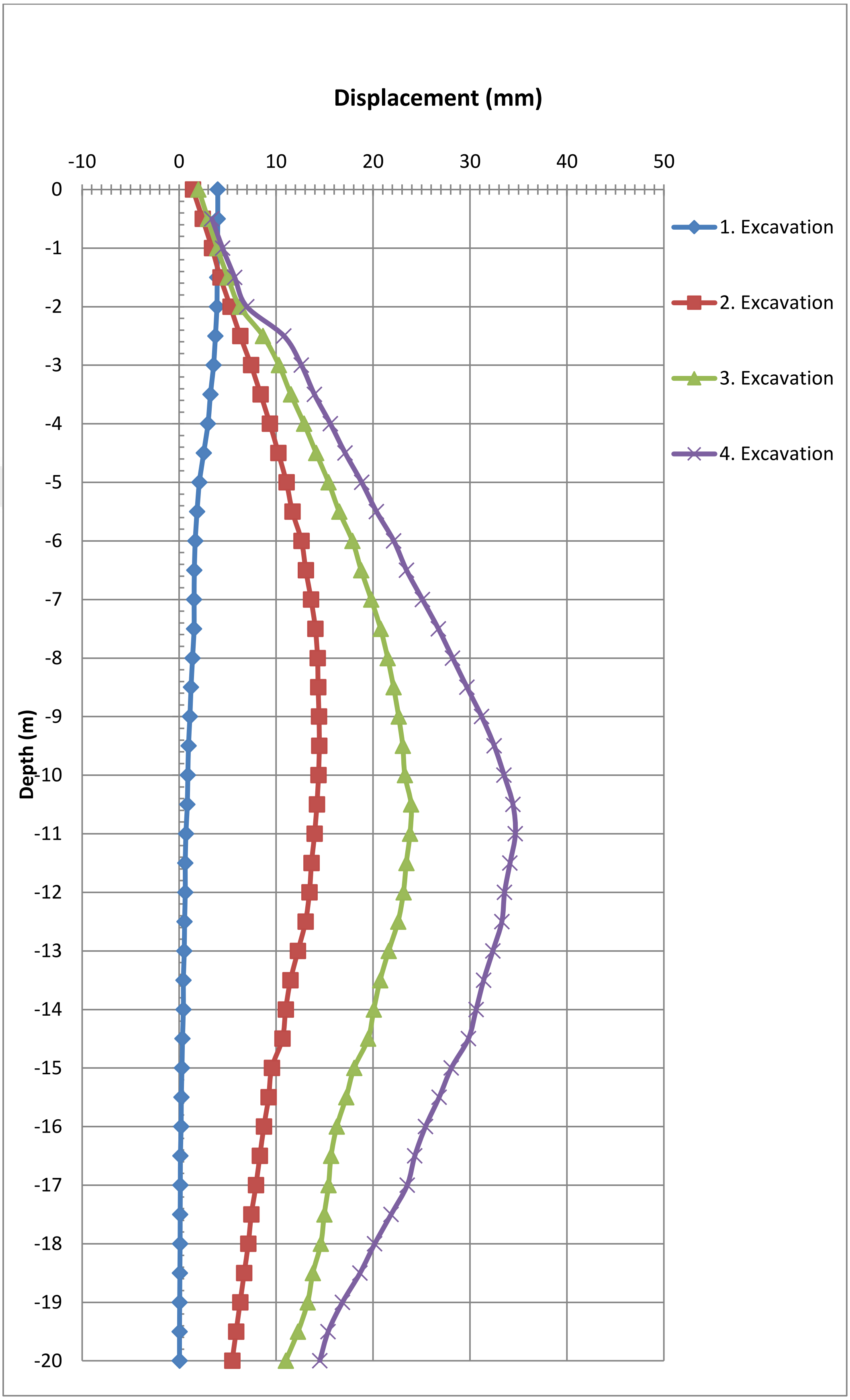

Figure 4.8 Inclinometer-4 reading results

4.3 Strain-Gauges Observations

The strain gauges are used to determine a degree of deformation due to mechanical strain to determine forces. Resistance strain gauges and the vibrating wire strain gauges are more commonly used in excavation observations. Resistance type of strain gauges as illustrated in Figure 4.9 will discuss in this Chapter.

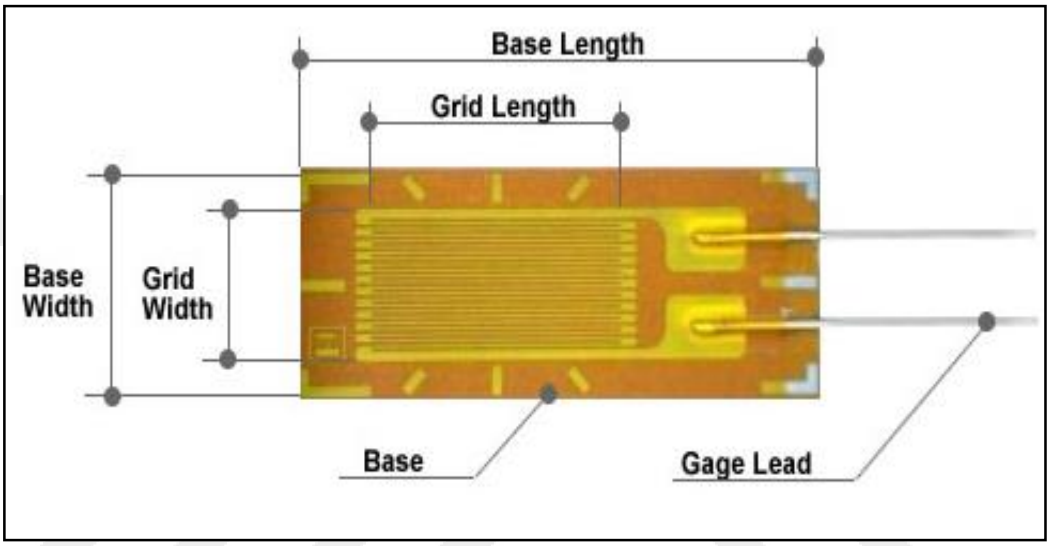

Figure 4.9 Resistance type strain sauge

When material is streched or compressed, the force generates stress. This stress deforms the material by $(\boldsymbol{L} + \Delta\boldsymbol{L})$ or $(\boldsymbol{L} - \Delta\boldsymbol{L})$. The ratio of $\Delta\boldsymbol{L}$ to $\boldsymbol{L}$ is called strain. The material produces a change of electrical resistance corresponding to the deformation. A strain gauge is the element that senses this change and converts it into an electrical signal.

$$\varepsilon = \frac{\Delta L}{L} = \frac{\Delta R/R}{K} \tag{4.1}$$

$\boldsymbol{\varepsilon}$ = strain measured

$\boldsymbol{R}$ = gauge resistance

$\Delta\boldsymbol{R}$ = resistance change due to strain

$\boldsymbol{K}$ = gauge factor

The strain induced change of resistance is too small to be measured directly. For this reason, Wheatstone bridge is used to convert resistance to voltage output (Figure 4.10).

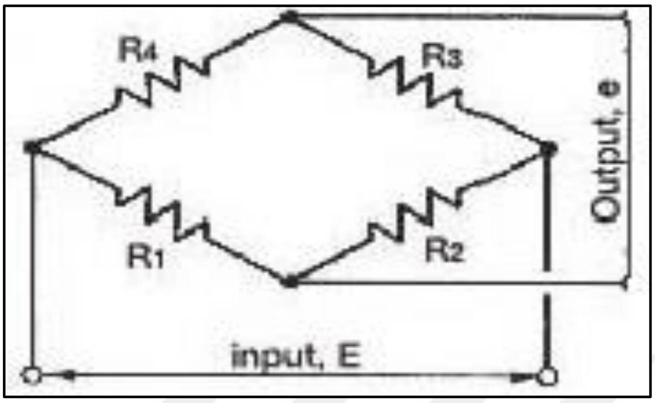

Figure 4.10 Wheatstone bridge schematic

Assuming the value $\boldsymbol{R}$ such that $\boldsymbol{R} = \boldsymbol{R_1} = \boldsymbol{R_2} = \boldsymbol{R_3} = \boldsymbol{R_4}$ the active gauge resistance varies to $\boldsymbol{R} + \Delta\boldsymbol{R}$ due to strain. Thus the output voltage ($\Delta\boldsymbol{e}$):

$$\Delta \boldsymbol{e} = \frac{1}{4}\boldsymbol{K}.\boldsymbol{\varepsilon}.\boldsymbol{E} \qquad (4.2)$$

$\boldsymbol{E} =$ Exciting voltage

To measure the strain gauge, the quarter bridge method, the half bridge method or full bridge method can be used. A single strain gauge is used for the quarter bridge method. The quarter bridge method is applied to measure the strain of structural elements but can not measure effects of the temperature. The half bridge method generates output twice from the generated by the quarter bridge method. Neverthless this method can be used for temperature correction. The full bridge method requires the installation of four strain gauges on a bridge. Schematic diagrams for these methods as follows;

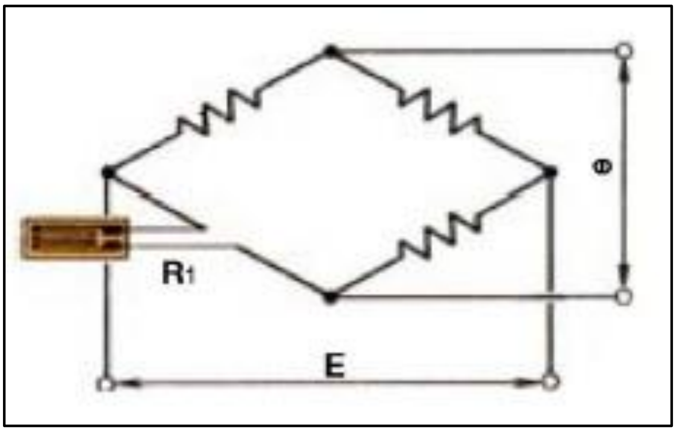

Figure 4.11 Quarter bridge method schematic

$$\Delta \boldsymbol{e} = \frac{1}{4}\boldsymbol{K}.\boldsymbol{\varepsilon}.\boldsymbol{E} \tag{4.3}$$

a)

b)

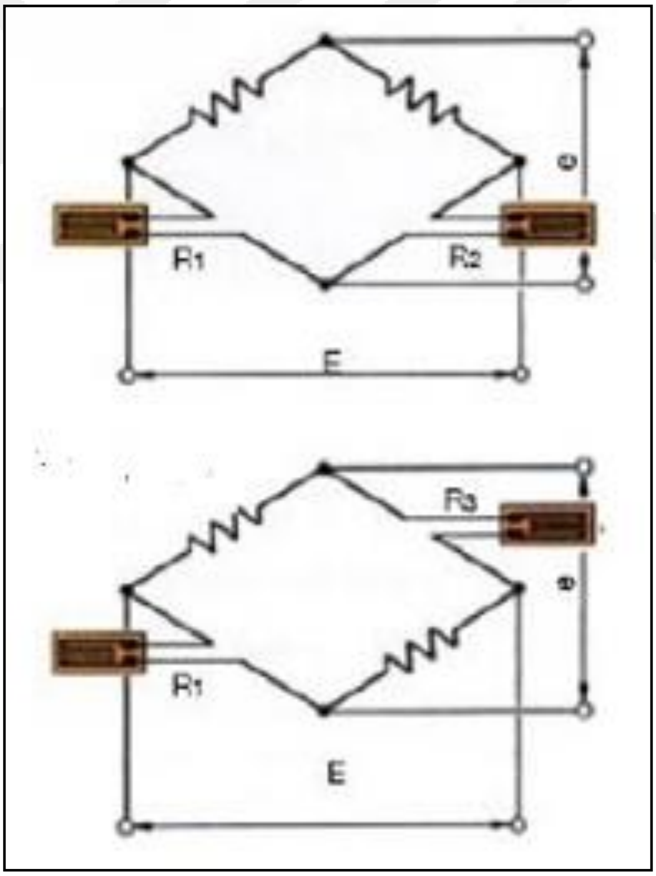

Figure 4.12 Half bridge method schematic

For figure 4.12a $\longrightarrow$ $$\Delta \boldsymbol{e} = \frac{1}{4}\boldsymbol{K}.(\boldsymbol{\varepsilon_1} - \boldsymbol{\varepsilon_2}).\boldsymbol{E} \tag{4.4}$$

For figure 4.12b $\longrightarrow$ $$\Delta \boldsymbol{e} = \frac{1}{4}\boldsymbol{K}.(\boldsymbol{\varepsilon_1} + \boldsymbol{\varepsilon_2}).\boldsymbol{E} \tag{4.5}$$

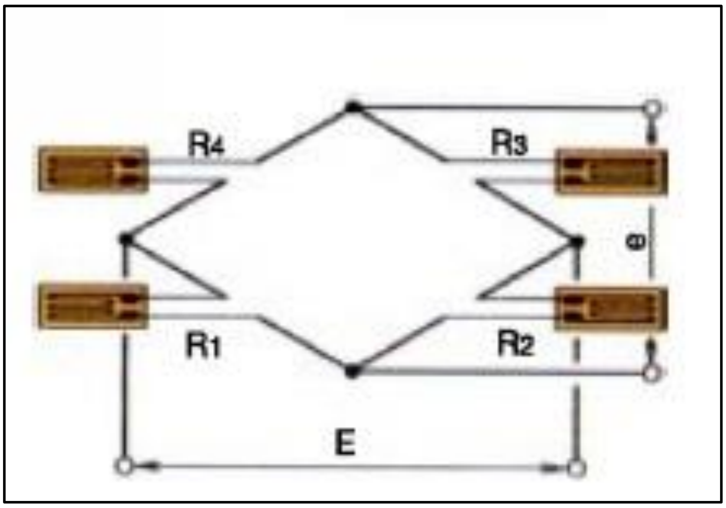

Figure 4.13 Full bridge method schematic

$$\Delta e = \frac{1}{4}K.(\varepsilon_1 - \varepsilon_2 + \varepsilon_3 - \varepsilon_4).E \tag{4.6}$$

The position of the strain gauge depends on the purpose of the measurement and the shape of the structural elements. Figure 4.14 shows typical strain gauge locations.

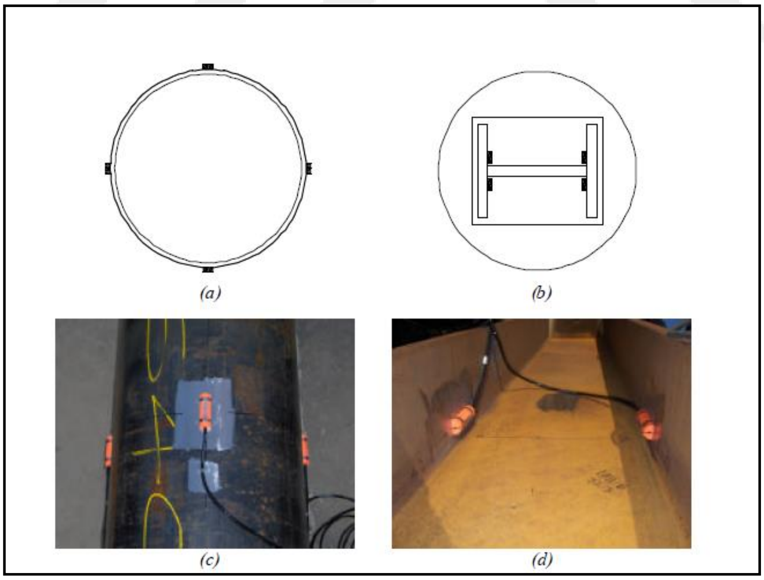

Figure 4.14 Typical strain gauge locations a and c a tubular, and b and d a welded channel section (Zaremba, 2007)

According to Dunnicliff (1988) a single gauge is sufficient for the elements which is not subject to bending stress. If the structural elements subjected to both axial and bending stresses and axial stres is required, a minimum of two gauges must be used.

These two gauges must be placed at equidistant from and on opposite sides of the neutral axis. If the maximum stres is required and the member may be subjected to bending about any axis, more than two gauges must be used. On a pipe strut, a minimum of three gauges spaced 120 degrees apart should be used for determination of maximum stress.

Temperature change can cause stress change. To eleminate temperature changes on strain gauges active dummy method can be used as illustrated in Figure 4.15.

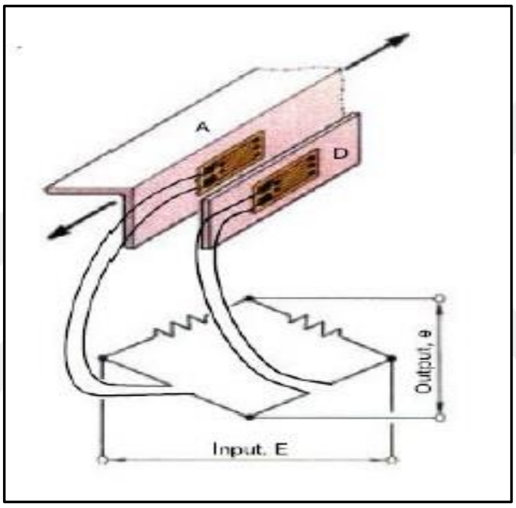

Figure 4.15 Active dummy method

Another method is the correct for any strain caused by temperature change. In this method when making measurements on strain gauges, temperature should be measured.

$$total\ strain = \frac{\Delta\sigma}{E} + \varepsilon * \Delta t \tag{4.7}$$

$\Delta\sigma$ = stress change

Δt = temperature change

E = modulus of elasticity of steel

ε = linear coefficient of thermal expansion of steel

Many researchers investigate the temperature change effects on strain gauges. Zaremba and Lehane (2007) founds that during a period of no construction activity, the strut force increases about approximately 182 kN for a 25$°C$ increase in temperature. Another research show that observed thermal loading compenent of the strut force as much as 40% of the total load observed (Finno et al., 2005).

Installing resistance strain gauge is an exacting work. First gauge position should be determined roughly and then bonding area should be purified from all grease and rust as illustrated in Figure 4.16. Surface of bonding area should be sanded with abresive paper. Sanded area should be cleaned with acetone. Strain gauge adhesive must be used for bonding, Figure 4.17. After soldering the gauge leads, terminal wires and lead wires, strain gauge should be protected from water and mechenical damage, as illustrated Figure 4.18, 4.19, 4.20, 4.21, 4.22, 4.23. Coating entire gauge with mastic and epoxy provides a moisture barrier and protects the gauge, Figure 4.24 and Figure 4.25. Gauge installation illustrated on the following Figures.

Figure 4.16 Purified bonding area

Figure 4.17 Resistance type strain-gauge

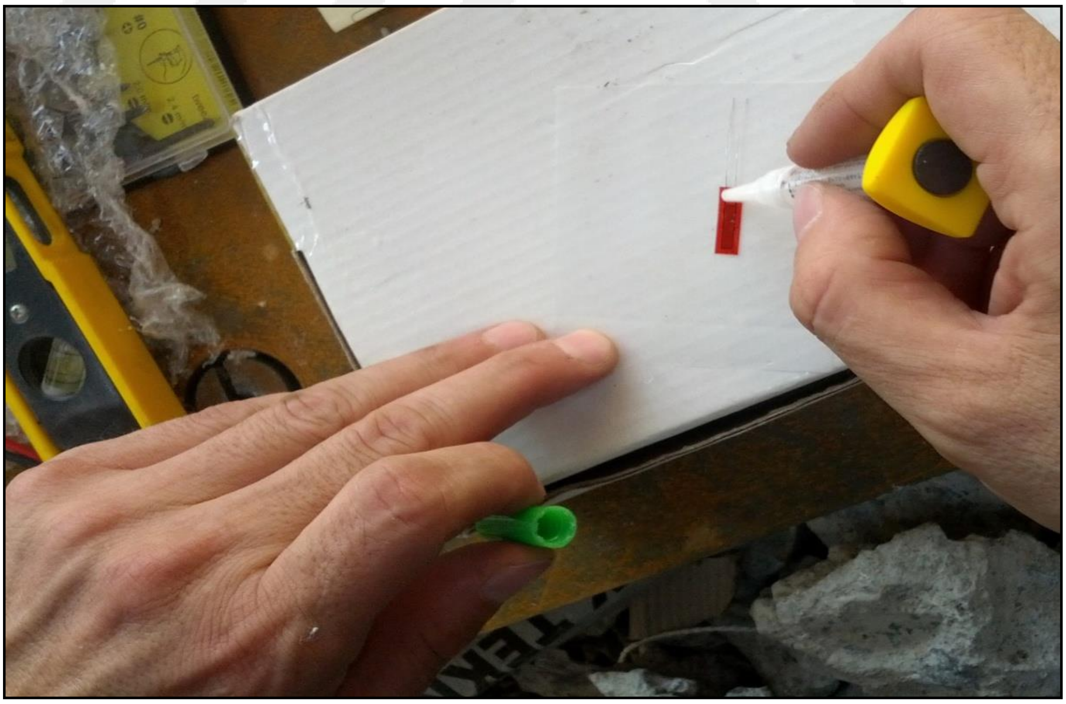

Figure 4.18 Strain-gauge bonding

Figure 4.19 Raising the gauge leads

Figure 4.20 Bonding connecting terminals

Figure 4.21 Soldering the gauge leads

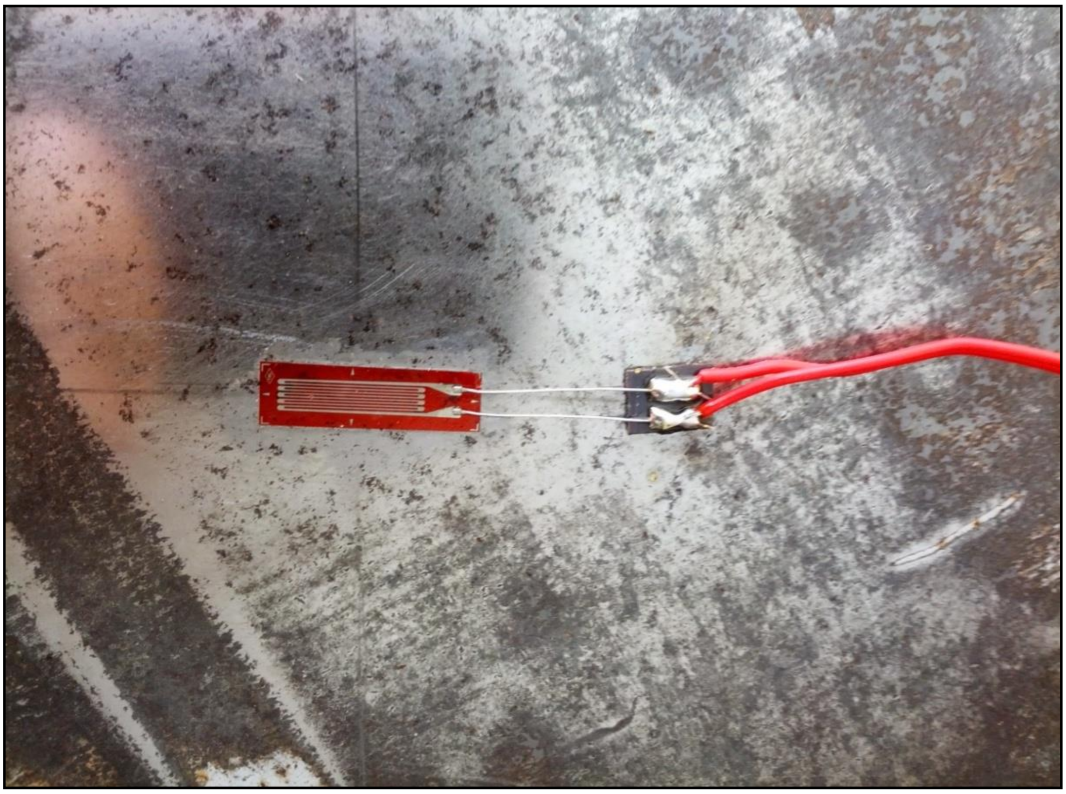

Figure 4.22 Soldered the gauge leads and lead wires

Figure 4.23 Controlling the resistance voltage

Figure 4.24 Coating the gauge with mastic

Figure 4.25 Coating the gauge with epoxy

Figure 4.26 Numbered strain gauges

Figure 4.27 Collecting strain gauge data

A total of sixteen resistance type of strain gauges were installed on selected bracing members. The locations were arranged to obtain a representative set of data from each of the three strut levels. Two gauges were installed on each selected struts.

Two gauges were installed on each selected struts. The axial load in a strut was calculated from the average of the two strain gauge readings when all two gauges were operational.

Many of the strain gauge datas contain obvious erroneous readings. In this readings strut forces measured more than 4 to 5 times it should be. The loads found at a reasonable level are listed in Table 4.2

Table 4.2 Strain gauge results

	1S3	1S4	1S11	2S3	2S4	2S11	3S3	3S4
1. Excavation	-	-	-	-	-	-	-	-
2. Excavation	-	-	-	-	-	-	-	-
3. Excavation	-	-	-	-	-	1085.4 kN	-	-
4. Excavation	-	-	-	-	-	3031.9 kN	1654.9 kN	2074.6 kN

CHAPTER FIVE
CONCLUSIONS AND RECOMMENDATIONS

The importance of the deep excavations was the main priority for this dissertation. The effect of deep excavation to the adjacent structures was considered by finite element method which is commonly used in practice. The details of the finite element method were described. Nevertheless, the stress-strain relationship of soil is well noted. Finally, the accuracy of numerical excavation analysis was validated by comparing to the observation data. According to the results from this study, several conclusion and recommendation can be drawn:

- As summarized in Table 5.1, the results of stability analyses using finite element methods and the conventional methods for six case histories.

Table 5.1 Calculated factors of safety against basal heave

Case History	Finite Element Analysis		Empirical Analysis	
	Strength Reduction Method	Intersection Method	Terzaghi's Method (1943)	Bjerrum and Eide's method (1956)
This Study	3.597	1.7	1.55	1.64
Taipei Rebar Broadway Case (Hsieh et al. 2008)	1.76	1.0	1.09	0.95
Taipei Shi-Pai Case (Hsieh et al. 2008)	2.46	1.0	0.9	0.79
Taipei Electricity Distribution Center Case (Wang and Su., 1996)	2.0	1.06	1.17	1.04
Oslo Case (Aas 1984)	1.17	1.01	0.86	0.83
Hangzhou, China Case (Chen et al., 2004)	1.10	0.94	1.05	0.74

- In conventional methods, a failure surface of soil is first assumed, and the factor of safety against basal heave is then calculated as the ratio of the resistant force to the driving force. Although this calculation procedure is convenient for practical application, the actual failure surface may not be the same as that assumed in the conventinal methods. In addition, these methods do not take into account the stiffness and embedment depth of the wall in the calculation. The strength reduction method provides the highest safety factor values among the finite element methods and generally overestimates basal heave stability of the case histories as can be seen in Table 5.1. Do et al., (2013) and Zhang et al., (2013) reported that the intersection method resulted in good agreement with the field measurements.

- The numerical prediction from finite element analysis, the observation data from the field measurements and the empirical analysis results were compared. Results show that finite element method is the most effective method for determining lateral wall deflections (Table 5.2). Also the prediction of surface settlements due to excavation were performed with finite element analysis and empirical analysis (Table 5.3).

Table 5.2 Calculated maximum lateral wall deflections

	Field Measurements	Finite Element Analysis	Empirical Analysis	
			Clough and O'Rourke (1990)	Ou et al., (1993)
This Study	4.5cm	4.32cm	5.175cm	$2.3cm < \delta_{hm} \leq 5.75cm$

Table 5.3 Calculated maximum ground surface settlements

	Finite Element Analysis	Empirical Analysis	
		Clough and O'Rourke (1990)	Ou et al., (1993)
This Study	4.32cm	5.175cm	$2.3cm < \delta_{hm} \leq 5.75cm$

- Comparisons between the field measurements and the numerical results show that field behavior could be fairly well predicted as illustrated following Figures 5.1, 5.2, 5.3. They showed similar tend and almost identical results were obtained. All the inclinometer results showed that occured displacements are less than expected except for Inclinometer-3 as illustrated in Figure 5.1. For west section of the wall, observed displacements exceed the numerical analysis results. The existence of the construction machine in west section of the wall may have the reason for the unexpected displacements occured in this part of the wall. Uncorrected inclinometer readings, corrected inclinometer readings and Plaxis results for each inclinometers are as follows.

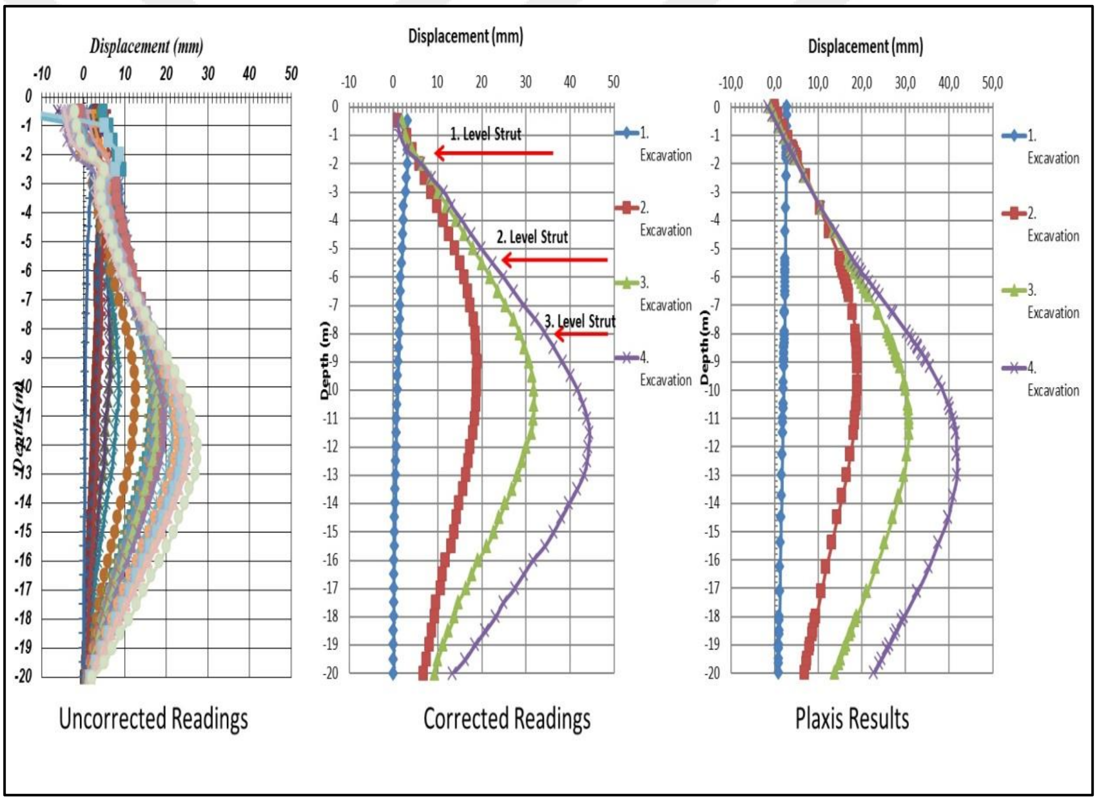

Figure 5.1 Inclinometer results for inclinometer-3

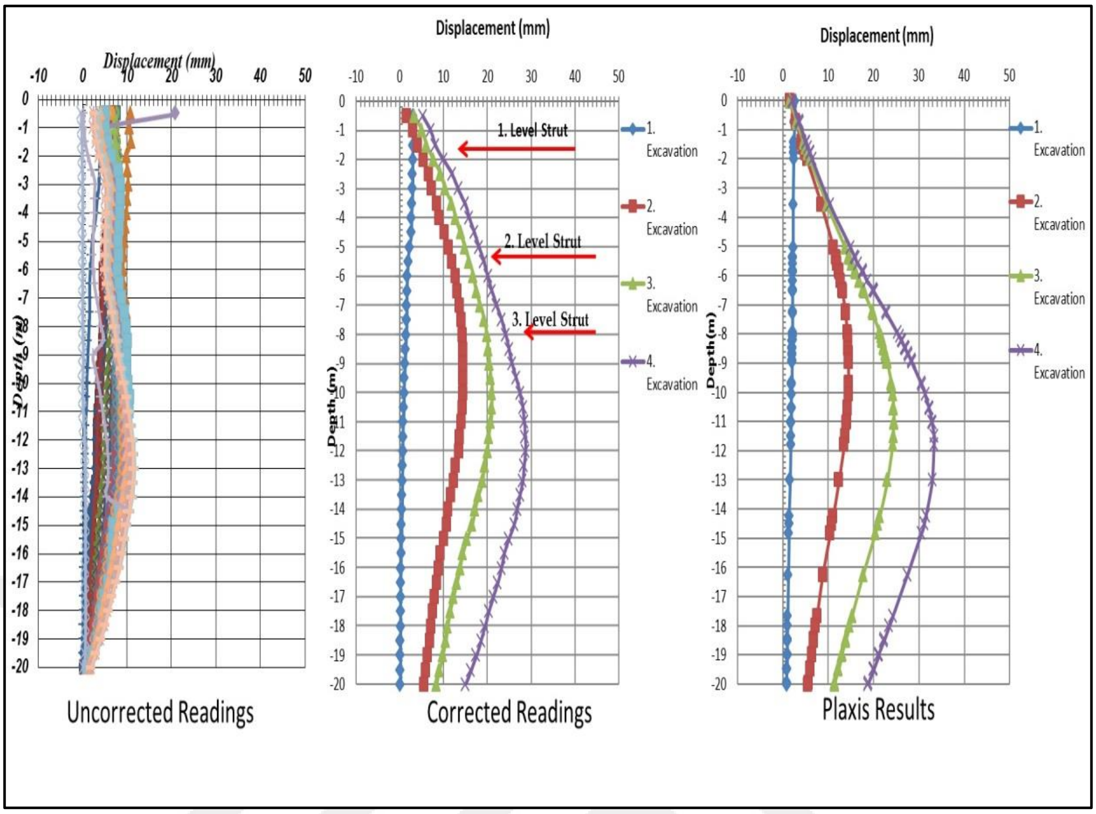

Figure 5.2 Inclinometer results for inclinometer-2

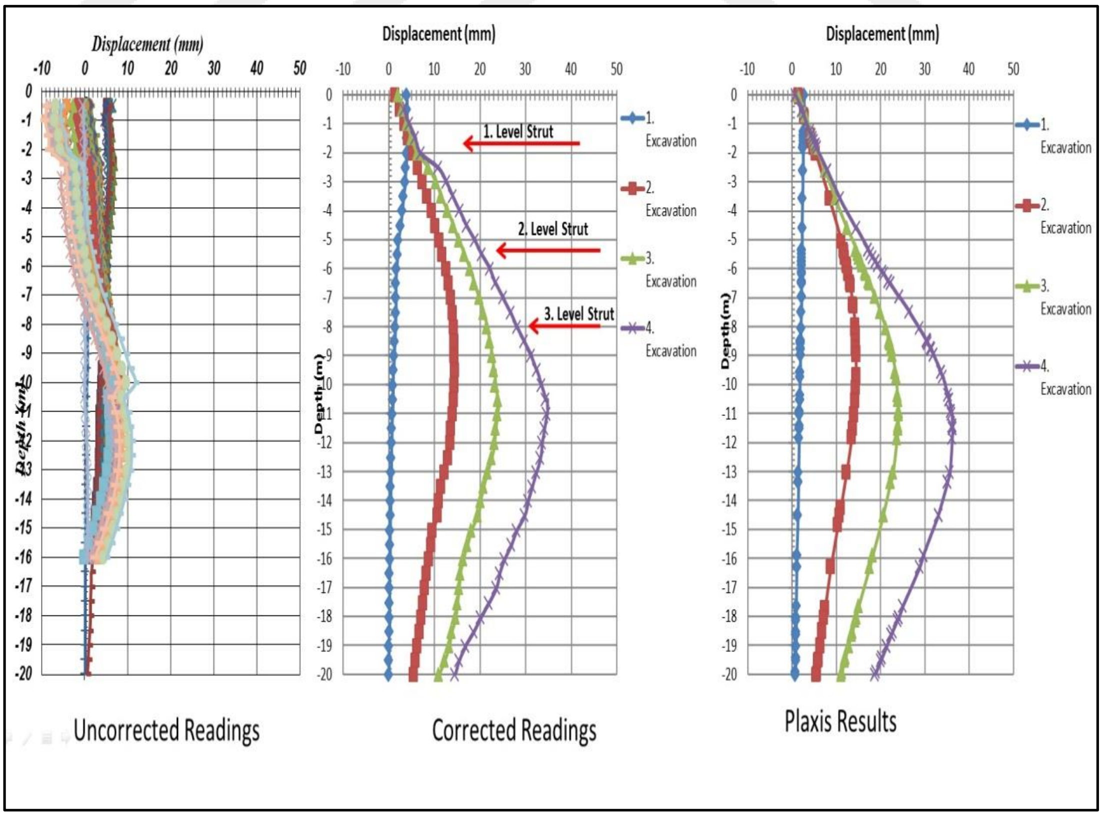

Figure 5.3 Inclinometer results for inclinometer-4

- The maximum wall deflection at the final excavation stage is equal to 4.32cm. The value of the $\boldsymbol{\delta_{hm}/H_e}$ was found as 0.38%.

- Studies on lateral retaining wall deflection caused by deep excavations in Asian soft clay were reported by some researchers. Liu et al. (2008) compared the results. Figure 5.4 shows the measured lateral wall deflection compared to the excavation depth. All the excavations were in soft clay and diaphragm walls were used for the retaining system.

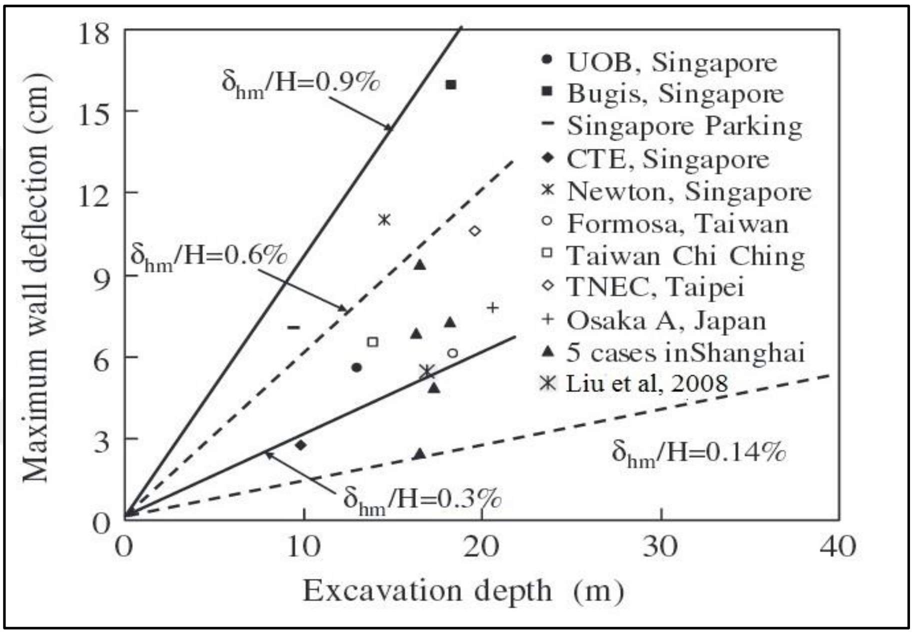

Figure 5.4 Relationship of the maximum lateral wall deflection to the excavation depth (Liu et al. 2008)

- Figure 5.5 and Figure 5.6 shows the relationship between the maximum ground surface settlement and the maximum lateral displacement of the wall. Figure 5.5 show that δ_{vm} ranges from $0.5\delta_{hm}$ and $1\delta_{hm}$. On the other hand, the upper and lower bound values of δ_{vm} are $0.4\delta_{hm}$ and $2\delta_{hm}$ in Figure 5.6. In this study the ratio of δ_{vm} and δ_{hm} was found as 0.61.

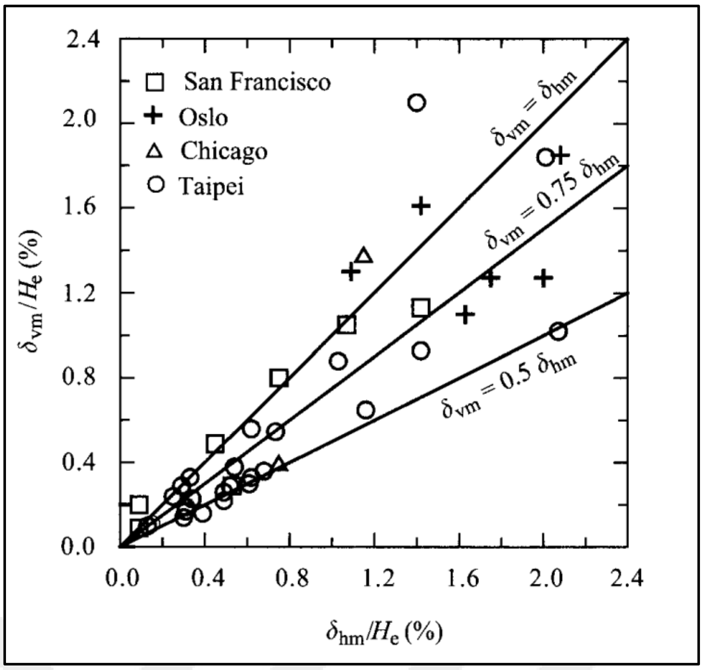

Figure 5.5 Maximum ground surface settlement and lateral wall deflection relation (Ou, 2006)

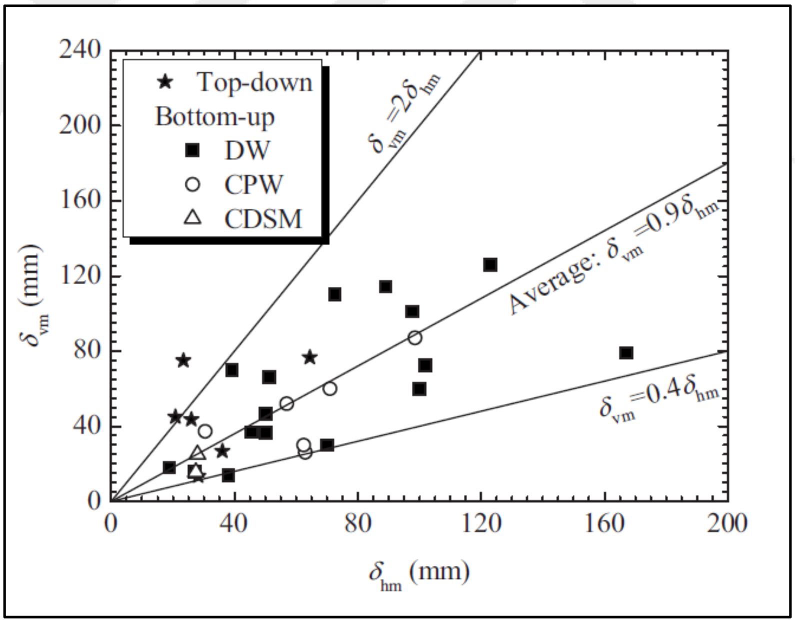

Figure 5.6 Maximum ground surface settlement versus lateral wall deflection (Wang et al., 2009)

- For a building behind the location of maximum ground surface settlement, angular distortion was found 1/830. This value remains within acceptable limits for angular distortion and differential settlement (Ou, 2006). In this study adjacent structures simulated as a plate. These simulations were simple to catch the real characteristic of building response to the excavation. Type of foundation, size of foundation, and structural system affected the building performance during excavation. The effect of deep excavation on the building damage potential can be evaluated by adopting SAP 2000. Furthermore, these simulation results should be checked with field measurements (e.g. tiltmeter). Finno and Bryson (2002) reported that angular distortions as large as 1/300 were observed at the three-story school which was affected by an adjacent 12.2m deep excavation in soft clay.

- No structural system damage was observed in the adjacent buildings during excavation stage. Field observations and numerical analysis results showed that the maximum wall displacements and settlements below the adjacent buildings remain within the acceptable limits. But it must be noted that, the building behind the location of maximum ground surface settlement has tilted towards the excavation zone at the early stages of the construction and then, after the completion of the construction, the deformations substantialy reversed.

- The results showed that three dimensional analysis can be used to obtain more realistic prediction of excavation behavior. The corner effect, irregular strut position and adjacent structure location significantly affected the resulting excavation behavior. Inclinometer measurements showed that displacements on the short sides of the diaphragm wall are small compared to the displacements on the long sides besides lateral movements were restrained by the wall corner. The wall and ground displacement exhibit peak values at the middle section and become smaller at the corners. And also type of foundation, length of excavation side, size of foundation affected the adjacent construction performance as we can see in Figure 3.14. In the lights of this information it can be said that wall movement below excavation level is much better predicted by 3D analyses.

- In the early stage of excavation, displacements are observed in the upper part of the wall. The wall is to behave as a cantilever at the first stage of excavation because the steel struts at the first level have not installed. In later stages more displacement are observed at the excavation level of the wall.

- The obtained information will be more reliable when the inclinometer extends to a hard stratum. In this study inclinometer readings were calibrated by assuming the strut level of the wall will no longer move or move inward by only small amounts. Uncorrected inclinometer readings were given in the Appendix A section.

- Also quality of the construction workmanship may affect the excavation behavior. Consequently, unexpected displacements can be observed.

    - Struts should be fixed on the wales. If the connection of the struts to the wales is weak, i.e. struts just located on the wales without any fixtures, supports will not work, and the effective length of each strut is increased. In addition, struts should be located with effective welding, otherwise there would be poor connection between the steel strut and the diaphragm wall. All of these effects will lead to a decrease in the stability of the retaining system.

    - In normal soil condition excavation is performed using a grab suspended by cables to a crane. The grab can easily cut through soft ground and the sides inside the trench cut can collapse easily. Bentonite slurry is used to protect the sides of soil. Therefore, quality of bentonite slurry effects the displacements before excavation stages.

    - The soil is expected to collapse at any time during construction of the wall. However, if any collapse occurred during concreting, the contaminated concrete must be removed immediately. Concreting must be continued until soil contaminated concrete is taken out.

- Diaphragm wall must provide low water permeabilty. Gaps between diaphragm wall panel joints may cause more thane expected water leakage and settlements.

- Maximum strut loads force is observed at the lowest strut location and numerical results showed that stress relief is observed at previous strut levels.

- In this thesis, the strain gauge observations may be considered as a failed experimental study. Unsatisfactory results were obtained from six struts. Although there are some efficient results, they are not reliable because of errors in the other struts. The data obtained from the gauges is difficult due to errors in the collected data set. Great care has to be exercised. Due to environmental conditions, impacts and vandalism, protection of the experimental measuremet equipments is a very difficult job in the field. Once for all, waldeble gauges may be preferred to bonded gauges because waldeble gauges may provide more reliable results due to environmental conditions but their price is much higher. In addition to all these at least three strain gauges should be prefered instead of two strain gauges to obtain more accurate results.

- As mentioned earlier stage field and laboratory tests can be tricky. Variations of input parameters elasticity modulus, shear modulus are significantly influence the predictions, so parameter selection must be checked and improved with back analysis.

REFERENCES

Aas, G. (1984). Stability problems in a deep excavation in clay. *Proc., 1st Int. Conf. on Case Histories in Geotechnical Engineering,* Univ. of Missouri-Rolla, Rolla, MO, 315-323.

Bjerrum, L. & Eide, O. (1956). Stability of strutted excavations in clay. *Geotechnique*, *6*(1), 32-47.

Bjerrum, L. (1963, October). Allowable settlement of structures. In *Proceedings of the 3rd European Conference on Soil Mechanics and Foundation Engineering, Wiesbaden, Germany* (Vol. 2, pp. 135-137).

Brinkgreve R. B. J. (Ed.). (1999). *Beyond 2000 in computational geotechnics*. Rotterdam: Balkema Publishers.

Blackburn, J. T., & Finno, R. J., (2007). Three- dimensional responses observed in an internally braced excavation in soft clay. *Journal of Geotechnical and Geoenvironmental Engineering. 133, 1364- 1373.*

Bowles, J. E. (1997). *Foundation analysis and design.* Singapore: McGraw- Hill Book Co.

Caspe, M. S. (1966). Surface settlement adjacent to braced open cuts. *Journal of Soil Mechanics & Foundations Div*, *92*(ASCE# 4867 Proceeding).

Chen, W. F., & Saleeb, A. F. (1982). Uniaxial behavior and modeling in plasticity. *West Lafayette: Purdue University*.

Chen, R. P., Li, Z. C., Chen, Y. M., Ou, C. Y., Hu, Q., & Rao, M. (2013). Failure investigation at a collapsed deep excavation in very sensitive organic soft clay. *Journal of Performance of Constructed Facilities*, *29*(3), 04014078.

Clough, G. W., & O'Rourke, T. D. (1990). Construction induced movements of insitu walls. In *Design and performance of earth retaining structures* (pp. 439-470). ASCE.

Do, T. N., Ou, C. Y., & Lim, A. (2013). Evaluation of factors of safety against basal heave for deep excavations in soft clay using the finite-element method. *Journal of Geotechnical and Geoenvironmental Engineering*, *139*(12), 2125-2135.

Duncan, J. M., & Bentler, D. J. (1998, October). Evolution of deep excavation technology. In *International conference on soil-structure interaction in urban civil engineering, Darmstadt Geotechnics, Darmstadt* (pp. 139-150).

Dunnicliff, J. (1988). *Geotechnical instrumentation for monitoring field performance*. Canada: A Wiley- Interscience Publication.

Finno, R. J., Voss Jr, F. T., Rossow, E., & Blackburn, J. T. (2005). Evaluating damage potential in buildings affected by excavations. *Journal of Geotechnical and Geoenvironmental Engineering*, *131*(10), 1199-1210.

Finno, R. J., Bryson, S., & Calvello, M. (2002). Performance of a stiff support system in soft clay. *Journal of Geotechnical and Geoenvironmental Engineering, 128*(8), 660-671.

Hsieh, P. G., & Ou, C. Y. (1998). Shape of ground surface settlement profiles caused by excavation. *Canadian Geotechnical Journal*, *35*(6), 1004-1017.

Hsieh, P. G., Ou, C. Y., & Liu, H. T. (2008). Basal heave analysis of excavations with consideration of anisotropic undrained strength of clay. *Canadian Geotechnical Journal*, *45*(6), 788-799.

Hsiung, B., & Dao, S.D (2014). Evaluation of constitutive soil models for predicting movements caused by a deep excavations in sands. *Electronic Journal of Geotechnical Engineering, 19, 17325-17343.*

Hwang, R. W., Moh, Z.C., & Wang, C. H. (2007). Toe movements of diaphragm walls and correction inclinometer readings. *Journal of GeoEngireering*, 2, 2, 61-71.

Jaky, J. (1944). The coefficient of earth pressure at rest. *Journal of the Society of Hungarian Architects and Engineers*, *78*(22), 355-358.

Khoiri, M., & Ou, C. Y. (2013). Evaluation of deformation parameter for deep excavation in sand through case histories. *Computers and Geotechnics*, *47*, 57-67.

Kung, G. T. C. (2009). Comparison of excavation-induced wall deflection using top-down and bottom-up construction methods in Taipei silty clay. *Computers and Geotechnics*, *36*(3), 373-385.

Likitlersuang, S., Surarak, C., Wanatowski, D., Oh, E., & Balasubramaniam, A. (2013). Finite element analysis of a deep excavation: A case study from the Bangkok MRT. *Soils and Foundations*, *53*(5), 756-773.

Lin, G.D., & Woo, S. M. (2007). Three dimensional analyses of deep excavation in Taipei 101 construction project. *Journal of GeoEngineering*, 2, 1, 29-41.

Liu, K. X. (1995). Three dimensional analyses of deep excavation in soft clay. *M. Eng. Thesis, National University of Singapore, Singapore*.

Liu, G. B., Ng, C. W., & Wang, Z. W. (2005). Observed performance of a deep multistrutted excavation in Shanghai soft clays. *Journal of Geotechnical and Geoenvironmental Engineering*, *131*(8), 1004-1013.

Liu, G. B., Jiang, J., & Ng, C. W. (2008). Performance of a deep excavation in soft clay. In *Geotechnical Aspects of Underground Construction in Soft Ground: Proceedings of the 6th International Symposium (IS-Shanghai 2008)* (p. 419). CRC Press.

Liu, G. B., Jiang, R. J., Ng, C. W., & Hong, Y. (2011). Deformation characteristics of a 38 m deep excavation in soft clay. *Canadian Geotechnical Journal*, *48*(12), 1817-1828.

Mikkelsen, E. P. (2003). Advances in inclinometer data analysis. *Symposium on Field Measurements in Geomechanics, 1-13.*

Ng, C. W. W., Hong, Y., Liu, G. B., & Liu, T. (2012). Ground deformations and soil-structure interaction of a multi-propped excavation in Shanghai soft clays. *Géotechnique*, *62*(10), 907-921.

Obrzud, R. F.(2010). On the use of the hardening soil small strain model in geotechnical practice. *Numerics in Geotechnics and Structures*.

Ou, C. Y., Hsieh, P. G., & Chiou, D. C. (1993). Characteristics of ground surface settlement during excavation. *Canadian Geotechnical Journal*, *30*(5), 758-767.

Ou, C. Y., & Shiau, B. Y. (1998). Analysis of the corner effect on excavation behaviors. *Canadian geotechnical journal*, *35*(3), 532-540.

Ou, C. Y., Liao, J. T., & Cheng W. L. (2000). Building response and ground movements induced by a deep excavation. *Geotechnique.* No: 3, 209- 220.

Ou, C. (2006). *Deep excavations theory and practice*. Balkema: Taylor & Francis.

PLAXİS 3D Reference Manual. 2016. Retrieved August 5, 2016, from http://www.plaxis.nl/files/files/3D-2-Reference.pdf

PLAXİS 3D Material Models Manual. 2016. Retrieved August 5, 2016, from http://www.plaxis.nl/files/files/3D-3-Material-Models.pdf

Peck, R. B. (1969). Deep excavations and tunnelling in soft ground. In *Proceedings of the 7th International Conference on Soil Mechanics and Foundation Engineering, Mexico City, State-of-the-Art Volume,* (pp. 225-290).

Schanz, T., & Vermeer P. A. (1998). On the stiffness of sands. *Pre-failure Deformation Behaviour of Geomaterial,* 383-387.

Schanz, T., Vermeer P. A., & Bonnier, P. G. (2000). *Beyond 2000 in computational geotechnics: the hardening soil model: formulation and verification*. Rotterdam: Balkema Publishers.

Schanz, T., Vermeer P. A., & Bonnier P.G. (2000). The hardening soil model: Formulation and verification. *Computational Geotechnics,* 281-296

Schweiger, H. F. (2009). Influence of constitutive model and EC7 design approach in FEM analysis of deep excavations. In *Proceeding of ISSMGE International Seminar on Deep Excavations and Retaining Structures, Budapest* (pp. 99-114).

Surarak, C., Likitlersuang, S., Wanatowski, D., Balasubramaniam, A., Oh, E., & Guan H. (2012). Stiffness and stregnth parameters for hardening soil model of soft and stiff Bangkok clays. *Soils and Foundations*, 52(4), 682-697

Surarak, C., Likitlersuang, S., Wanatowski, D., Balasubramaniam, A., Oh, E., & Guan H. (2012). Finite element analysis of a deep excavation: A case study from the Bangkok MRT. *The Geotechnical Society: Soils and Foundations,* 53(5), 756-773.

Tang, Y. G., & Kung, G. T. C. (2009). Application of nonlinear optimization technique to back analyses of deep excavation. *Computers and Geotechnics*, *36*(1), 276-290.

Terzaghi, K. (1943). *Theoretical soil mechanics*. New York, John Wiley & Sons.

Terzaghi, K., & Peck, R. B. (1967). Settlement of Point Bearing Pile Foundation;, Settlement of Floating Pile Foundation. *Soil Mechanics in Engineering Practice*, 540-555.

Tjie-Liong, G. O. U. W. (2014). Common Mistakes on the Application of Plaxis 2D in Analyzing Excavation Problems. *International Journal of Applied Engineering Research*, *9*(21), 8291-8311.

Tung, G., & Kung, C. (2009). Comparison of excavation- induced wall deflection using top- down and bottom-up construction methods in Taipei silty clay. *Computers and Geotechnics,* 36, 373-385.

Wang, J. H., Xu, Z. H., & Wang, W. D. (2009). Wall and ground movements due to deep excavations in Shanghai soft soils. *Journal of Geotechnical and Geoenvironmental Engineering*, *136*(7), 985-994.

Zhang, J. F., Chen, J. J., Wang, J. H., & Zhu, Y. F. (2013). Prediction of tunnel displacement induced by adjacent excavation in soft soil. *Tunnelling and Underground Space Technology*, *36*, 24-33.

Zaremba, N. L. (2007). Experiences in strut load monitoring in excavations for the new metrorail city project. *School of Civil Resource Engineering, 1-12.*

Zaremba, N. L., & Lehane, B. M. (2007). The performance of steel struts in a braced excavation in Perth CBD. *Australian Geomechanics*, *42*(3).

APPENDICES

APPENDIX A:

Uncorrected Inclinometer Results

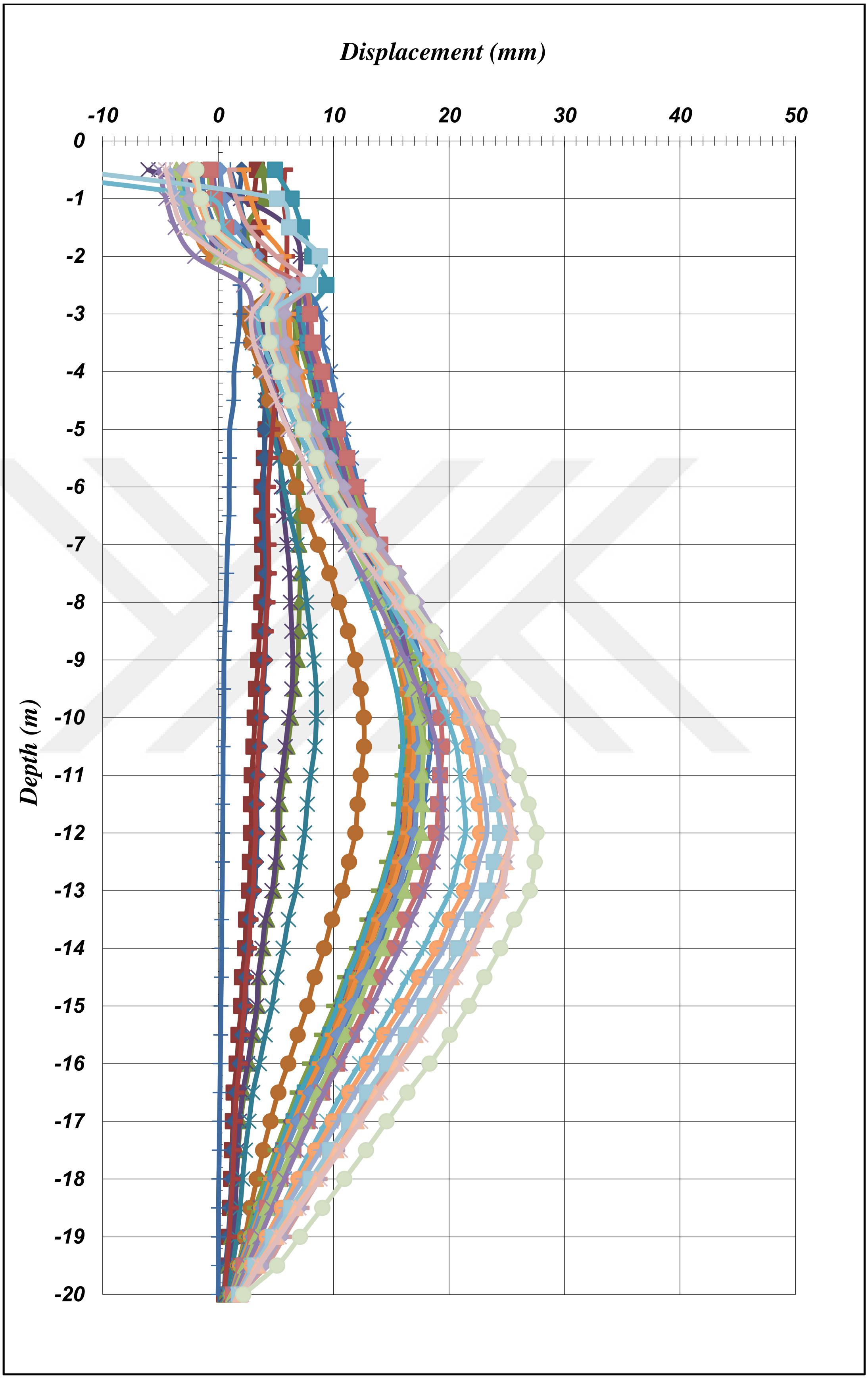

Figure A-1 Uncorrected reading results (Inclinometer-3)

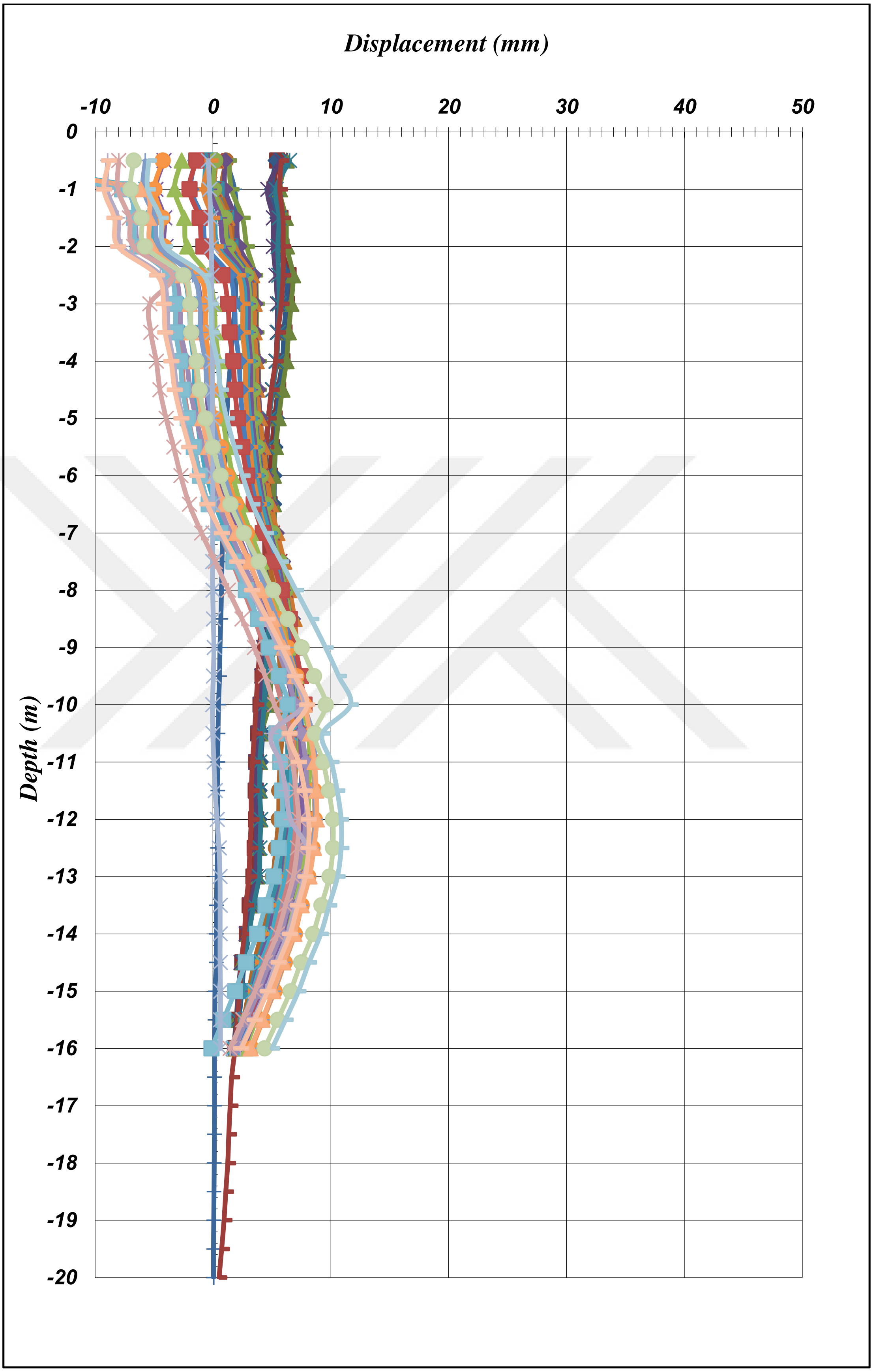

Figure A-2 Uncorrected reading results (Inclinometer-4)

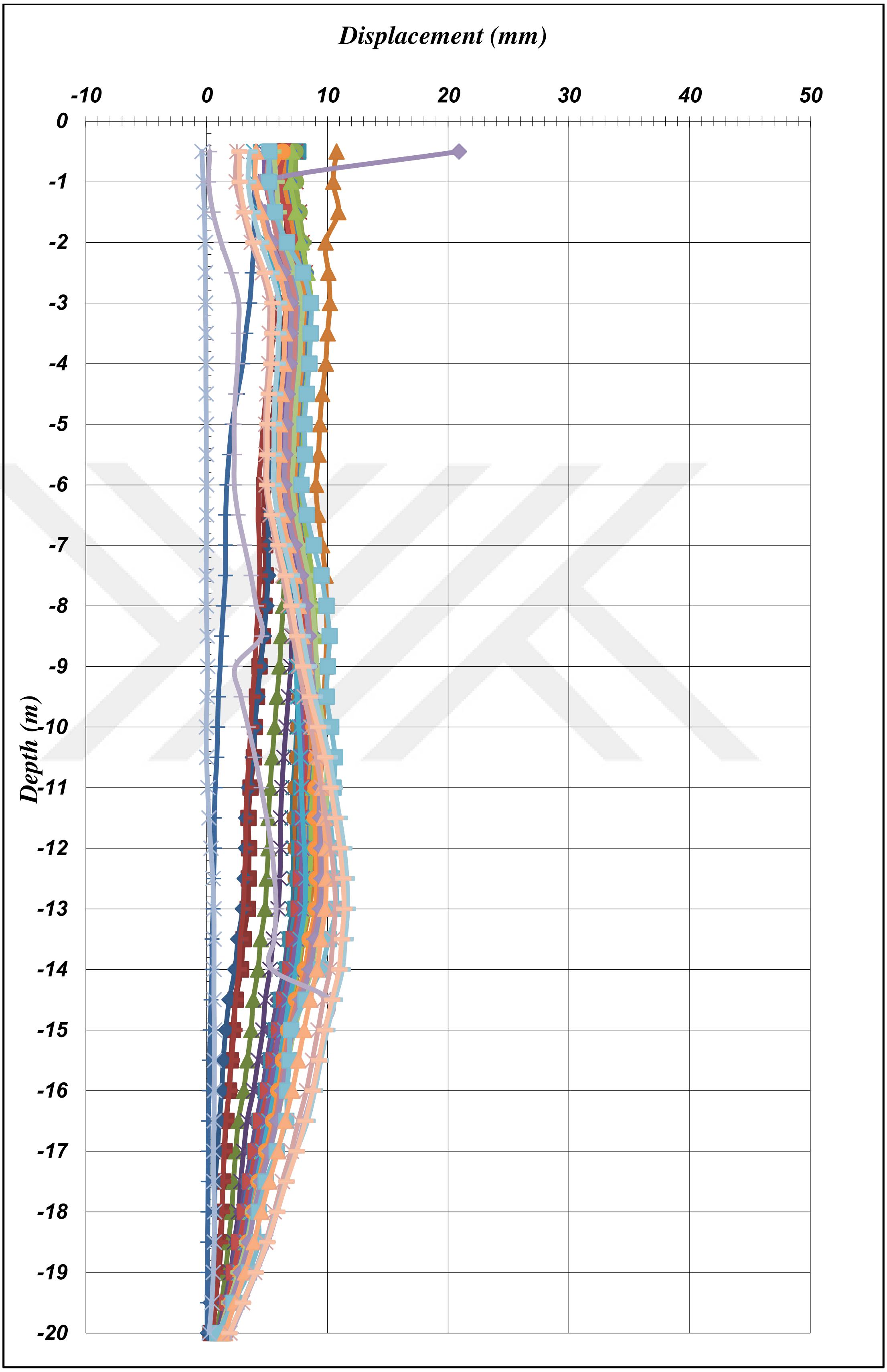

Figure A-3 Uncorrected reading results (Inclinometer-2)

APPENDIX B:
Construction Stage Figures

Figure B.1 Preparing the guide wall

Figure B.2 Preparing the guide wall - 2

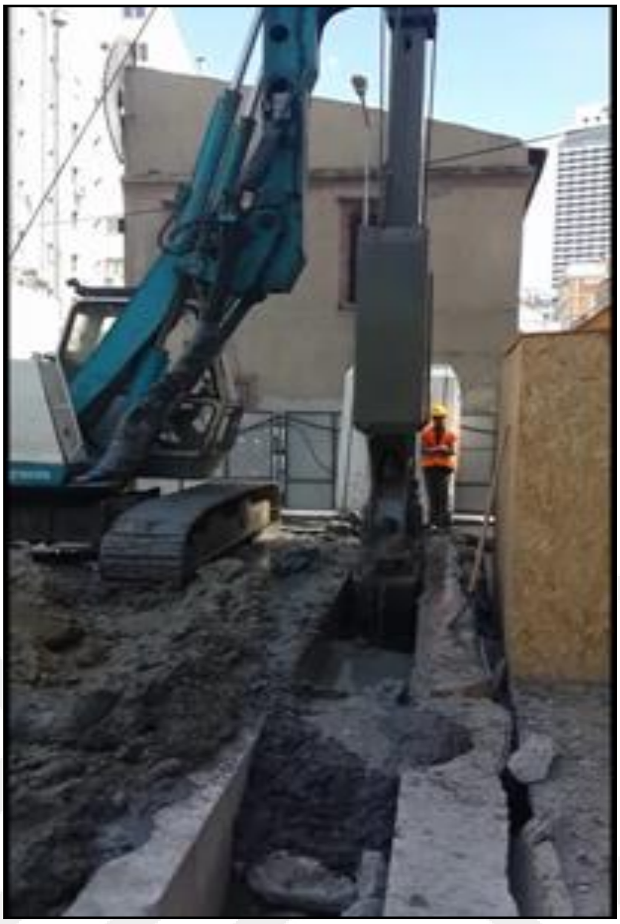

Figure B.3 Trench excavation

Figure B.4 Placing reinforcement cage

Figure B.5 Concreting stage

Figure B.6 Struts

Figure B.7 During excavation stage-1

Figure B.8 During excavation stage-2